

Jornada de
**Escoamentos
Multifásicos**
JEM - 2023



The 7th Multiphase Flow Journey

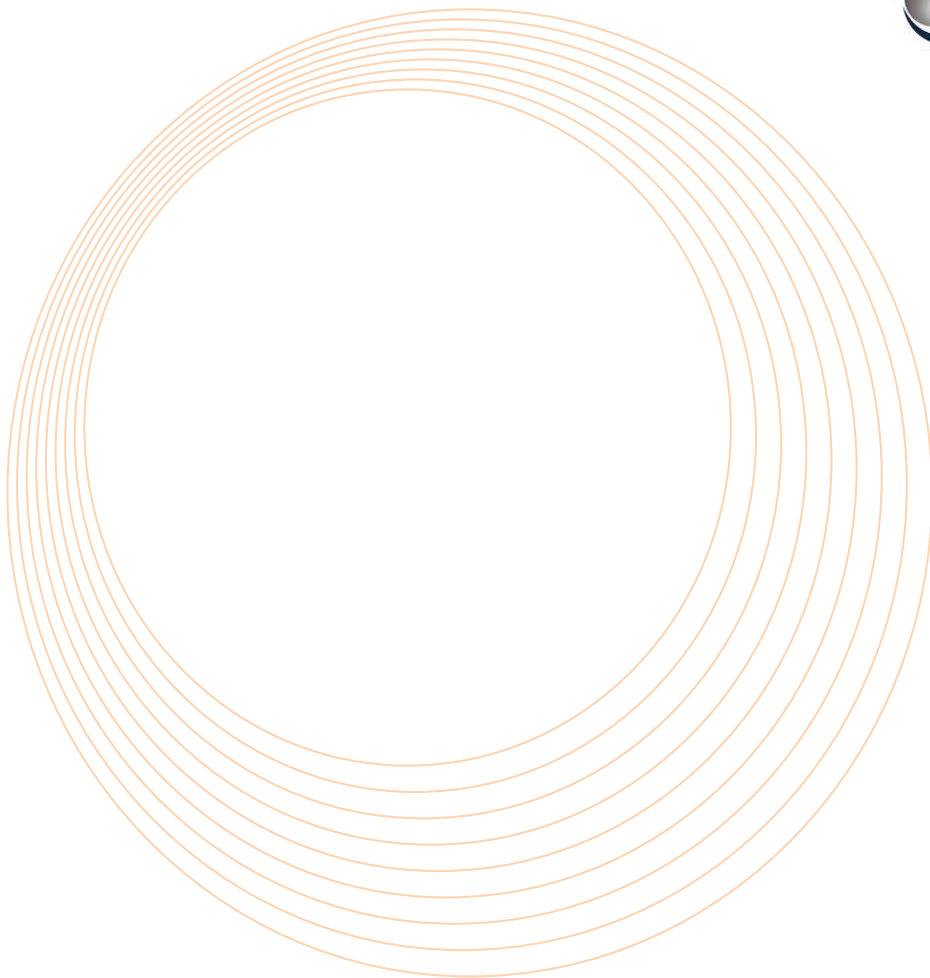


The local organizing committee of JEM2023 welcomes the scientific and industry community to attend the 7th Multiphase Flow Journey, to be held at the Technology Center II of the Federal University of Rio de Janeiro on May 29–31, 2023.

The Multiphase Flow Journey is a biannual event, organized by the Brazilian Society of Mechanical Sciences and Engineering (ABCM). JEM2023 is a merger between the former School of Multiphase Flows (EEM) and the former Brazilian Meeting on Boiling, Condensation and Multiphase Flows (EBECEM).

The general expectation of the organizing committee is that after the recent hiatus in in-person meetings, the opportunity for the Brazilian national community in mechanics to meet in scientific events is to be well perceived by people.

We look forward to welcome you in person in Rio de Janeiro!



Local Organizing Committee

- Fábio Pereira dos Santos
- Gustavo Rabello dos Anjos
- Juliana Loureiro
- Ricardo Medronho
- Tânia Suaiden Klein

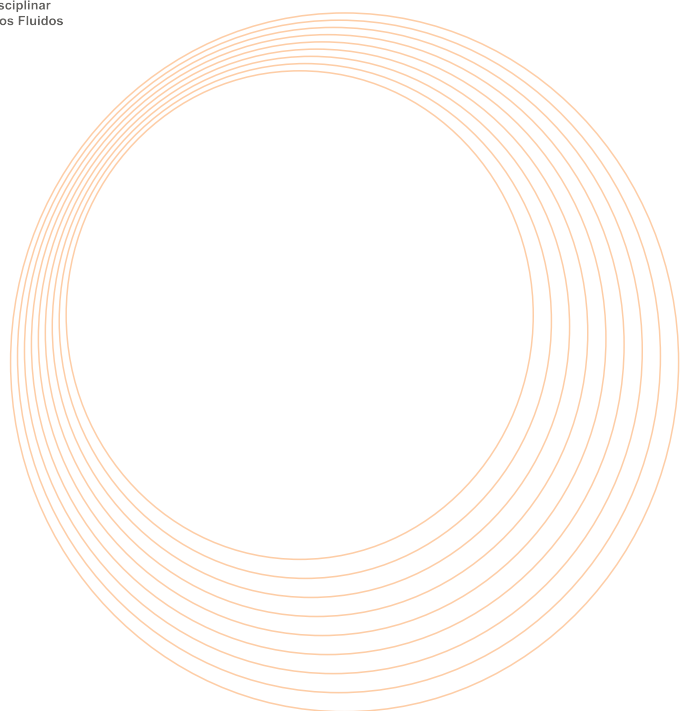
Scientific Committee

- Aline Melchuna, Equinor
- Aloísio Orlando
- Angela Nieckele, PUC-Rio
- André S. Monteiro, Petrobras
- Antonio Bannwart, UNICAMP
- Débora C. Moreira, USP/SC
- Elaine M. Cardoso, UNESP
- Enio P. Bandarra Filho, UFU
- Erick M. Franklin, UNICAMP
- Fabio Kanizawa, UNICAMP
- Geraldo Spinelli, Petrobras
- Igor de Paula, PUC-Rio
- Jacqueline Copetti, Unisinos
- Jader Barbosa Jr., UFSC
- Jorge L. Balino, USP
- Júlio C. Passos, UFSC
- Luiz Machado, UFMG
- Marcelo Castro, UNICAMP
- Moisés Marcelino, UTFPR
- Oscar M.H. Rodriguez, USP/SC
- Ricardo Mazza, Unicamp
- Rigoberto Morales, UFTPR
- Rogério Ramos, UFES



Sponsors

Associação Brasileira de Engenharia e Ciências Mecânicas (ABCM)
Fundação de Amparo à Pesquisa do Estado do Rio de Janeiro (Faperj)
Programa de Apoio aos Núcleos de Excelência (Pronex)
Universidade Federal do Rio de Janeiro (UFRJ)
Centro de Tecnologia da UFRJ (CT/UFRJ)
Instituto Alberto Luiz Coimbra de Pós-Graduação e Pesquisa de Engenharia (Coppe/UFRJ)
The Interdisciplinary Center of Fluid Dynamics (NIDF)



Contents

Local Organizing Committee
Scientific Committee
Sponsors
Contents

1 – Droplets

Total internal reflection technique applied to analyze the contact area between droplets and heated substrates

A. C. Araya, L. P. Leitão, A. V. S. Oliveira

Characteristics of droplet stream generation for different diameters of the nozzle hole

J. M. M. Silva Filho, G. Castanet, M. Gradeck, A. V. S. Oliveira

Characteristics of multiple droplet stream generation using high-speed shadowgraphy

J. M. M. Silva Filho, G. Castanet, M. Gradeck, A. V. S. Oliveira

Deformations of confined magnetic fluid droplets subjected to different magnetic field configurations

R. M. Oliveira

Using the Monte Carlo method to evaluate droplets interaction during spray cooling

C. E. B. M. Rocha, A. V. S. Oliveira

2 – Phase Change, Phase Flow Characterization

Assessment of flow boiling prediction methods for pressure drop and heat transfer coefficient under high temperature and pressure conditions

D. B. Marchetto, G. Ribatski

Flow boiling of R1336mzz(Z) in a copper microgap with tapered manifold

D. C. Moreira, V. S. Do Nascimento Jr., S. G. Kandlikar, G. Ribatski

Nitrogen thin film evaporation applied to cryopreservation

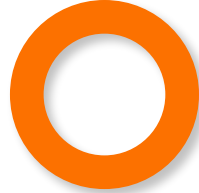
H. Vidaletti, Á. S. da Silva; J. B. Copetti, J. D. de Oliveira, E. M. Cardoso, L. L. Manetti

Study of phase fraction distribution in horizontal gas/liquid flow via collimated gamma-ray densitometry

C.E. Alvarez-Pacheco, C.M. Ruiz-Diaz and O.M.H. Rodriguez

A machine learning approach on two-phase flow characterization and calculation based on a large experimental dataset

A. C. Faller, P. H. C. Paulo, S. C. Vieira, A. T. Fabro, M. S. Castro



3 – Stratified Flow, Annular Flow

Study on hydrodynamic stability of stratified liquid–liquid flow using optical techniques

P. J. Miranda–Lugo, Jorge E. Arrollo–Caballero and O. M. H. Rodriguez

Analysis of the wave characteristics for stratified–wavy flow during in–tube convective condensation

Neumeister, R. F., Kohlmann, A. L. G., Moreira, T. A. and Ribatski, G

Experimental investigation on upward–vertical adiabatic–inverted annular flow

E. Orati, O. M. H. Rodriguez

Liquid film behavior regarding pipe diameter on vertical downward annular flow

A. L. B. Santana, G. K. de Souza, E. N. dos Santos, M. J. da Silva, M. A. Marcelino Neto, R. E. M. Morales

Characterization of horizontal oil–water core–annular flow using particle image velocimetry (PIV) and planar laser induced fluorescence (PLIF) techniques

J. E. Arrollo–Caballero, P. J. Miranda–Lugo and O. M. H. Rodriguez

4 – Slug Flow, Phase Flow Characterization

Influence of the flow loop configuration on the slug flow characteristic parameters in vertical pipes

C. C. Rodrigues, P. A. D. Maldonado, E. N. dos Santos, M. A. Marcelino Neto, R. E. M. Morales

Slug flow of gas and shear thinning fluids in horizontal pipes

R. Baungartner, G.F.N. Gonçalves, J.B.R. Loureiro, A.P. Silva Freire

Experimental investigation of horizontal two–phase slug flow with high density gases

B. P. Naidek, M. V. R. Pereira, I. S. Veiga, E. M. Baggio, P. L. N. Machado, R. Fonseca Junior, M. A. Marcelino Neto, R. E. M. Morales

Analytical and numerical study of the Benjamin’s bubble using a rock flow cell

G. D. Dextre, E. Mancilla, M. A. Marcelino Neto, R. E. M. Morales

Characterization of two–phase flow pattern for qualitative flow induced vibration analysis in subsea Xmas tree

M. C., Oliveira, L. L. Palladino, S. T. Griffo





5 – Numerical Methods

Three Dimensional Two-Phase finite element simulation using a Front – Tracking Method

D. B. V. Santos and G. R. Anjos

Simplified lattice Boltzmann implementation of the Brinkman equation with applications in the viscous fingering instability

H. S. Tavares

Numerical Simulation of a Multiphase Flow inside a Diesel Particulate Filter

F. F. Ferreira, G. R. dos Anjos

Simulation of multiphase flow and analysis of droplet formation patterns in a microchannel

K. L. Pinto, V. L. P. Amorin, R. J. Lobosco, E. G. A. Costa, G. B. Lopes Junior

A semi-lagrangian finite element method for two-phase flows

G. R. dos Anjos, R. A. Vidal

6 – Centrifugal Flows, Gas Flow

Using electrical submersible pump mechanical vibrations and Fourier convolution neural network to estimate the water cut in two-phase liquid-liquid flows

F. C. T. Carvalho, A. L. Serpa

Surging parametrization for gas-liquid centrifugal pumps

L. E. M. Carneiro, G. S. O. Martins, C. M. P. Rosero, J. B. R. Loureiro, A. P. Silva Freire

A coupled PIV/PTV framework for the determination and assessment of interfacial momentum closure in dispersed two-phase rotating flows

W. D. P. Fonseca, R. F. L. Cerqueira, R. M. Perissinotto, W. Monte Verde, M. S. Castro and E. M. Franklin

Experimental methodology to simulate leaks in dense-gas/liquid pipe flow

C. M. Ruiz-Díaz, C. E. Álvarez-Pacheco, M. da Silva Carr, Oscar M. H. Rodríguez

Influence of the Slip parameter in pressure wave propagation in wet gas flow

J. E. C. Bolívar, O. M. H. Rodríguez

7 – Non-Newtonian Fluids, Experimental Methods

Effect of drag reducing polymer on flow patterns of horizontal air-water flow

P. B. P. Panisset, I. B. de Paula, L. F. A. Azevedo

Numerical study of capillary thinning dynamics with FENE-P model

R. A. Figueiredo, C. M. Oishi and A. M. Afonso





Measurement system for the airflow of an EA211 1.0 MPI Volkswagen engine

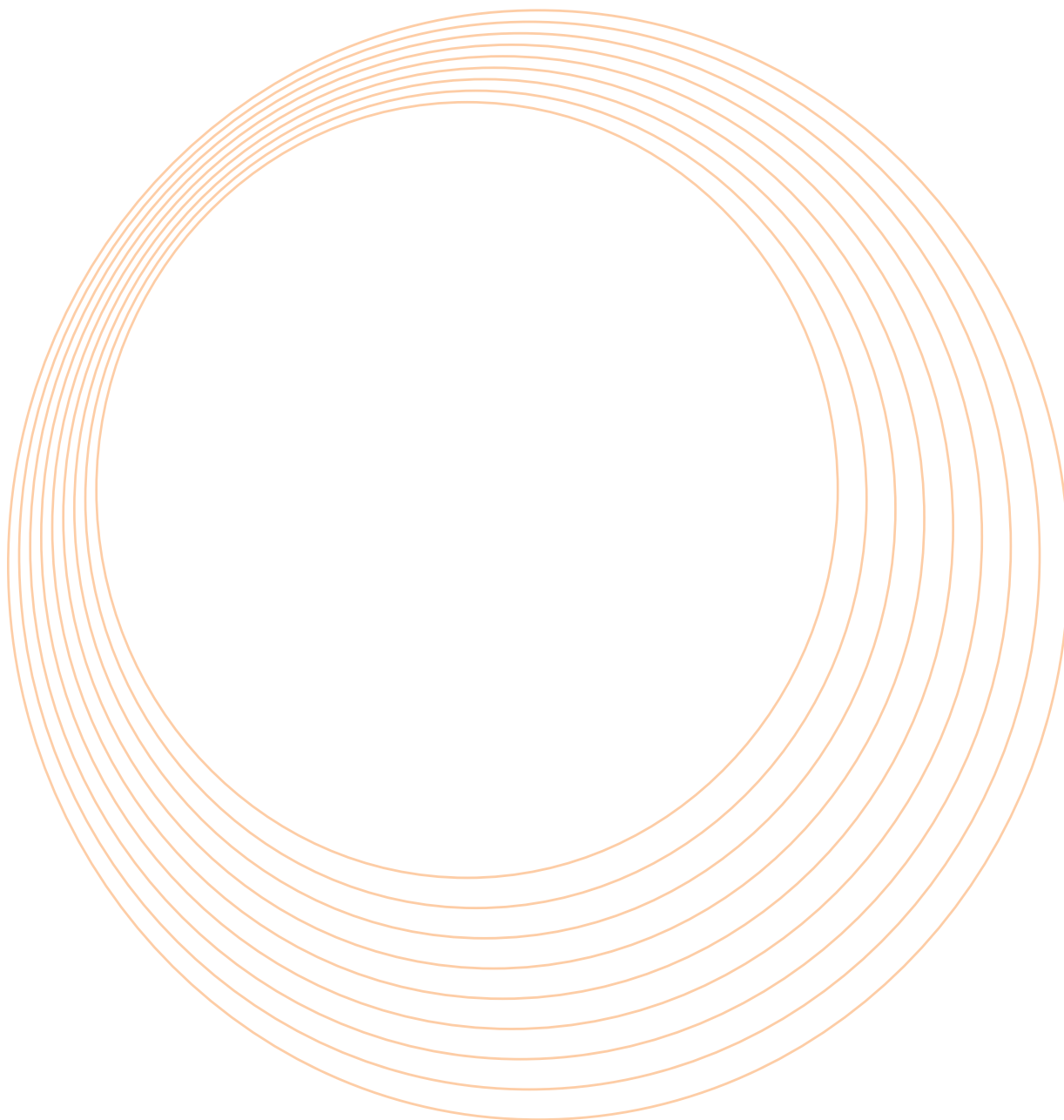
F. Frejat, F. Lisboa

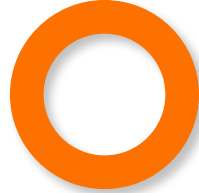
Implementation of low cost espectrophotometer for MEG detection in water

R. Baldin, M. J. da Silva, E. N. dos Santos

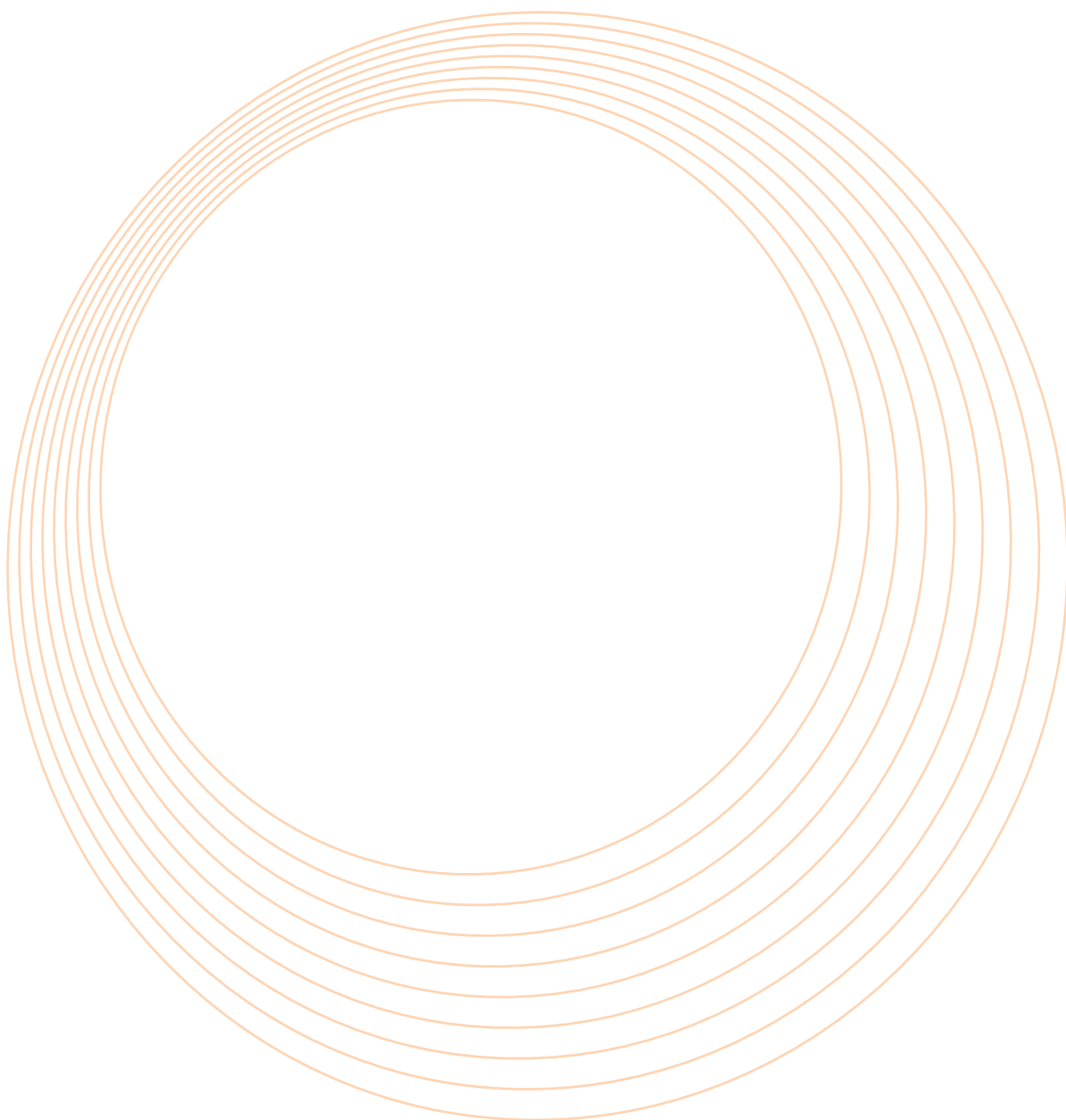
Analysis of velocity fields during hydrogen production by electrolysis

J. D. de Oliveira, T. W. Leite, E. M. Cardoso, J. B. Copetti





1 - Droplets



Total internal reflection technique applied to analyze the contact area between droplets and heated substrates

Álvaro Campos Araya, Luigi Paero Leitão, Arthur V. S. Oliveira

Department of Mechanical Engineering, São Carlos School of Engineering, University of São Paulo, São Carlos, Brazil.

Email: afc.araya@usp.br, luigi.leitao@usp.br, avs.oliveira@usp.br

ABSTRACT – Spray cooling has many industrial applications, which motivates many studies on droplet impact on heated wall and wall rewetting. The main objective of this work is to apply the Total Internal Reflection (TIR) technique to study the real contact area between a single droplet of fluid and a heated surface. Single droplet impact results are presented for different substrate temperatures. This is the first step for future studies with multiple drops and sprays given their complex phenomenology.

INTRODUCTION

Spray cooling is a highly complex process both from the hydrodynamic and thermal point of view. Authors such as Khavari (2017) focused their study on single droplets, due to greater feasibility to perform behavior analysis and development of methods eventually useful for sprays. Single droplet studies have proven to be essential to understand the behavior of sprays, but the complex interactions between droplets are not being considered Moreira et al. (2010). In this study, we used TIR to evaluate the solid-liquid contact area during a droplet impact on a heated wall.

METHOD

TIR consists essentially of a laser beam directed by mirrors getting into a dove prism at a certain angle as shown on figure 1. If the angle is greater than a critical value, then the light will not be refracted but totally reflected, then the beam comes out and ends up projected on a viewing screen. The resulting images are recorded by a high-speed camera where the darker zones represent the wetted or contact area.

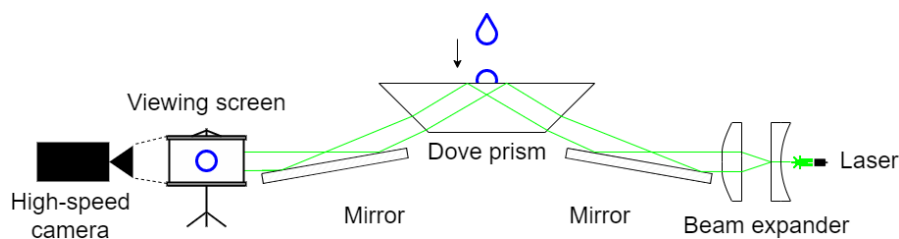


Figure 1: TIR experimental setup.

RESULTS

Several tests were performed for different substrate temperatures: 70°C on figure 2, 170°C on figure 3 and 210°C on figure 4. For the 70°C case, the drop is deposited on the surface and, as time progresses, no significant changes are observed given the low temperature of the substrate. For the 170°C case, given a higher temperature of the substrate, the heat transfer increases, generating some displacement of the droplet and also a rupture into smaller droplets. Eventually the volume of fluid evaporates completely. For the 210°C case, in general terms, the behavior of the droplet was similar to the previous case. The main difference was that the process was at least three times faster.

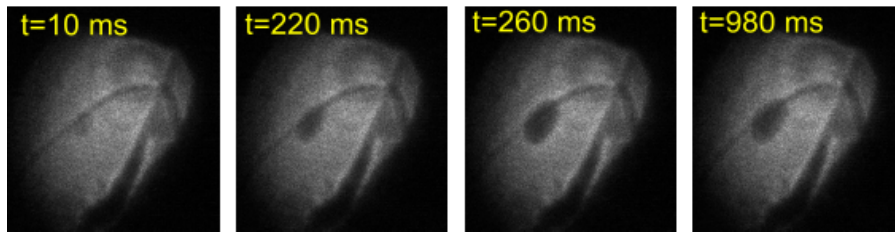


Figure 2: Recorded images for a wall temperature of 70°C.

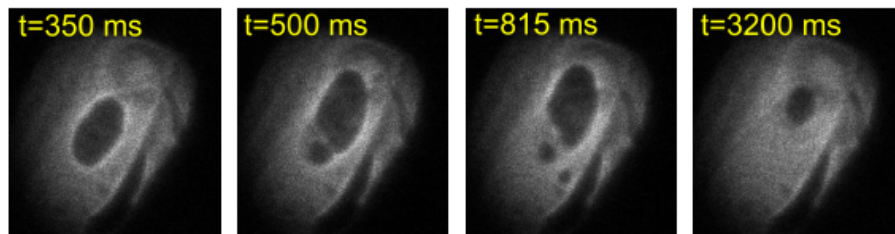


Figure 3: Recorded images for a wall temperature of 170°C.

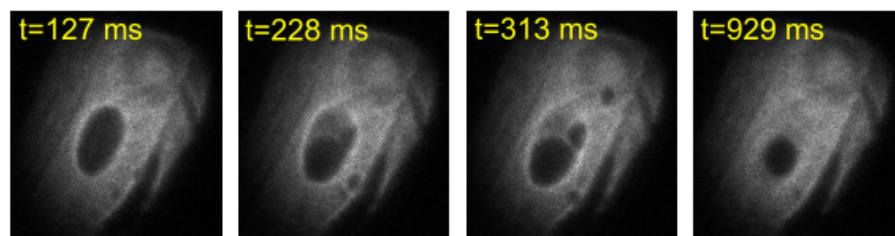


Figure 4: Recorded images for a wall temperature of 210°C.

CONCLUSIONS AND FUTURES WORK

Images for different wall temperatures and times are shown, the solid-liquid contact area is visible but it is still not optimal. The aim for future results is to improve the quality of the images to identify and classify the droplet phenomena, also develop post processing codes on Matlab which are meant to facilitate the extraction of quantitative results. Finally the tests must cover a wide range of wall temperatures to find the Leidenfrost temperature, one of the most important parameter for experiments in this matter.

ACKNOWLEDGMENTS

The authors gratefully acknowledges São Paulo Research Foundation (FAPESP) for the Young Investigator research grant (2021/01897-0), the scholarship given to the author Álvaro Campos Araya (2022/08694-0) and to Luigi Paero Leitão (2022/13480-0).

REFERENCES

Khavari, M. (2017). Droplet impact on superheated surfaces. Nanyang Technological University.
 Moreira, A., Moita, A., & Panão, M. (2010). Advances and challenges in explaining fuel spray impingement: How much of single droplet impact research is useful? *Progress in Energy and Combustion Science*, 36, 554-580.

Characteristics of droplet stream generation for different diameters of the nozzle hole

João Marcelo M. Silva Filho¹, Guillaume Castanet², Michel Gradeck², Arthur V. S. Oliveira¹

¹Department of Mechanical Engineering, São Carlos School of Engineering, University of São Paulo, São Carlos, Brazil

²Université de Lorraine, CNRS, LEMTA, F-54000 Nancy, France

Email: jmarcelofilho@usp.br, guillaume.castanet@univ-lorraine.fr, avs.oliveira@usp.br

ABSTRACT

The quality of a generated droplet stream by Plateau-Rayleigh instability is directly related to the nozzle design, including the hole diameter. We present in this study experimental results of droplet streams generated by nozzles with different hole diameters. While the repeatability was excellent for smaller holes, a well-behaved droplet stream could not be obtained with higher diameters.

INTRODUCTION

When a jet is injected in air, small perturbations in the jet diameter along its length are amplified until break up takes place, generating a droplet stream. This hydrodynamic instability is called Plateau-Rayleigh (Charru, 2011) and there are several solutions of droplet stream generators based on this phenomenon. These devices can generate small, periodic and highly repeatable droplets in a row, and they are very useful, for example, to study droplet impact heat transfer (Dunand, Castanet, Gradeck, Lemoine, & Maillat, 2013). As indicated by Breslouer (2010), the generated droplets have a diameter of approximately 2.1 times the nozzle diameter. In this study, we tested and evaluated the quality of droplet streams generated by a nozzle equipped with membranes of different hole diameters.

METHOD

Figure 1 presents the experimental apparatus, which consists of a droplet stream generator – a tube with a piezoelectric slab attached to its bottom and a pierced membrane in the other end where the jet is formed. This pierced membrane was changed for each experiment, so we could vary the hole diameter from 112 to 822 μm . All of the membranes were 0.2-mm thick. The piezoelectric part was excited using a signal generator, which induced Plateau-Rayleigh instabilities in the jet that, eventually, broke into small droplets. We used deionized water as test fluid, which was pressurized at 1 bar using compressed air and a pressure regulator. A high-intensity lamp was used as back-light source for the shadowgraphy, and a high-speed camera (Phantom Miro M110) captured the images at 1600 fps. We also used a teleconverter (Sigma 2x EX DG APO) to amplify the image.

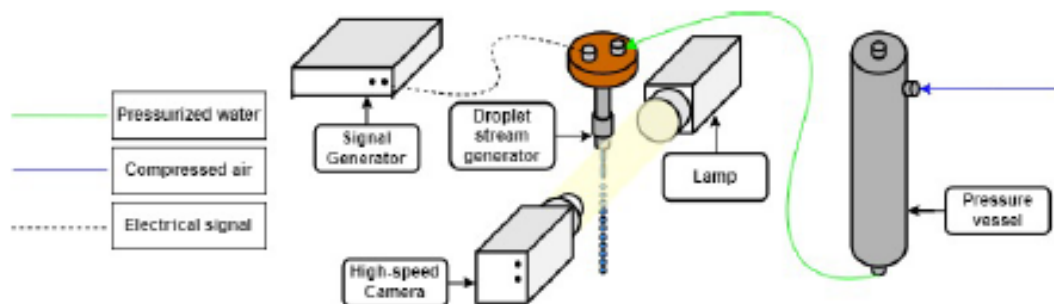


Figure 1: Experimental apparatus.

RESULTS

Figure 2 shows the droplet streams and their respective jets resulted from three different single-hole membrane sizes: 112 μm , 322 μm , and 822 μm . Using shadowgraphy we could characterize the average droplet diameter (d_{droplet}) for the 112 μm and 322 μm membranes, and later obtain other relevant parameters, as: droplet velocity (v), spacing parameter (C) and volumetric flow rate (\dot{V}). We also present values for the voltage frequency applied to the piezoelectric (f), in all conditions.

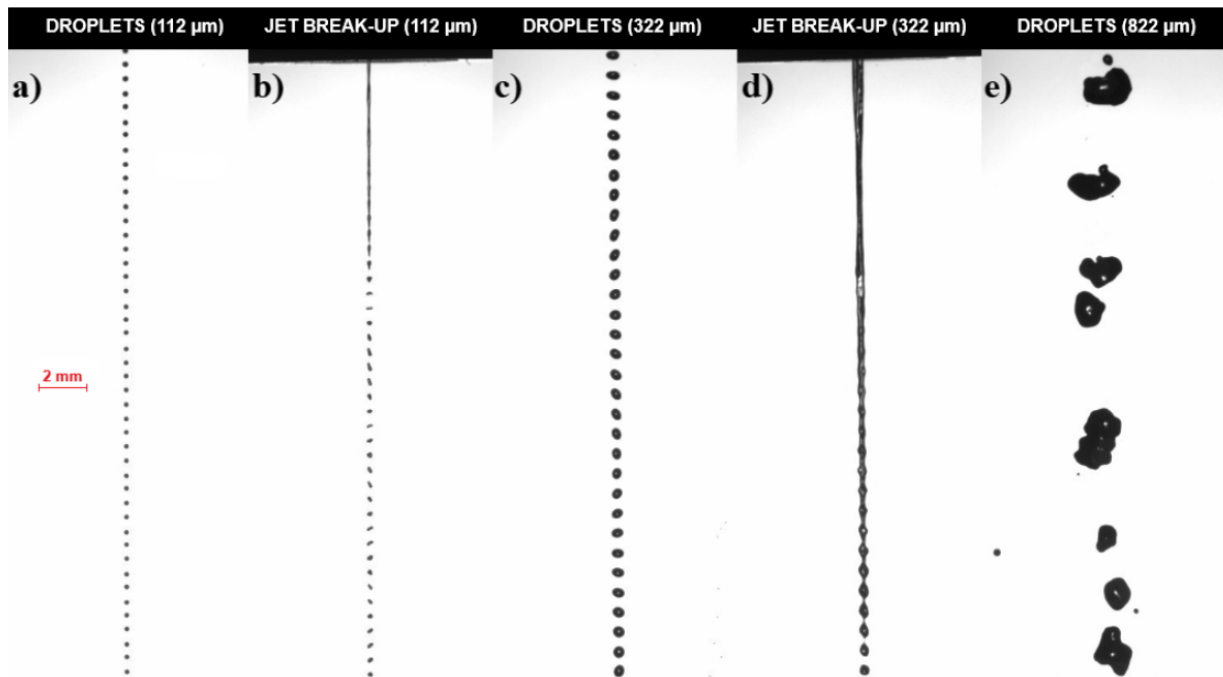


Figure 2: Droplets streams (downstream distance from the nozzle was 80 mm) and jets obtained for different single-hole membrane sizes — a,b) $f = 21.49$ kHz, $d_{\text{droplet}} = 206$ μm , $v = 12$ $\frac{\text{m}}{\text{s}}$, $C = 2.75$, $\dot{V} = 98$ $\frac{\text{mm}^3}{\text{s}}$; c,d) $f = 16.3$ kHz, $d_{\text{droplet}} = 454$ μm , $v = 13$ $\frac{\text{m}}{\text{s}}$, $C = 1.76$, $\dot{V} = 798$ $\frac{\text{mm}^3}{\text{s}}$; e) $f = 16.91$ kHz.

As it can be induced from the images, we achieved a great droplet repeatability for smaller nozzle sizes (112 μm and 322 μm) and could not obtain spherical and repeatable droplets for a larger hole (822 μm). Also, the break-up length for the 322 μm nozzle diameter was greater than the break-up length for the 112 μm hole size. That result was already expected, since the jet breaking criterion is directly dependent on the diameter of the droplet generated.

CONCLUSIONS

A great droplet repeatability was obtained for smaller nozzle sizes. Conversely, spherical and repeatable droplets could not be obtained for a larger hole diameter. Therefore, we can infer that, for the tested membranes and considering their 0.2-mm thickness, the nozzle diameter limit that generates repeatable droplets should be between 300 and 800 μm .

ACKNOWLEDGMENTS

The authors gratefully acknowledge São Paulo Research Foundation (FAPESP) for the Young Investigator research grant (2021/01897-0) and the BEPE scholarship (2022/14365-0).

REFERENCES

- Breslouer, O. (2010). Rayleigh-plateau instability: falling jet. Project Report. Charru, F. (2011). Hydrodynamic instabilities. (Vol. 37; C. U. Press, Ed.).
- Dunand, P., Castanet, G., Gradeck, M., Lemoine, F., & Maillet, D. (2013). Heat transfer of droplets impinging onto a wall above the leidenfrost temperature. *Comptes Rendus Mécanique*, 341 (1), 75–87. (Combustion, spray and flow dynamics for aerospace propulsion).

Characteristics of multiple droplet stream generation using high-speed shadowgraphy

João Marcelo M. Silva Filho¹, Guillaume Castanet², Michel Gradeck², Arthur V. S. Oliveira¹

¹Department of Mechanical Engineering, São Carlos School of Engineering, University of São Paulo, São Carlos, Brazil

²Université de Lorraine, CNRS, LEMTA, F-54000 Nancy, France

Email: jmarcelofilho@usp.br, guillaume.castanet@univ-lorraine.fr, avs.oliveira@usp.br

ABSTRACT

Droplet streams are very useful in droplet impact studies, especially those where highly repeatable droplet characteristics are necessary. In this study we present experimental results of shadowgraphy to characterize multiple droplet streams generated by perforated membranes with two to four holes. Results with a single-hole membrane are also presented for comparison. It was possible to generate monodisperse droplets for all configurations and in-phase droplet streams for the two-hole membrane.

INTRODUCTION

Droplet impact studies are very common in the literature because of the many engineering applications that involve droplet-surface dynamic interactions (Liang & Mudawar, 2017). The repeatability of experiments is crucial to have reliable experimental data to validate mechanistic models of fluid dynamics and heat transfer – if the wall is at a different temperature. Although we find several droplet generators in the literature (Wang & Liu., 2022), either for single droplet on-demand or single droplet stream, less options are found to generate multiple droplets, especially to ensure the droplets will impact the surface at the same time. In this study, we used a droplet stream generator using a multi-hole membrane to generate two to four droplet streams, and characterized the generated droplets using high-speed shadowgraphy.

METHOD

Figure 1 presents the experimental apparatus we used in this study. The droplet generator consists mainly of a tube with a piezoelectric slab attached to its bottom and a membrane in the other end that has one to four holes where jets are formed and, consequently, the droplets streams. The singlehole membrane is the reference to compare with the multi-hole membranes. The piezoelectric part was excited using a signal generator, which induced Plateau-Rayleigh instabilities in the jet that, eventually, broke into small droplets. We used deionized water as test fluid, which was pressurized at 0.5 bar using compressed air and a pressure regulator. A high-intensity lamp was used as backlight source for the shadowgraphy, and a high-speed camera (Phantom Miro M110) captured the images at 1600 fps. We also used a teleconverter (Sigma 2x EX DG APO) to amplify the image.

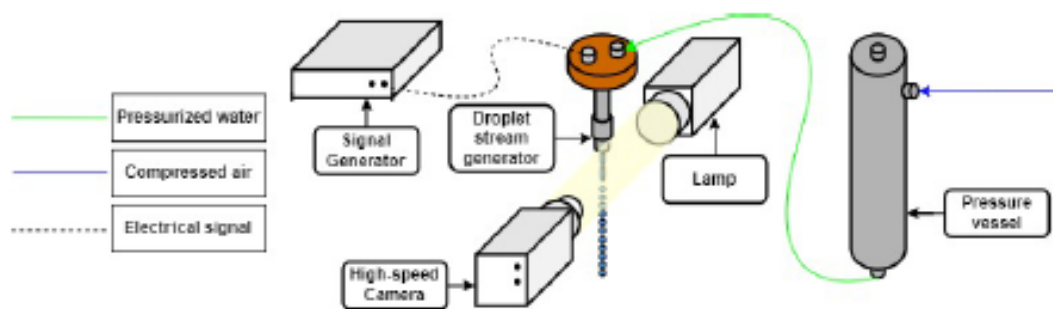


Figure 1: Experimental apparatus.

RESULTS

Figure 2 shows the droplet streams and their respective jets resulted from four different membranes, with one to four holes. The diameters of the nozzles are 112 μm (single-hole), 200 μm (two-hole), 204 μm (three-hole), and 185 μm (four-hole). The distance between holes for the in-line configurations (two-hole and three-hole) were 1 mm and 0.5 mm, respectively. For the square configuration (four-hole), the side distance was 0.62 mm. Other important parameters are the signal frequency applied to the piezoelectric piece, f , and the volumetric flow rate, \dot{V} .

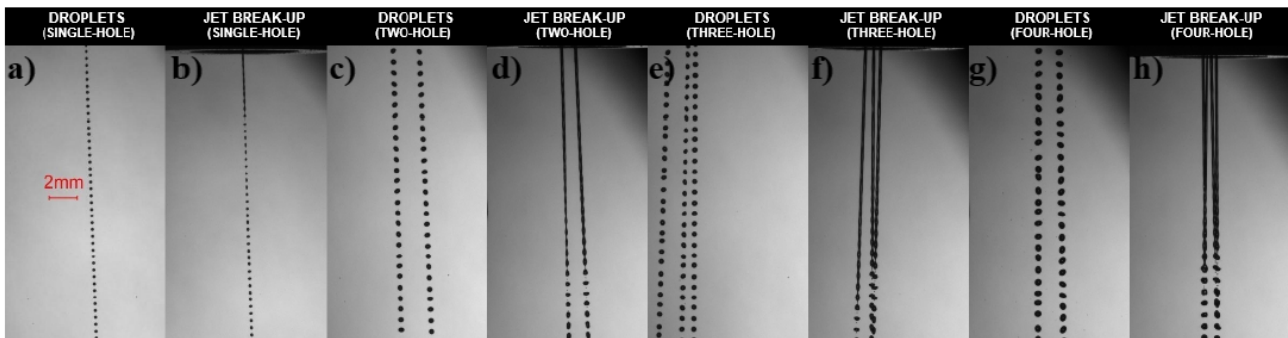


Figure 2: Droplet streams (downstream distance from the nozzle was 40 mm) and jets obtained for membranes with one to four nozzles — a,b) $f = 20.59$ kHz, $\dot{V} = 96 \frac{\text{mm}^3}{\text{s}}$; c,d) $f = 12.60$ kHz, $\dot{V} = 685 \frac{\text{mm}^3}{\text{s}}$; e,f) $f = 11.45$ kHz, $\dot{V} = 908 \frac{\text{mm}^3}{\text{s}}$ and g,h) $f = 8.63$ kHz.

As shown by the images, we achieved a great droplet size repeatability amongst jets for the two-hole and three-hole membranes. For the two-hole nozzle, the droplet streams were in-phase and had the same break-up length. For the three-hole membrane, the first stream was not in-phase with the other two, which may be resulted from the difference in the break-up lengths. For the four-hole configuration, there were two merges, resulting in two droplet streams that were not in-phase, since one of the merged jets was unstable. Both three-hole and four-hole membranes presented deflection in the direction of their jets, which resulted in different jet phases and merge of jets, respectively.

CONCLUSIONS

We obtained great repeatability in the droplet size results for the two-hole membrane. For the three-hole and four-hole configurations, jet deflection had an impact in the results, causing a difference in the break-up lengths and jet stability. Therefore, a major attention must be given in order to avoid jet deflection in multi-hole membranes.

ACKNOWLEDGEMENTS

The authors gratefully acknowledge São Paulo Research Foundation (FAPESP) for the Young Investigator research grant (2021/01897-0) and the BEPE scholarship (2022/14365-0).

REFERENCES

- Liang, G., & Mudawar, I. (2017). Review of spray cooling – part 1: Single-phase and nucleate boiling regimes, and critical heat flux. *International Journal of Heat and Mass Transfer*, 115, 1174–1205. doi: <https://doi.org/10.1016/j.ijheatmasstransfer.2017.06.029>.
- Wang, W. K. P. B. F. W., Liping, & Liu., H. (2022). Experimental investigation on the performances of a valve-based and on-demand droplet generator producing droplets in a wide size range. *AIP Advances*, 12 (9). doi: <https://aip.scitation.org/doi/10.1063/5.0107610>

Deformations of confined magnetic fluid droplets subjected to different magnetic field configurations

Rafael M. Oliveira

Departamento de Engenharia Mecânica, Pontifícia Universidade Católica do Rio de Janeiro, Rio de Janeiro, 22451-900, Brazil

ABSTRACT

We conduct nonlinear simulations to determine the interfacial morphology of magnetic fluid droplets confined to the parallel plates of a Hele-Shaw cell in the presence of different magnetic field configurations. Both ferrofluids and magnetorheological fluids are considered. The former is stable colloidal suspensions containing a carrier fluid and nanometer-sized magnetic particles. They have a Newtonian viscosity and behave superparamagnetically, thus presenting a prompt response to even modest magnetic fields. Magnetorheological fluids, on the other hand, are composed of much larger, micron-sized particles suspended in the carrier fluid. This renders the fluid viscoelastic properties in the form of a magnetic field-dependent yield stress. Magnetic fluids are smart controllable materials that have a wide range of applications, including the clean-up of oil spills, the active control of suspension for vehicles, the external magnetic actuator for microfluidic devices, and the diagnosis and treatment of diseases such as cancer. In our simulations, we investigate the fully nonlinear behavior of the interface dynamics by employing an accurate boundary integral method based on the vortex-sheet formalism. The shapes of the confined magnetic fluid droplets are calculated by considering the competition between capillary, viscous, and magnetic influences, in addition to viscoelastic effects when a magnetorheological fluid is considered. The discretization method is discussed and results considering the influence of different magnetic field configurations are presented.

INTRODUCTION

Magnetic fluids are smart materials with the outstanding feature of combining magnetic tunable properties of solids with typical fluidity behaviors of liquids [1,2]. Because of their easiness to manipulate, control, and shape, they have attracted increasing interest in various areas including physics, chemistry, engineering, material science, biology, medicine, and art. In particular, these materials are ideal to study interfacial instability and pattern formation [3,4].

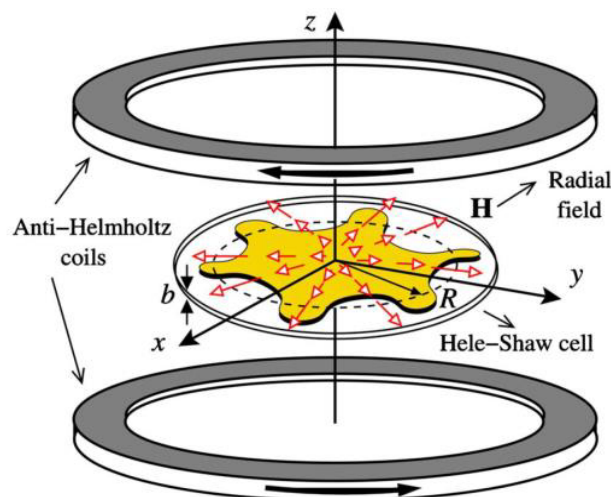


Figure 1

These are usually investigated by confining the magnetic droplet between the parallel plates of a Hele–Shaw cell. When surrounded by a nonmagnetic fluid and submitted to a uniform magnetic field, applied perpendicularly to the cell’s plates, the droplet goes through morphological transitions leading to a labyrinthine instability. However, the droplet shapes are strongly dependent on the applied field configuration and type of magnetic fluid, i.e. if it is a ferrofluid or a magnetorheological fluids [5]. Here, we consider the influence of two magnetic field configurations: a radially growing magnetic field acting on the Hele–Shaw plane, and an azimuthal one generated by a current-carrying wire (cf. Figure 1). The radial field tends to stretch the magnetic droplet turning the ferrofluid into starfish-like, spiked patterns [6].

However, when a magnetorheological fluid is considered, the field-dependent yield stress acts to attenuate deformations. The interfacial patterns are also dependent on the surface tension acting on the interface, which has a stabilizing influence on the instabilities, and on the viscosities of both fluids. The azimuthal field tends to align the magnetic dipoles along the azimuthal direction, which creates and radial force that pulls the fluid radially inwards. It has a stabilizing influence on interface deformations when the magnetic droplet is the internal fluid. However, the superposition of both radial and azimuthal fields has surprising effects and may generate steady-state skewed shapes that rotate like a rigid body [7]. Moreover, if the order of the fluids is reversed, i.e., if we consider a droplet of nonmagnetic fluid surrounded by a ferrofluid, the azimuthal field becomes destabilizing.

Methods and Results

We conduct accurate boundary integral simulations based on the vortex-sheet formalism to track the interfacial deformations of these magnetic droplets. The vortex-sheet is a measure of the vorticity distribution of the problem, which is concentrated in the sharp interface between the fluids. It is defined as the jump in the tangential component of velocity as one crosses the interface. The distribution of vortex-sheet needs to be calculated in every time step and is coupled to evolution equations to determine the shape of the interface [6,7,8]. Examples of interfacial patterns subjected to different magnetic field configurations can be seen in Figure 2.

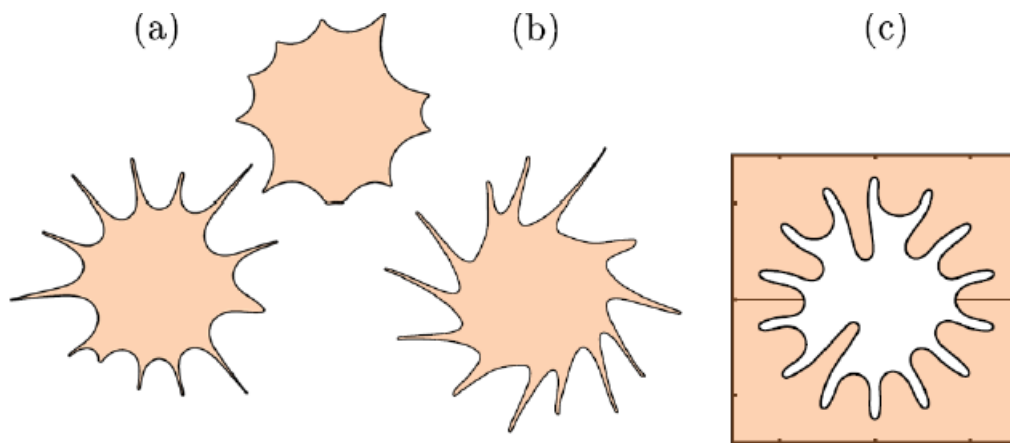


Figure 2: (a) Spiked pattern obtained from the stretch imposed by the radial magnetic field on a ferrofluid. The inset shows a corresponding result for a magnetorheological fluid; (b) Skewed spiked fingers result from the superposition of the radial and azimuthal magnetic fields. The whole ferrofluid pattern rotates in the counterclockwise direction; (c) When the internal fluid is nonmagnetic, the azimuthal field pulls the ferrofluid inwards, deforming the interface.

REFERENCES

- [1] R. E. Rosensweig, *Ferrohydrodynamics* (Cambridge University Press, Cambridge, UK, 1985).
- [2] I. Torres-Díaz and C. Rinaldi, Recent progress in ferrofluids research: novel applications of magnetically controllable and tunable fluids, *Soft Matter* 10, 8584 (2014).
- [3] Y. Zhang and N.-T. Nguyen, Magnetic digital microfluidics—a review, *Lab Chip* 17, 994 (2017).
- [4] K. Ulbrich et al., Targeted drug delivery with polymers and magnetic nanoparticles: Covalent and noncovalent approaches, release control, and clinical studies, *Chem. Rev.* 116, 5338 (2016).
- [5] S. A. Lira, J. A. Miranda and Rafael M. Oliveira, Field-induced patterns in confined magnetorheological fluids, *Phys. Rev. E* 81, 046303 (2010).
- [6] Rafael M. Oliveira and J. A. Miranda, Fully nonlinear simulations of ferrofluid patterns in a radial magnetic field, *Phys. Rev. Fluids* 5, 124003 (2020).
- [7] Rafael M. Oliveira, I. M. Coutinho, P. H. A. Anjos and J. A. Miranda, Shape instabilities in confined ferrofluids under crossed magnetic fields, *Phys Rev. E*, 104, 065113 (2021).
- [8] T. Y. Hou, J. S. Lowengrub and M. J. Shelley, Removing the stiffness from interfacial flows with surface tension, *J. Comput. Phys.* 114, 312–338 (1994).

Using the Monte Carlo method to evaluate droplets interaction during spray cooling

Carlos Eduardo B. M. Rocha, Arthur V. S. Oliveira
São Carlos School of Engineering, University of São Paulo, São Carlos, Brazil

Email: carlosbmrocha@usp.br, avs.oliveira@usp.br

ABSTRACT

In this study, we used the Monte Carlo method to determine the droplet size and impact location to simulate spray cooling. The objective was to quantify how the volume flow rate and the droplet size affected droplet interactions, so we can identify the transition from disperse to intermediate spray, which can be useful when designing spray systems for several engineering applications.

INTRODUCTION

Spray applications in engineering are numerous (Liang & Mudawar, 2017), which motivated many droplet impact studies in the literature. However, sprays are much more complex than single droplets because interactions take place, which affects the hydrodynamics of droplet spreading and breakup, for example. As a consequence, if the surface is heated, the heat transfer is affected as well. In this study, we present the first results of using the Monte Carlo method to simulate multiple droplet impacts using global spray characteristics, like volume flow rate and droplet size.

METHOD

We used the Monte Carlo method (Rubinstein & Kroese, 2017) to guess the droplet size and impact location during spray cooling. We considered that the spray-generated droplets were uniformly distributed in size in the range $[D_{min}, D_{max}]$, all of them impacting the wall at the same velocity ($V_d = 2$ m/s), and also with a uniform probability of impacting a 30x30-mm² wall in any part of the surface. We considered water as the working fluid and a parabolic model for the droplet spreading and receding during impact (Breitenbach, Roisman, & Tropea, 2017), which is characteristic of the Leidenfrost regime. The number of droplets per second N that was generated by the Monte Carlo method was found respecting volume balance as follows:

$$N = 6Q / \pi \overline{D}^3 \quad (1)$$

where Q is volume flow rate, and D is the droplet mean diameter – which is the average between D_{min} and D_{max} because of the uniform distribution hypothesis. To evaluate the droplet interaction, we created a droplet interaction parameter I_d that considers the average number of droplets occupying all the wet areas of the surface. For example, an area where there is only one droplet's lamella is labeled as "1", while the areas where two or three droplets interact are respectively labeled as "2" and "3". Hence, I_d is the average label of the entire wet surface. Note that "0" is excluded, which means dry areas, so $I_d \geq 1$.

RESULTS

Figure 1a shows how I_d varies with the mean diameter, D , for different volume flow rates, Q , (0.1 to 5 l/min). In turn, Fig 1b shows an instant of the spray cooling simulation for $D = 500 \mu\text{m}$, $V_d = 2 \text{ m/s}$ and $Q = 1 \text{ l/min}$. At the instant represented in Fig. 1b, we have a maximum intersection of four droplets and $I_d = 1.228$. As expected, the I_d is elevated, on average, when we increased Q . For $Q = 5 \text{ l/min}$, I_d was virtually greater than 2, which means that for all the mean diameters simulated, we got that, on average, we have two or more droplets interacting with each other at a certain moment. For a small Q , we observed that the mean diameter, for the simulated range, I_d not have a strong influence on the I_d , but as we increase the Q the influence increase as well. With this higher influence, we can see an upward concave shape, which has a minimum point and increases when moving away in either direction from this point. On the one hand, the increment for lower diameters can be associated with the rapid growth of the number of droplets since N is proportional to $1/D^3$, which raises the probability of interactions. On the other hand, the increase in I_d for higher diameters is related to a larger spreading diameter when the droplet hit the wall.

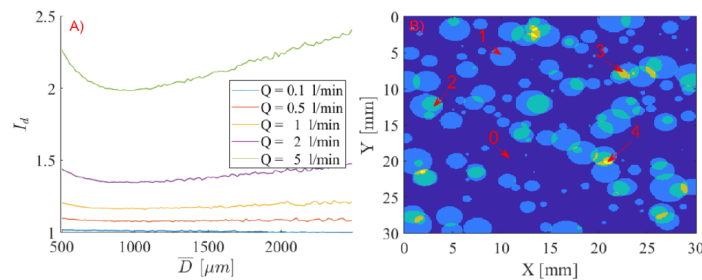


Figure 1: A) Interaction parameters as a function of the droplets mean diameter for different volume flow rates; B) Simulated wet areas for $\bar{D} = 500 \mu\text{m}$, $V_d = 2 \text{ m/s}$ and $Q = 1 \text{ l/min}$

CONCLUSIONS

This study shows that some spray parameters can have a direct impact on how the droplets interact with each other, in particular the volume flow rate and the mean diameter. In a spray with a small volume flow rate, which characterizes a dilute spray, it is possible to obtain very few interactions, and, with that, we can treat the spray as a combined action of multiple isolated drops, since the droplets do not interfere with the impact hydrodynamics of other droplets, thus simplifying the analysis of sprays problems. The size of the droplets also has importance in the analysis of the sprays problems if the spray works at a high volumetric flow, since, if the multiple droplets hypothesis will be utilized, is important to seek the optimal diameter, which minimizes the interaction of the droplets, so the hypothesis is more valid. For future works, it is possible to better refine the results by using a different distribution to the diameter. We used a constant distribution in these simulations, while a real spray usually produces droplets following a normal or log-normal distribution.

ACKNOWLEDGEMENT

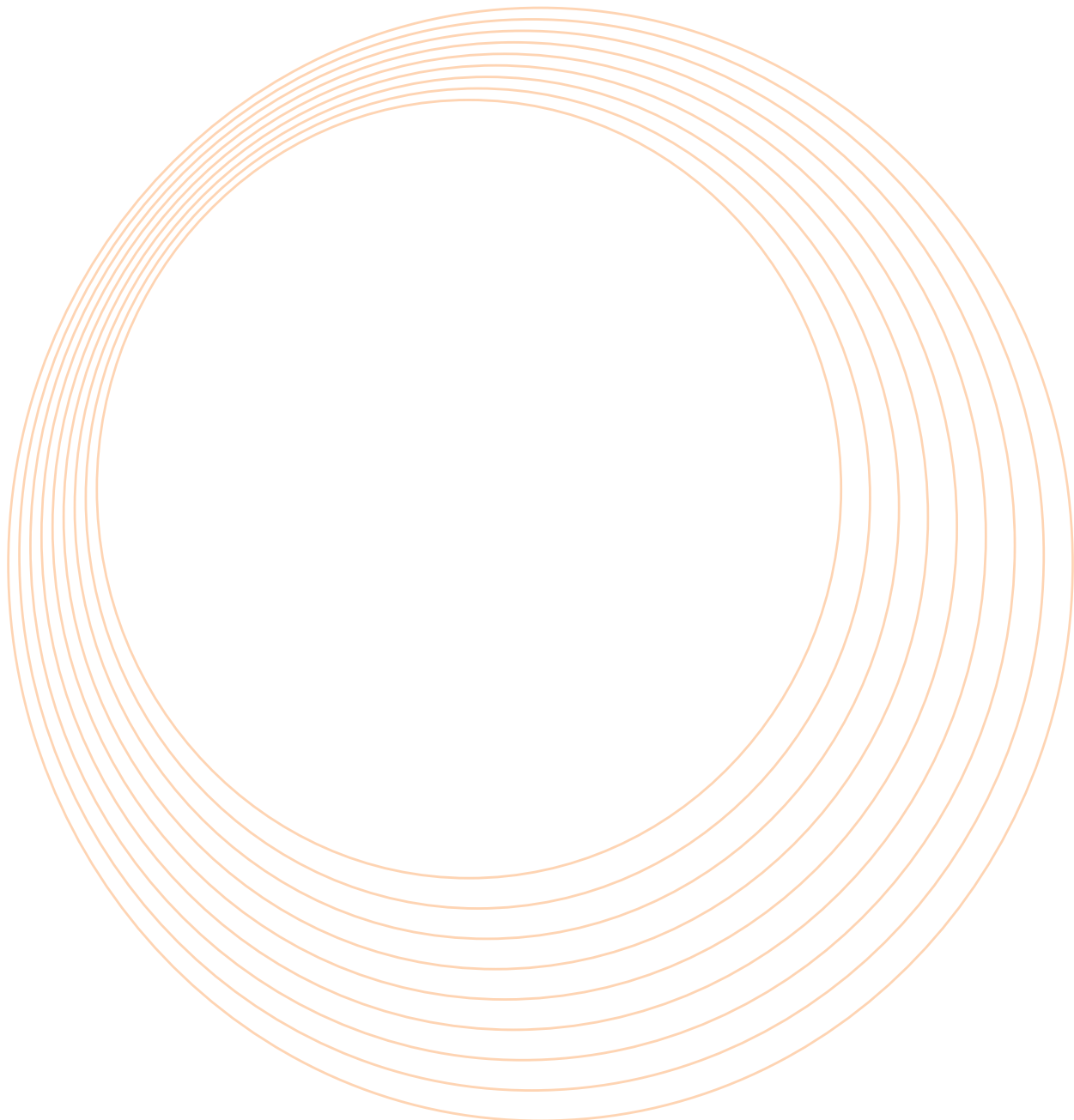
The authors gratefully acknowledge São Paulo Research Foundation (FAPESP) for the Young Investigator research grant (2021/01897-0) that supported this study.

REFERENCES

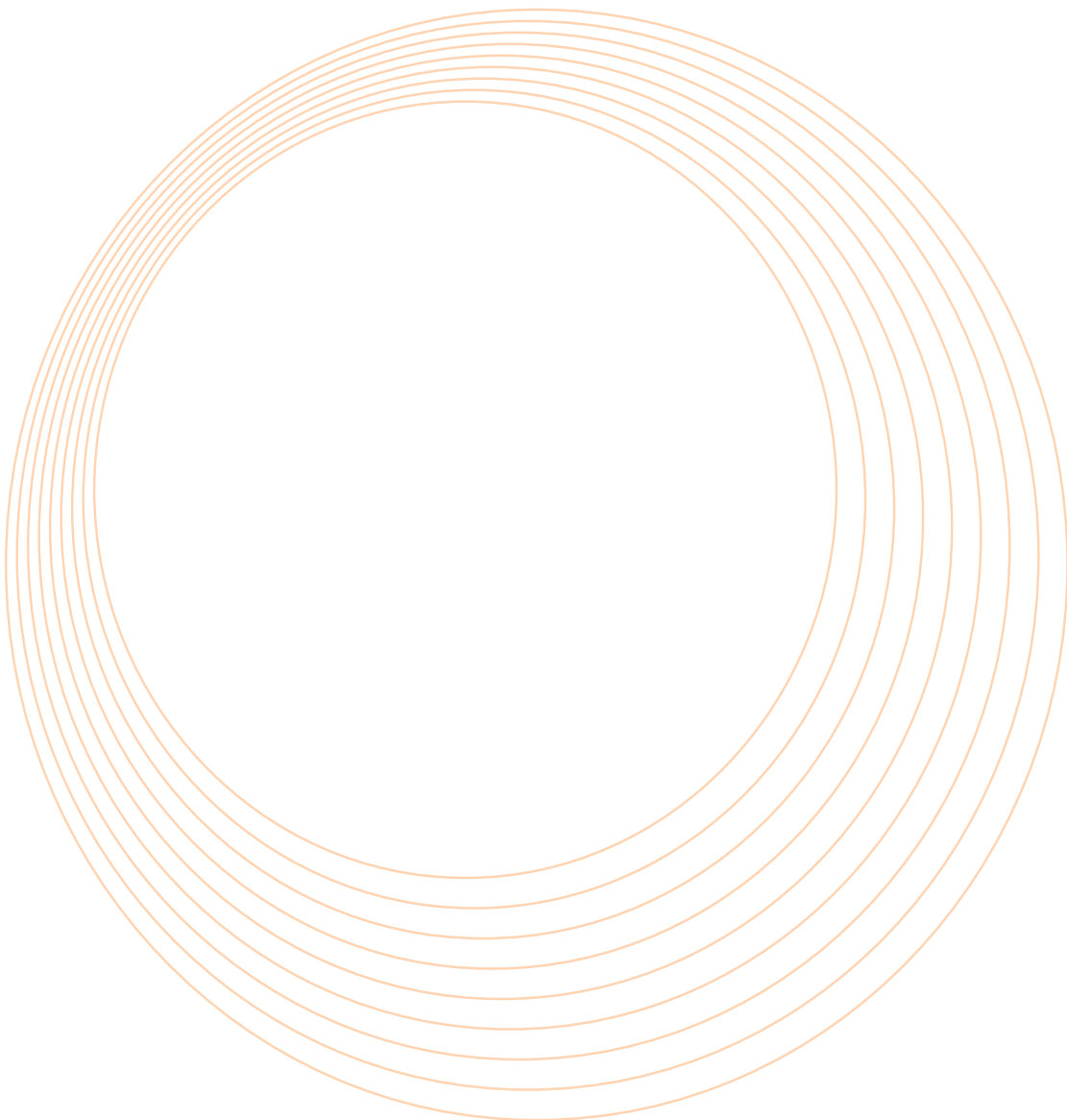
Breitenbach, J., Roisman, I. V., & Tropea, C. (2017). Heat transfer in the film boiling regime: Single drop impact and spray cooling. *International Journal of Heat and Mass Transfer*, 110, 34-42. doi: <https://doi.org/10.1016/j.ijheatmasstransfer.2017.03.004>.

Liang, G., & Mudawar, I. (2017). Review of spray cooling – part 1: Single-phase and nucleate boiling regimes, and critical heat flux. *International Journal of Heat and Mass Transfer*, 115, 1174-1205. doi: <https://doi.org/10.1016/j.ijheatmasstransfer.2017.06.029>.

Rubinstein, R. Y., & Kroese, D. P. (2017). *Simulation and the Monte Carlo method*. (Wiley, Ed.).



2 – Phase Change, Phase Flow Characterization



Assessment of flow boiling prediction methods for pressure drop and heat transfer coefficient under high temperature and pressure conditions

Daniel Borba Marchetto, Gherhardt Ribatski

Heat Transfer Research Group, São Carlos School of Engineering, University of São Paulo, 13566-590, São Carlos, Brazil

Email: daniel.marchetto@usp.br, ribatski@sc.usp.br

ABSTRACT

The reduced pressure increase considerably modifies the fluid thermophysical properties, especially in the vicinity of the critical point. As a consequence, the flow behavior during evaporation is highly affected, which can lead to possible loss of accuracy of prediction methods, generally, developed based on databases characterized by low reduced pressure fluids. Due to the growing interest in high temperature and pressure flow boiling applications, it is indispensable to verify if the prediction methods currently available in the literature are applicable for these conditions. In this context, the present paper presents a comparison between high pressure and temperature flow boiling data and prediction methods. The pressure drop database is composed by 1763 experimental results extracted from 16 studies from literature. None of the 21 evaluated methods was able to predict 70% of the pressure drop data within error bands of $\pm 30\%$.

Methods based on the homogeneous model presented the highest errors for $Pr < 0.1$, but were the most accurate at $Pr \geq 0.5$, which is justified by the slip velocity ratio reduction at high pressures. A heat transfer coefficient database composed by 6329 experimental results from 46 studies was also compiled in the present investigation. Considering the 30 prediction methods evaluated, none of them predicted more than 60% of the database within errors bands of $\pm 30\%$, and only 8 of them were able to predict more than 50% of the data with this accuracy. This was not only associated with limitations of the methods but also to strong divergences between the experimental data, and anomalous behaviors, specially at near critical pressures.

INTRODUCTION

Accurate predictions during flow boiling processes have been a recurring concern in both industry and academy. Despite the wide scope of application, in the past years most of the flow boiling studies were focused on refrigeration and air conditioning. As consequence, in general, the prediction methods currently available were developed or validated based on low saturation temperature (T_{sat}) and pressure (P_{sat}) experimental data. However, the interest in applications involving evaporation at high T_{sat} and P_{sat} has continuously grown in recent years. In order to meet current and future energy demands, and provide an efficient use of resources as well as a progressive replacement by renewable solutions, two approaches have been recurrently highlighted in the literature: organic Rankine cycles (ORCs) and high temperature heat pumps (HTHPs).

The fluid progressively approaches the critical point when the evaporation temperature and pressure increase. Increasing the reduced pressure (Pr) changes the thermophysical properties, affecting the two-phase flow characteristics and heat transfer mechanisms, and leading to a possible loss of accuracy of prediction methods. In this context, the present paper presents a comparison of experimental data for pressure drop (Δp) and heat transfer coefficient (HTC) during high T_{sat} and P_{sat} flow boiling against prediction methods.

METHODOLOGY

In our previous study [1], two databases composed of 1486 and 4753 experimental results from the literature were raised for pressure drop and HTC, respectively. Studies that reported data at $Pr \geq 0.5$ for any working fluid were considered. These databases were complemented in the present investigation with experimental results for organic refrigerants at $T_{sat} \geq 50^\circ\text{C}$, which corresponds to the experimental range of ORCs and HTHPs applications. Therefore, the new databases contain 1763 and 6329 experimental data.

Figure 1 presents the data distribution according to reduced pressure for both databases. It is important to remark that, the studies from which the experimental results were extracted, also reported data at low reduced pressures, which were included in the databases, in order to compare the accuracy of the prediction methods in both high and low Pr . Therefore, different from other studies, the present databases include data for all Pr ranges, representing operational conditions of several flow boiling applications: electronics cooling, ORCs, CO₂ trans-critical ORCs, HTHPs, water-cooled nuclear reactors, water circulating fluidized beds, refrigeration and air conditioning. It should also be highlighted that 352 ΔP and 1300 HTC data points correspond to low-global warming potential refrigerants, which have received special interest in recent years.

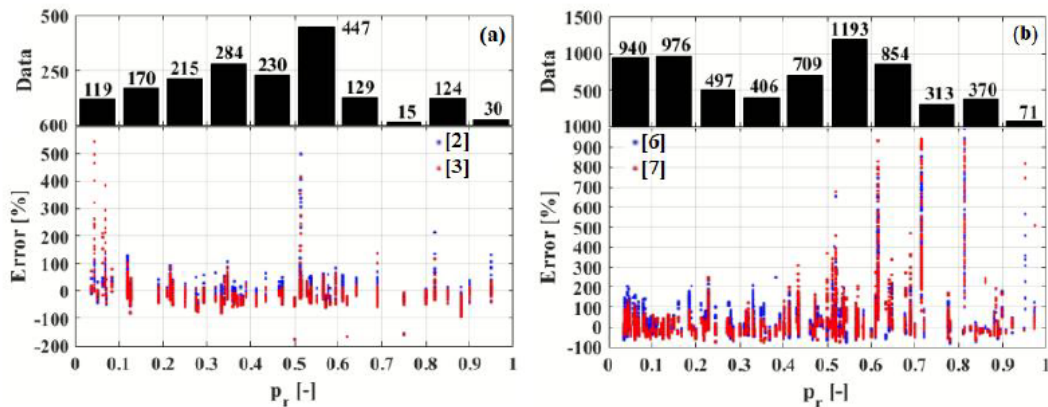


Figure 1: Data and error distribution against Pr .

RESULTS

Pressure drop data were compared against twenty one prediction methods, classified as: based on the homogeneous model, based on two-phase multipliers, and strictly empirical. Considering the entire database, the methods proposed by Müller-Steinhagen and Heck [2] and Kim and Mudawar [3] presented the lowest mean absolute errors (MAE), 28.1% and 28.4%, predicting 64.0% and 68.3% of the data within error bands of $\pm 30\%$, respectively.

Pressure drop data were compared against twenty one prediction methods, classified as: based on the homogeneous model, based on two-phase multipliers, and strictly empirical. Considering the entire database, the methods proposed by Müller-Steinhagen and Heck [2] and Kim and Mudawar [3] presented the lowest mean absolute errors (MAE), 28.1% and 28.4%, predicting 64.0% and 68.3% of the data within error bands of $\pm 30\%$, respectively.

Figure 1a presents the effect of the reduced pressure on the error achieved by the method of Müller-Steinhagen and Heck [2]. It should be highlighted that, although this method did not consider high pressure data in its development, no progressive loss of accuracy was verified with increasing Pr . The errors presented only aleatory variations with reduced pressure, with exception of the sharp increase close to $Pr=0.5$, which corresponds to the experimental data of Grauso et al. [4] for R410A at low mass velocity ($152 \text{ kg/m}^2\text{s}$). However, all the prediction methods evaluated presented errors higher than 100% for these data points.

Figure 1a also presents the error distribution against Pr for the method based on the homogeneous model proposed by Cicchitti et al. [5]. Strong deviations are verified at $Pr < 0.1$, but for the rest of the reduced pressure range, the errors are comparable to those of [2]. It is important to remark that all the 8 homogeneous-based methods evaluated presented lower MAEs for $Pr \geq 0.5$ than $Pr < 0.5$,

which is justified by the reduction of the slip velocity ratio at high reduced pressures. Considering the HTC data, none of the 30 prediction methods evaluated was able to predict the entire database with reasonable accuracy, which is not only associated with limitations of these methods, but also with divergences between the experimental results reported in the literature. Data obtained for independent studies at the same experimental conditions presented differences higher than 100%. In addition, unusual behaviors were also verified, such as HTC increases with reducing heat flux at near critical pressures.

The method proposed by Kanizawa et al. [6] predicted the largest parcel of the database within error bands of $\pm 30\%$, 57.7%, followed by the method of Liu and Winterton [7], which predicted 56.2% of the data with the same deviation range. The effect of the reduced pressure on the errors obtained by these methods is presented in Fig. 1b. The errors become higher with increasing Pr , with sharp increments for some specific datasets. Data at $Pr=0.99$ were excluded from Fig. 1b to improve visualization, since errors higher than 1000% were achieved, indicating that HTC prediction methods are not applicable near the critical point.

CONCLUSIONS

The results of the present study indicate that further improvements are still necessary to accurately predict pressure drop and HTC at high T_{sat} and P_{sat} . The best prediction methods evaluated were not able to predict 70% of the Δp data, and 60% of the HTC results. However, data at the experimental conditions evaluated in the present study are still scarce in the literature, and strong deviations between independent datasets are verified. Therefore, the development of new prediction methods should occur simultaneously with the advancement of experimental studies.

REFERENCES

- [1] Marchetto, D. B., Moreira, D. C., Revellin, R., Ribatski, G. A state-of-the-art review on flow boiling at high reduced pressures. *International Journal of Heat and Mass Transfer*, 193 (2022), 122951.
- [2] H. Müller-Steinhagen, K. Heck, A simple friction pressure drop correlation for two-phase flow in pipes, *Chem. Eng. Process.* 20 (1986) 297–308.
- [3] S.M. Kim, I Mudawar, Universal approach to predicting two-phase frictional pressure drop for mini/micro-channel saturated flow boiling, *Int. J. Heat Mass Transf.* 58 (2013) 718–734.
- [4] S. Grauso, R. Mastrullo, A.W. Mauro, G.P. Vanoli, Two-phase adiabatic frictional pressure gradients for R410A and CO₂ in a macro channel: Experiments and a simplified predictive method for annular flow from low to medium reduced pressures, *Exp. Therm Fluid Sci.* 52 (2014) 79–87.
- [5] A. Cicchitti, C. Lombardi, M. Silvestri, G. Soldaini, R. Zavattarelli, Two-phase cooling experiments—pressure drop, heat transfer and burnout measurements, *Energia Nucleare* 7 (1960) 407–425.
- [6] F.T. Kanizawa, C.B. Tibiriçá, G Ribatski, Heat transfer during convective boiling inside microchannels, *Int. J. Heat Mass Transf.* 93 (2016) 566–583.
- [7] Z. Liu, R.H.S. Winterton, A general correlation for saturated and subcooled flow boiling in tubes and annuli, based on a nucleate pool boiling equation, *Int. J. Heat Mass Transf.* 34 (1991) 2759–2766.

Flow boiling of R1336mzz(Z) in a copper microgap with tapered manifold

Debora C. Moreira¹, Valter S. Do Nascimento Jr.¹, Satish G. Kandlikar², Gherhardt Ribatski^{*}

¹Heat Transfer Research Group (HTRG), São Carlos School of Engineering (EESC), University of São Paulo (USP) Av. Trabalhador São-Carlense, 400, São Carlos-SP, 13.566-590, Brazil

²Thermal Analysis, Microfluidics, and Fuel Cells Laboratory (TA μ FL), Rochester Institute of Technology (RIT) Rochester, New York, 14623, USA

Email: ribatski@sc.usp.br

KEYWORDS

Cooling, Microchannel, low-GWP refrigerant, High-speed visualization, HFO

ABSTRACT

This work comprises an experimental investigation of flow boiling of the Hydro-fluoroolefin R1336mzz(Z) in a tapered microgap with diverging cross-section. Experiments were conducted for inlet mass fluxes varying from 400 to 1000 kg/m²s and the applied heat flux reached 46.1 W/cm², while the saturation temperature was set to 41 °C and the inlet temperature was 20 or 30 °C. A strong influence of the flow patterns observed with a high-speed camera in heat transfer and pressure drop could be verified, showing that nucleate boiling effects dominate heat transfer and fluid flow behaviors in this range of experimental conditions.

INTRODUCTION

Performance improvement of flow boiling in microchannel heat sinks has been continuously sought, with the proposition of diverse geometries and surface structuration and the use of diverse working fluids (Benam et al., 2021). It should be noted, however, that traditionally used refrigerants are frequently associated with negative environmental impacts, which motivated the substitution of these fluids by modern options with minimum global warming and ozone depleting potentials, but extensive investigation on the flow boiling behavior of these new fluids in microchannels heat sinks is still required to contribute to a thorough understanding of their boiling mechanisms (Lv et al., 2022). Recently, Marchetto and Ribatski (2020) evaluated the flow boiling heat transfer in microchannels-based polymeric heat sinks with inlet restrictors using R1336mzz(Z) as working fluid. In order to extend the ranges of heat flux and temperatures during the experiments, Moreira et al. (2021) analyzed the flow boiling behavior of the same fluid in a copper microchannel heat sink combined with an open tapered manifold proposed by Kandlikar et al. (2013). In the present study, the flow boiling behavior of R1336mzz(Z) in a plain copper surface combined to the previously used tapered manifold was experimentally evaluated, in order to produce benchmark data for future investigations with this relatively new fluid. Values of heat transfer coefficient and pressure drop are reported and their relations to the flow patterns observed with a high-speed camera are discussed.

EXPERIMENTAL FACILITY

Detailed information regarding the experimental apparatus that was used in the current experiments can be found in previous works (Marchetto and Ribatski, 2020; Moreira et al., 2021). Figure 1 illustrates the copper chip test section. Heat was provided to the test section by a copper block containing eight embedded cartridge heaters powered by a DC source. The heated footprint is a square with 10 mm x 10 mm, and polysulfone housing and cover served as manifold and defined the flow area. The cover was milled to create a gap with minimum height equal to 150 μ m and a taper corresponding to 6% of the gap length aligned to the heated footprint, so the gap height at the outlet was 750 μ m. An absolute pressure transducer indicated the pressure at the inlet of the test section, and a differential pressure transducer measured the pressure drop.

Two K-type thermocouples measured inlet and outlet fluid temperatures, and three K-type thermocouples were lodged in the copper chip below the heated surface, shown in Fig. 1 as T1, T2 and T3, which were used in wall temperature calculations.

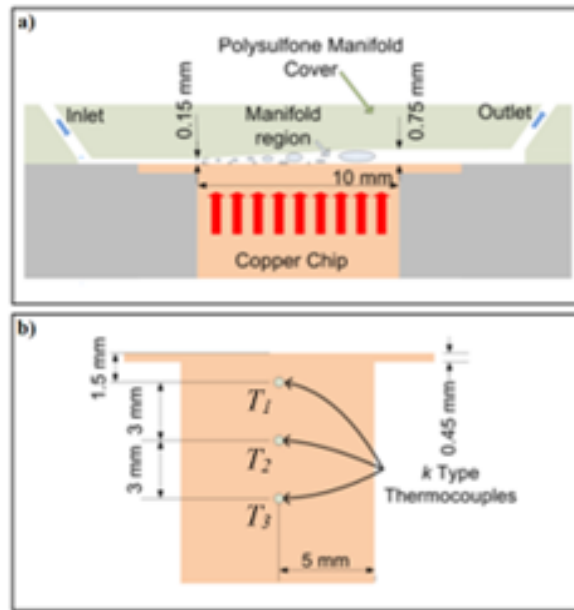


Figure 1: Schematics of the test section.

The input power applied to the cartridge heaters and the pump were controlled using LabView, which also provided the data acquisition. The saturation temperature of the working fluid R1336mzz(Z) was set to 41°C, and the experimental conditions are summarized in Tab. 1. Heat losses were estimated based on energy balances for single-phase experiments and extrapolated to flow boiling experiments, so the heat flux effectively transferred to the fluid could be calculated. The wall temperature was calculated considering one-dimensional heat conduction through the neck of the copper chip combined with the temperature measurements T1, T2 and T3.

Table 1: Experimental Conditions for flow boiling tests.

G_{in} (kg/m ² s)	ΔT_{sub} (°C)	q'' (W/cm ²)
400	20	10.5-45.6
600	20 / 10	13.6-46.1 / 11.0-44.7
800	20	14.5-45.1
1000	20	15.6-43.1

RESULTS AND CONCLUSIONS

Boiling curves and pressure drop from experiments at four mass fluxes and for an inlet subcooling (ΔT_{sub}) of 20°C are shown in Fig. 2. The critical heat flux was not reached during this experimental campaign, and the applied heat flux was limited by the maximum temperature of the cartridge heaters ($T_{max}=160^\circ\text{C}$).

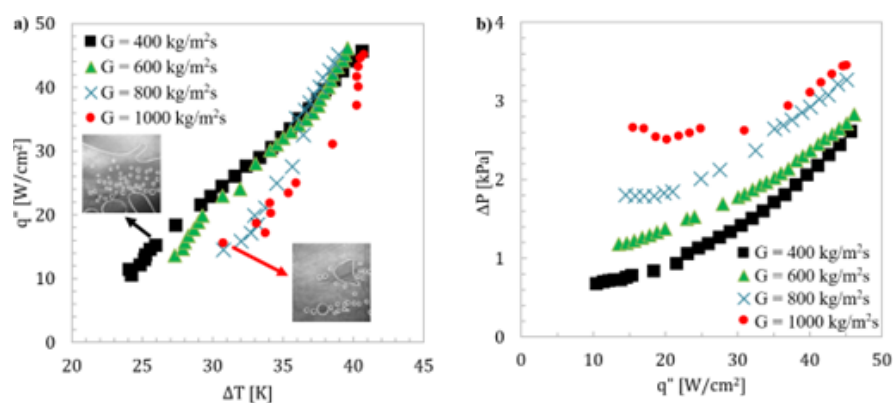


Figure 2: Boiling curve of R1336mzz(Z) (a) and pressure drop (b) as functions of heat flux for all experimental conditions.

It is possible to observe that for heat fluxes lower than 30 W/cm^2 , the wall superheat increases with the mass flux, which is directly related to the higher heat flux required to the onset of nucleate boiling and lower exit vapor qualities that are achieved at higher flow rates. As also seen in Fig. 2(a), the density of active nucleation sites decreases as the mass flux rises, which deteriorates nucleate boiling heat transfer and results in the increase of wall superheat, a behavior that is in accordance with that observed by Kalani and Kandlikar (2015). Based on the trends observed in Fig. 2(a), it can be speculated that under conditions of greater heat flux than those reached in the present experiments higher mass fluxes would correspond to lower wall superheats, resulting in higher values of HTC, as reported in our previous investigation (Moreira et al., 2021).

The increase in pressure drop with heat and mass fluxes seen in Fig. 2(b) can be attributed to variations in inertia forces and vapor quality, due to the variation of the effective density. Moreover, it is possible to notice a change in the slope of the pressure drop curve due to change in flow pattern. Nevertheless, it should be remarked that the reported values of pressure drop are low and do not imply in significant increase in the required pumping power nor in relevant variation of the saturation temperature along the microgap.

ACKNOWLEDGMENTS

The authors would like to acknowledge the financial support provided by FAPESP through the grants #2015/24834-3, #2016/09509-1, #2017/12576-5, and #2018/23538-0. The technical support provided by Rick Würzer and Craig Arnold from RIT's ME Department, and by José Roberto Bogni and Jorge Nicolau dos Santos from the Department of Mechanical Engineering at the São Carlos School of Engineering in the fabrication of the components of the experimental apparatus and instrumentation of the experimental setup is also recognized and deeply appreciated.

REFERENCES

- Benam, B. P., Sadaghiani, A. K., Yağcı, V., Parlak, M., Sefiane, K. and Koşar, A., 2021. Review on high heat flux flow boiling of refrigerants and water for electronics cooling. *International Journal of Heat and Mass Transfer*, 180, 121787.
- Kalani, A. and Kandlikar, S. G., 2015. Flow patterns and heat transfer mechanisms during flow boiling over open microchannels in tapered manifold (OMM). *International Journal of Heat and Mass Transfer*, 89, 494-504.
- Kandlikar, S. G., Widger, T., Kalani, A. and Mejia, V., 2013. Enhanced flow boiling over open microchannels with uniform and tapered gap manifolds. *Journal of heat transfer*, 135(6).
- Lv, H., Ma, H., Mao, N. and He, T., 2022. Boiling heat transfer mechanism of environmental-friendly refrigerants: A review. *International Journal of Refrigeration*, 133, 214-225.
- Marchetto, D. B. and Ribatski, G., 2020. An experimental study on flow boiling heat transfer of HFO1336mzz (Z) in microchannels-based polymeric heat sinks. *Applied Thermal Engineering*, 180, 115815.
- Moreira, D.C., Nascimento Jr, V.S., Ribatski, G. and Kandlikar, S.G. 2021. Flow Boiling of R1336mzz(Z) in Open Microchannels with Diverging Manifold". In 26th International Congress of Mechanical Engineering.

Nitrogen thin film evaporation applied to cryopreservation

Henrique Vidaletti, Álisson Stochero da Silva e Jacqueline Biancon Copetti

University of Vale do Rio dos Sinos, Mechanical Engineering Graduate Program, São Leopoldo, 93022-750, RS, Brazil

Jéferson Diehl de Oliveira

FSG - University Center, Center of Innovation and Technology, Caxias do Sul, 95020-472, RS, Brazil.

Elaine Maria Cardoso

UNESP - Faculdade de Engenharia de Ilha Solteira - Avenida Brasil, 56, 15385-000, Ilha Solteira, SP, Brazil

Leonardo Lachi Manetti

IFMS - Instituto Federal de Mato Grosso do Sul / Campus Campo Grande, Campo Grande - MS

ABSTRACT

Thin film evaporation is fundamental to many processes, including energy conversion, microelectronic cooling, boiling, transpiration, and others. The current work presents the application of nitrogen thin film evaporation for the cryopreservation of biological material (BM).

KEYWORDS

Cooling rate, Evaporation, Thin films, DMSO, Heat transfer.

INTRODUCTION

Cryopreservation has evolved as a technology for medical applications, such as therapy with stem cells, tissue engineering, assisted reproduction and gene therapy. This process allows for preserving the BM at low temperatures, usually between -80 and -196 °C, suppressing biological aging and maintaining viability. Freezing and storage are made through the contact of the material with cryogenic fluid and cryoprotective agents (CPA), minimizing the osmotic damage and preventing the formation of intra and extracellular ice crystals, reducing cryoinjuries.

In conventional protocols - with the sample immersion in liquid nitrogen (LN₂) or slow freezing, with gradual temperature reduction - the cooling rates are low and crystallization problems may appear. The vitrification of the sample with the direct transition from the liquid state to the vitrified and amorphous state is the alternative to achieve higher

cooling rates, but it requires a higher concentration of CPA. Thus, new vitrification technologies associating an increase in the cooling rate with small volumes of material and low CPA concentrations have been investigated in order to achieve appropriate conditions, reducing toxicity and injuries caused by ice crystals during the process (Li et al., 2019).

Methods like Cryoloop, Open Pulled Straw (OPS), Droplet Vitrification, and Electron Microscope Grids can achieve complete or partial vitrification of the samples, but it is necessary to use a high concentration of CPA. Some works have tested the nitrogen thin film evaporation process for vitrification and have achieved significant results regarding the freezing rate (Sait et al., 2009; Su et al., 2018). However, much remains to be improved regarding surface conditions for evaporation, sample volume, and preparation.

The heat transfer process in thin film evaporation can be analyzed regarding different regions and their associated thermal resistances (Plawsky et al., 2014). Such regions correspond to the adsorbed or non-evaporating thin film region; the transition region, where the attractive forces of the liquid on the solid are weak and the liquid-vapor interface has measurable curvature; and the meniscus region or bulk fluid, where the curvature of the liquid-vapor interface becomes almost constant, acting as a liquid reservoir for the transition region.

The thermal resistances associated with it are the conduction through the solid substrate; the conduction through the liquid, which is a linear function of the film thickness; and the heat transfer resistance at the liquid-vapor interface, which depends on the intermolecular forces and, therefore, on the film thickness, the liquid-vapor curvature and bulk vapor state.

The enhancement in phase change heat transfer is associated with maximizing the region where overall thermal resistance is reduced and minimizing the hydrodynamic resistances associated with the liquid flow into and vapor flow out of this region. Surface modification techniques, such as microstructured surfaces, have been used to control the transport processes in these films. The surface morphology can alter solid/liquid/vapor interactions, maximizing the region where phase change is most active. The microstructured surface increases the solid-liquid surface area, which may increase the capillary absorption (Liu et al., 2011) and nucleation sites, improving the phase change heat transfer (Maroo and Chung, 2013). Moreover, the wetting behavior may change, and consequently, the fluid flow processes may be altered.

Thus, this research aims to study the thin film evaporation phenomenon applied to the vitrification of a biological sample using a surface coated with metal foam to improve the phase change heat transfer.

EXPERIMENTAL FACILITY AND METHODOLOGY

In this study, an experimental apparatus consisting of a vacuum chamber and two nitrogen-containing cryocauteries was developed, as seen in Fig. 1a. The sample is stored in a PDMS device between two copper plates coated with nickel foam (Fig. 1c). This system is suspended inside the chamber (Fig. 1b), and, nitrogen jets (rates from 0.4 to 1.2 g/s) are applied to the porous surfaces promoting evaporation. The pressure inside the chamber and temperatures in the sample are recorded during the experiments. Tests were carried out using samples of DMSO, glycerol and sucrose in PBS (Phosphate-buffered saline) at different concentrations and volumes to evaluate the vitrification and cooling rates. Images and videos of the evaporation process were recorded with a Motion Pro Y4 camera.

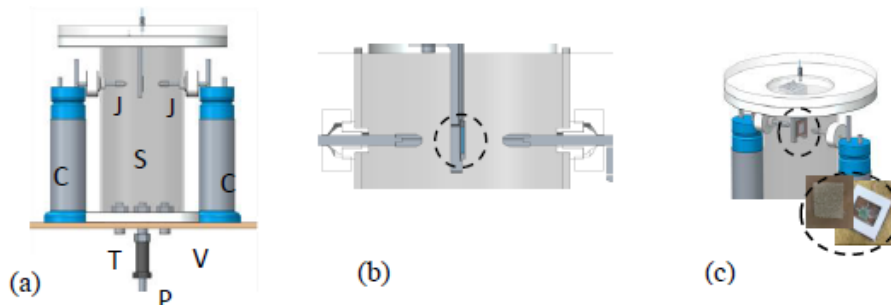


Figure 1 – (a) test bench: vacuum chamber, cryo-cauterics (C) with liquid nitrogen, injection nozzles (J), BM sample (S) and instrumentation: temperature (T), pressure (P), vacuum pump (V); (b) details of test section; (c) sample packaging in a PDMS device between two copper plates coated with Ni foam.

Table 1 shows the main characteristics of nickel metal foam in terms of porosity (ϵ), density (ρ), cell diameter (a), pore and fiber (d_p and d_f), respectively.

Table 1 – Characteristics of nickel metal foam (Manetti et al., 2020).

SEM image	Structure	ρ_{foam} (kg/m ³)	ϵ (%)	d_p (mm)	a (mm)	d_f (mm)
		138 ± 14.12	98.4 ± 0.15	0.25 ± 0.09	0.46 ± 0.10	0.07 ± 0.02

RESULTS AND CONCLUSIONS

Figure 2 presents images of the nitrogen jets on the porous surface at different instants of the phase change process, and Fig. 3 shows the cooling-freezing curve of the sample.

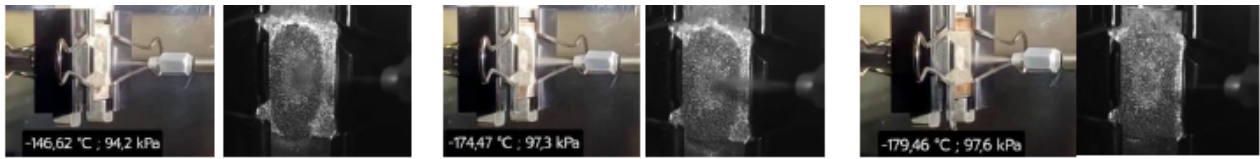


Figure 2 – Images of nitrogen film evaporation on metal foam.

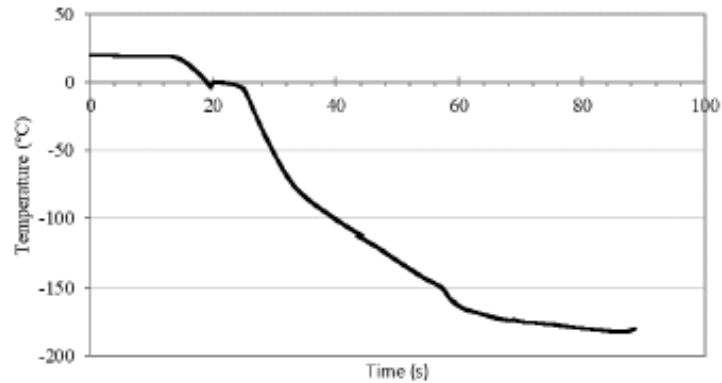


Figure 3 - Sample cooling and freezing curve.

The volume and concentration effects were evaluated, and it was found that lower volumes and higher concentrations allowed the vitrification of the samples. Moreover, it was found that the pre-cooling condition and pressure inside the chamber influenced the cooling rate. A 300 °C/min rate was obtained for larger volumes, about 30 μ l; however, the cooling rate tends to increase with a decrease in volume.

ACKNOWLEDGMENTS

The authors gratefully acknowledge the financial support of MCT/CNPq (Brazilian National Council of Research) under contract 403825/2021-0. The authors also acknowledge the grants provided by the agencies Capes and CNPq and the company HemoCord-Umbilical Cord Blood Bank for technical and material support.

REFERENCES

- Liu,W., Li,Y., Cai,Y., Sekulic,D.P. Capillary Rise of Liquids over a Microstructured Solid Surface, *Langmuir*, Vol. 27, pp. 14260–14266, 2011.
- Manetti,L.L, Ribatski, G., de Souza, R.R., Cardoso, E.M. Pool boiling heat transfer of HFE-7100 on metal foams, *Exper. Therm. Fluid Sci.* 113, 2020.
- Maroo S.C., Chung, J.N. A Possible Role of Nanostructured Ridges on Boiling Heat Transfer Enhancement, *Journal of Heat Transfer*, 041501, 2013.
- Plawsky, J.L.; Fedorov, A.G.; Garimella, S.V.; Ma, H.B.; Maroo, S.C.; Chen, L.; Nam, Y. Nano and microstructures for thin-film evaporation – A review. *Nanoscale and Microscale Thermophysical Engineering*. 18, 251–269, 2014.
- Su, F., Zhao, N., Deng, Y., and Ma, H.: An Ultrafast Vitrification Method for Cell Cryopreservation. *ASME. J. Heat Transfer*. 140, 012001, 2018.

Study of phase fraction distribution in horizontal gas/liquid flow via collimated gamma-ray densitometry

C.E. Alvarez-Pacheco, C.M. Ruiz-Diaz and O.M.H. Rodriguez

Industrial Multiphase Flow Laboratory (LEMI), Mechanical Engineering Department, São Carlos School of Engineering (EESC), University of São Paulo (USP), Av. Trab. São Carlense, 400 - Parque Arnold Schimidt, São Carlos - SP, 13566-590, Brazil.

Email: cristhianeap@usp.br, carlosruiz978@usp.br, oscarmhr@sc.usp.br

KEYWORDS

Gas-liquid flow, gamma-ray densitometry, chordal phase fraction distribution, phase fraction distribution.

ABSTRACT

Knowledge about the behavior of gas-liquid two-phase flow is essentially both in field development and in the oil and gas production process. Therefore, experiments for gas-dense/liquid two-phase flow will be developed in a horizontal steel pipe which has a length of 15 m and 2-inch-i.d diameter. Using mineral oil ($\rho = 867.2 \text{ kg/m}^3$ e $\mu = 22 \text{ cP}$) and sulfur hexafluoride (SF6) ($\rho = 100 \text{ kg/m}^3$ e $\mu = 1,617 \times 10^{-5} \text{ cP}$) at operating pressures of 15 Bar.

The characterization of flow patterns from the determination of the phase fraction distribution in the pipe is of great importance for the study of multiphase flow. Therefore, a high-speed camera will be implemented for this study, which will provide a detailed view of the flow pattern for validation purposes. In addition, a Cesium 137 (Cs137) gamma ray densitometer will be used together with a collimator that ensures good spatial sensitivity. A homemade mechanical displacement system that allows to automatically make a micrometric scan of the pipe cross-section is applied to obtain the phase fraction distribution data.

INTRODUCTION

The oil production process occurs in near-horizontal wells, where the fluids adopt different spatial configurations, known as flow patterns. For horizontal pipelines, gas-liquid flow patterns are composed of stratified, intermittent, annular, and dispersed flow patterns. In the petroleum industry, it is very common to have two-phase flows that occur throughout the production process, from the reservoir to the final product on the platform Amundsen (2011). These kinds of flows are classified into different flow patterns that depend directly on the pipe geometry (inclination and internal diameter), operating conditions (temperature, pressure, velocity and flow rate) and also on the physical properties of the fluids (viscosity, density and surface tension) Meng, W., Chen, X., Kouba, G., Sarica, C. & Brill, J. (2001).

To determine the phase fraction distribution in the different flow patterns, the technique of gamma ray densitometry (GRD) is used, which is a non-intrusive technique that emits ionizing radiation (which has sufficient energy to scrape electrons from atoms). Thus, work done by Elseth, G. (2001); Rodriguez, O.M.H. & Oliemans, R.V.A. (2006); Amundsen (2011) implement the gamma ray densitometry technique to determine the phase fraction in two-phase oil/water flow. Consequently, Shmueli, A. Unander, T. & Nydal, O. (2013, 2015); Vestøl, S., Kumara, W. A.S. & Melaaen, M.C. (2018) used the concept of gamma ray attenuation, making a chordal measurement from the top to the bottom of the tube and with the intensity data measured it was possible to determine the chordal phase fraction.

In this study, a micrometer scan along the pipe cross-section will be performed by implementing the non-intrusive collimated gamma ray densitometry technique to determine the phase fraction distribution in two-phase gas/liquid flows in a 15 m long, 2-inch-i.d. diameter horizontal pipe.

EXPERIMENTAL APPARATUS AND METHODS

The development of this study will be carried out in the experimental apparatus of LEMI (Industrial Multiphase Flow Laboratory) of the University of São Paulo (USP), campus São Carlos.

A 2-inch-i.d. U-shaped steel tubing, is 15 m long and has a length-to-diameter ratio (L/D) of 449 and 918. The system operates in a closed system. and it can operate with an inclination of -90° to 90° . The test section is composed of a bypass, quick closing valves, an acrylic visualization section, collimated gamma ray densitometry equipment, differential pressure sensor and local temperature and pressure sensors. In addition, the working fluids are turbine oil x-22 and dense gas (SF6). In Fig. 1 you can graphically see the test section.

The data of the phase fraction distribution in the SF6/Oil two-phase flow, obtained experimentally will be correlated using Eq. (1), which describes the absorption phenomenon of gamma radiation that is given by the attenuation law or also known as Lambert-Beers law, where the intensities emitted by the emitting source and I_0 and the transmission intensities measured by the receiver are I .

$$I = I_0 e^{-\gamma_1 X_1 - \gamma_2 X_2} \quad (1)$$

and

$$\gamma = \left(\frac{N_A}{A_M} \right) \rho \sigma \quad (2)$$

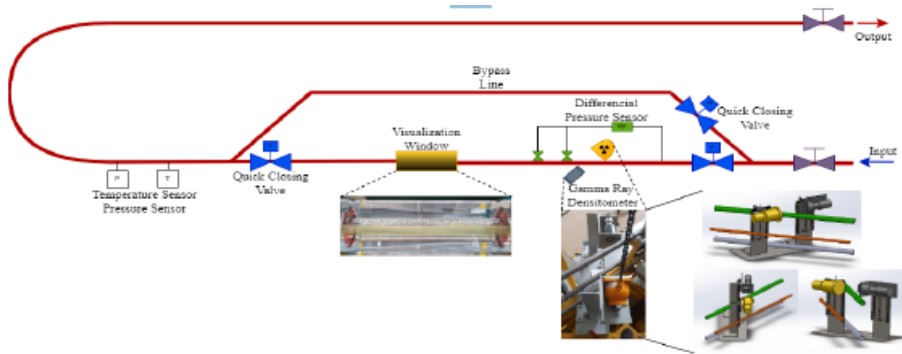


Figure 1: Schematic representation of the Dense-Gas (SF6)/Oil experimental setup.

where, X is defined as the thickness of the absorbing material [m], N_A is the Avogadro's number (6.022×10^{23}), A_M represents the atomic mass number of the material [kg/kmol] and σ is the atomic absorption section [kg/m³].

In addition, an expression can be obtained to determine the dense-gas fraction (SF6) (ϵ_g) from Eq (3) and also to obtain the Holdup (ϵ_l) as shown in Eq (4).

$$\epsilon_g = \frac{\ln(I/I_l)}{\ln(I_g/I_l)} \quad (3)$$

$$\epsilon_l = 1 - \epsilon_g \quad (4)$$

EXPECTED RESULTS

The expected results focus on the determination of phase distribution in gas-dense (SF6) and oil two-phase flow, with the implementation of the collimated gamma-ray densitometry technique.

CONCLUSION

Experiments will be performed to improve the knowledge in the gamma ray densitometry technique and to determine the distribution of the flow pattern in the pipe cross-section. The apparatus will provide new information for the study of the two-phase flow of oil and gas-dense (SF₆) and contribute to the development of improved phenomenological models.

REFERENCES

- Amundsen, L. An experimental study of oil-water flow in horizontal and inclined pipes. url:<http://hdl.handle.net/11250/231342>, pp. 309, (2011).
- Weng et al. Experimental Study of Low-Liquid-Loading Gas-Liquid Flow in Near-Horizontal Pipes. DOI: [//doi.org/10.2118/74687-PA](https://doi.org/10.2118/74687-PA), pp. 240–249 (2001).
- Elseth, G. An Experimental Study of Oil / Water Flow in Horizontal Pipes, pages = 270, url:<http://hdl.handle.net/11250/231212>, (2001).
- Rodriguez, O.M.H. & Oliemans, R.V.A. Experimental study on oil-water flow in horizontal and slightly inclined pipes, Vol. 32, DOI: 10.1016/j.ijmultiphaseflow.2005.11.001, (2006).
- Shmueli, A. Unander, T. & Nydal, O. liquid droplet entrainment in horizontal three-phase flow, pp. 1–6, (2013).
- Shmueli, A. Unander, T. & Nydal, O. Characteristics of gas/Water/Viscous oil in stratified-Annular horizontal pipe flows, DOI: 0.4043/26176-ms, isbn: 9781510814929, (2015).
- Vestøl, S., Kumara,W.A.S. & Melaaen, M.C. Gamma densitometry measurements of gas/ liquid flow with low liquid fractions in horizontal and inclined pipes, DOI: 10.2495/CMEM-V6-N1-120-131, isbn: 20460554, (2018).

A machine learning approach on two-phase flow characterization and calculation based on a large experimental dataset

Faller, A. C., Paulo, P. H. C., Vieira, S. C., Fabro, A. T., Castro, M.S.

Email: faller@petrobras.com.br, pedro.cardosopaulo@petrobras.com.br, saonvieira@petrobras.com.br, fabro@unb.br, mscastro@unicamp.br

INTRODUCTION

Two-phase flow calculations for pressure gradient and void fraction and flow pattern characterization are performed using empirical correlations or mechanistic modelling. We offer a machine learning data-driven approach to obtain such correlations. Our work is built upon a proprietary experimental dataset containing approximately 22k experimental data points featuring the fluid velocities: liquid and gas superficial velocities (v_{SL} , v_{SG}); the fluid properties: liquid and gas densities (ρ_L , ρ_G), liquid and gas viscosities (μ_L , μ_G) and the interfacial tension (σ_I); the pipe section geometry: roughness (ϵ), diameter (D) and inclination (θ); and the observed parameters: pressure gradient (dP/dL), void fraction (α) and flow pattern (dispersed, intermittent, annular or stratified). The goal is to obtain black box models that take the fluid properties and the geometry data as inputs and predict the pressure gradient, the void fraction, and the flow pattern.

METHOD

To obtain regressors for the continuous outputs (pressure gradient and void fraction) and classifiers for the discrete output (flow pattern), we used the following scikit-learn supervised learning algorithms: K-Nearest-Neighbors (KNN), Logistic Regression (LR), Decision Tree (DT), Random Forest (RF), Support Vector Machine (SVM), AdaBoost (AB), Gradient Boosting (GB) and Multi-Layer-Perceptron (MLP). The train/test split is 80%/20% and stratified. The regressors are evaluated with the fitness (R^2) score and the classifiers with the F1 score.

As input features to the models, besides the dimensional features contained in the dataset, we tested combinations with sets of dimensionless and augmented features, both inspired in dimensionless numbers used by empirical and mechanistic modeling techniques found in literature. Some of the dimensionless features used include: no-slip holdup (λ), relative roughness (ϵ/D), dimensionless pressure gradient (G), liquid and gas velocity numbers (N_{LV} and N_{GV}), liquid and gas viscosity numbers (N_L and N_G), diameter number (N_D), mixture Reynolds number Re_M , mixture, liquid and gas Froude number ($1/Fr_M$, $1/Fr_L$ and $1/Fr_G$) and several others. The augmented features combine the dimensionless ones and include $G \log \lambda$, $\lambda^2 \log Re_M$, $\sqrt{Fr_L} \log N_L$, $\cos^2 \lambda^2$, and so on. As part of the feature engineering process, all the features are ranked according to the impurity-based feature importance after fitting a Random Forest model.

RESULTS

Despite the dataset being large, it is somewhat biased towards the experiments' characteristics, which were performed mostly (more than 50%) on horizontal or near horizontal pipes, with fluids such as water, oil, kerosene, glycerol, air, among others. This bias is noticeable when a Random Forest model is fitted only with the dimensional input features (superficial velocities, fluid properties and pipe geometry) and the impurity-based feature importance reveals that the fluid properties have nearly zero importance, compared to the superficial velocities. This shows that a model trained only with these dimensional features won't be able to represent any physics related to the two-phase flow, which is in fact dependent of the fluid properties. Repeating the feature importance analysis, but with the dimensionless features set, though some other characteristics start to become relevant, the most

important features are still highly dependent on the superficial velocities, which are: no-slip holdup (λ), dimensionless pressure gradient (G) and liquid velocity number (N_{LV}). With the augmented features set, the feature importance analysis also showed that the most important ones are also related to the superficial velocities: $G \log \lambda$, mixture Reynolds number (Re_M) and $N_{LV} \log N_D$. However, the addition of such dimensionless and augmented features should increase the model's generalization capability, as they convey some physical meaning into the model.

Figure 1 shows the F1-score comparison between the beforementioned machine learning algorithms with each feature set as inputs, for the flow pattern classification. The best performers are the tree-based ones (DT, RF and GB). However, GB shows less degradation when evaluating the test dataset, because it is more robust and less susceptible to overfitting. Therefore, this model was selected for further analysis and hyperparameter optimization.

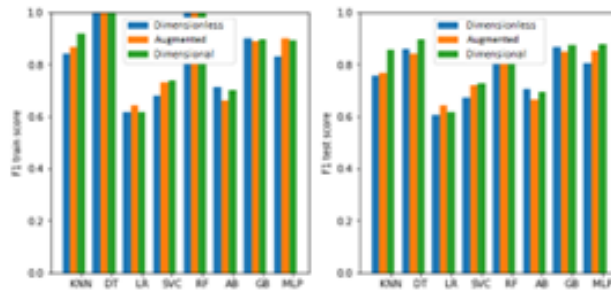


Figure 1 - Machine learning algorithms comparison

Evaluating the Gradient Boosting model with all the input sets combinations and tweaking hyperparameters (such as limiting the trees depth and increasing the minimum samples per leaf) to increase the generalization power, the best feature sets and results found for each output are: **Void fraction (α)**: only the dimensional inputs are enough to obtain a good fitness ($R^2_{train} = R^2_{test} = 0.99$, and $R^2_{xval} \in [0.98, 0.99]$). **Pressure gradient (dP/dL)**: the best fitness was found with the union of the dimensional and the dimensionless features sets ($R^2_{train} = 1.0$, $R^2_{test} = 0.98$ and $R^2_{xval} \in [0.85, 0.99]$). **Flow pattern**: the best F1-score is also obtained with the union of the dimensional and the dimensionless features sets ($F1_{train} = 1.0$, $F1_{test} = 0.93$ and $F1_{xval} \in [0.93, 0.94]$). Figure 2 show the results for all the models. In (a), (b) and (c), the good fitness for the void fraction and pressure gradient can be visualized. In (d), the model's generated flow pattern map resembles to the one generated by Barnea's method in (e).

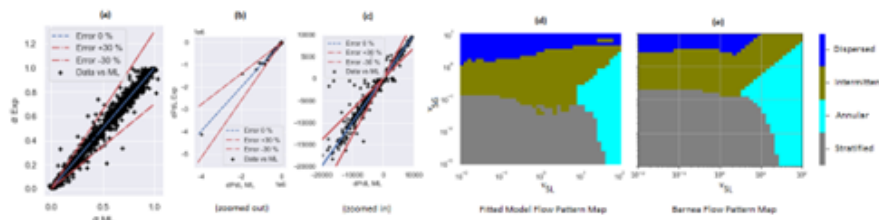
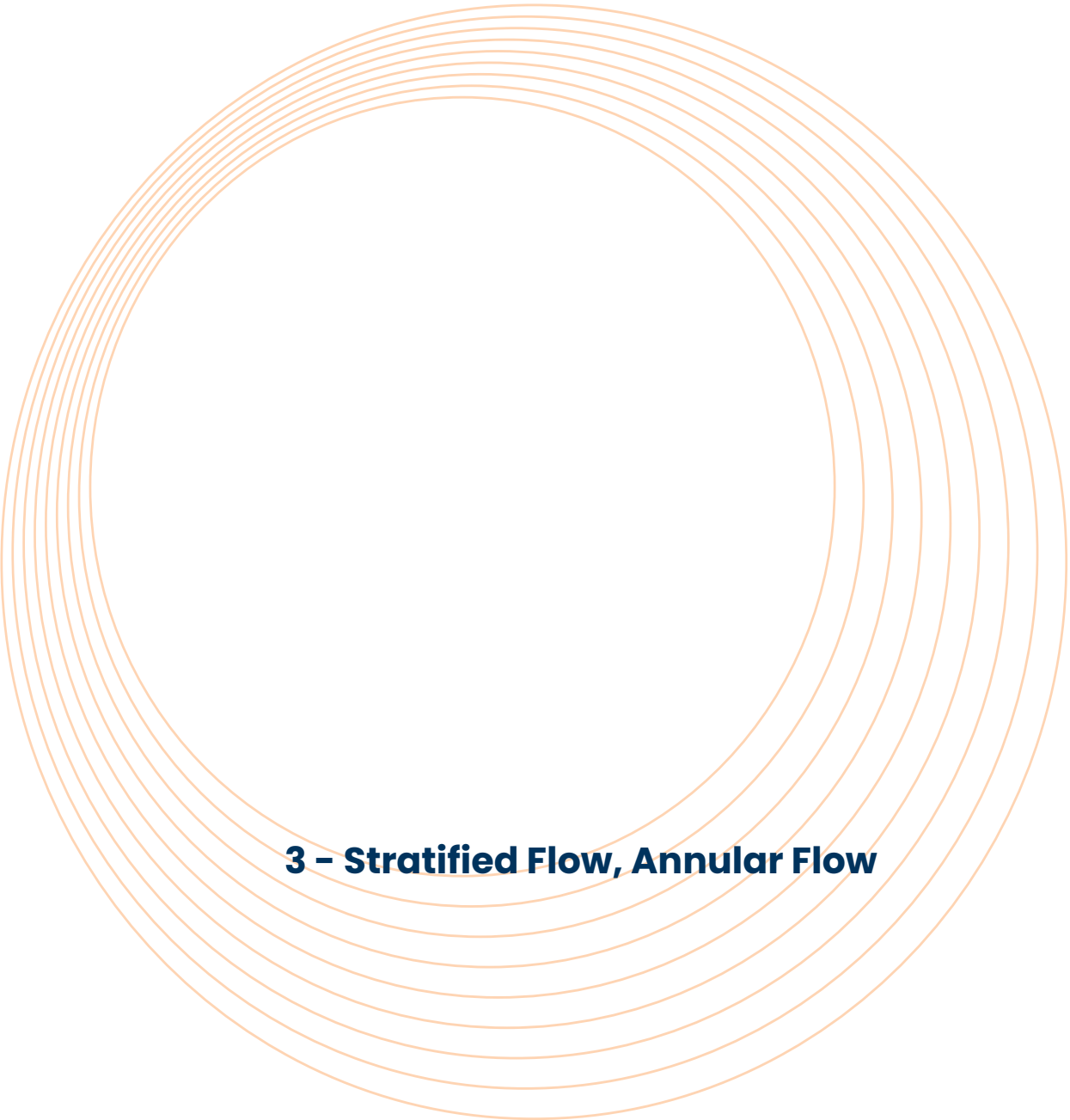


Figure 2 - Results: (a) Void Fraction; (b) Pressure Gradient; (c) Zoomed in Pressure Gradient; (d) Model's Flow Pattern Map; (e) Barnea's Flow Pattern Map.

CONCLUSION

The presented machine learning approach yields robust models that can accurately predict the void fraction, the pressure gradient, and the flow pattern in two-phase flow, within the dataset parameters range. It is not expected that the models can extrapolate to different pipe diameters and fluid properties, due to the lack of physics knowledge embedded in the model, which is limited to the engineered features, that improve generalization and robustness, but won't grant extrapolation capabilities.



3 - Stratified Flow, Annular Flow

Study on hydrodynamic stability of stratified liquid-liquid flow using optical techniques

P. J. Miranda-Lugo¹, Jorge E. Arrollo-Caballero¹, and O. M. H. Rodriguez¹

¹ University of São Paulo (USP), São Carlos School of Engineering (EESC), Mechanical Engineering Department, Industrial Multiphase Flow

Laboratory (LEMI), Av. Trab. São Carlense, 400 - Parque Arnold Schmidt, São Carlos - SP, 13566-590, Brazil.

Email: pjosemiranda@usp.br, jorgearrollo@usp.br, oscarmhr@sc.usp.br

ABSTRACT

The stratified liquid-liquid flow is still an open research subject due to its stability in specific operational conditions. This study aims to evaluate the hydrodynamic stability of a horizontal stratified oil-water pipe flow experimentally via Particle Image Velocimetry (PIV) and Planar Laser-Induced Fluorescence (PLIF). Velocity profiles and interface curvature radii at the pipe's lateral and cross-sections are measured. One expects that the larger the cross-section curvature of the interface, the stronger the influence of capillary instability and secondary flow on the stratified flow pattern transition.

KEYWORDS

Capillary instability, flow-pattern transition, oil-water flow, secondary flow, velocity contours.

INTRODUCTION

The study of the hydrodynamic stability of stratified flow considers the effect of several flow parameters that generate instabilities. Different theories on the stratified flow transition are found in the literature. One attributes such transition to instabilities resulting from the temporal amplification of a disturbance wave at the interface between the phases. Rodriguez and Castro (2014) suggested that for high-viscosity ratio stratified flow, the interface's cross-section curvature is related to capillary instability, which can be relevant at high water volumetric fractions. Eddy structures associated with secondary flows may be another destabilizing factor. However, no experimental study quantifies those effects upon the transition of stratified flow. We study the effects of the interface's cross-section curvature and secondary flow on the instability of a stratified oil-water pipe flow via 2-D PIV-PLIF.

EXPERIMENTAL SETUP

Figure 1 depicts a schematic view of the new test facility designed to study the dynamics of stratified liquid-liquid flows. It is composed by two independent supply lines, one for water and another for oil, and two test sections (G and O) made of borosilicate-glass pipes with lengths (L_p) of 4.5 and 7.5 m and internal diameters (i.d.) of 9.7 and 20.5 mm, respectively. The fluid distribution system is driven by pumping from water and oil reservoirs (A and I). The liquids are injected into the test section through flow straighteners (D, E, L, and M) and specially designed inlet sections (F and N). Both flow lines have an array of liquid flowmeters (1, 2, 4, 5), thermocouples (3, 6, 7, 8), and differential/gauge pressure transducers (9, 10, 11).

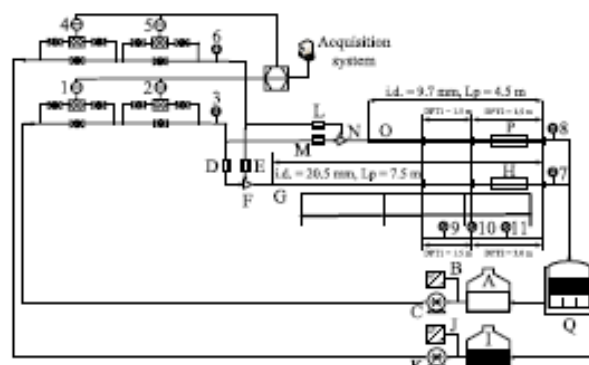


Figure 1: Schematic representation of the new liquid-liquid test facility at LEMI.

RESULTS

An image of the longitudinal view of the interface is presented in Fig. 2 (left). A homemade image-scanning routine is applied to define the liquid-liquid interface. Once the latter is identified, one can locate the interface's maximum and minimal local points. The curvatures that contain the minimal local points are used to fit circles through the least-squares method, Fig. 2 (center). On the other hand, a mapping technique is used to correct the distorted original images collected at -35° from the horizontal in a pipe's cross-section plane. The technique uses a calibration pattern and a polynomial function to correct distorted images. Once the original images are corrected, the scanning algorithm identifies the oil-water interface and fits a circle to it through the least-squares method, Fig. 2 (right). The interface's curvature radii R_1 and R_2 are determined by a probability density function of the circles' sizes.

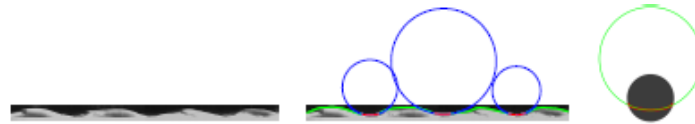


Figure 2: Image processing to determine the curvature radii of the liquid-liquid interface. Original image obtained via PLIF (left). Circle fitting to determine the longitudinal curvature radius R_1 (center) and cross-section curvature radius R_2 (right).

One can see in Fig. 3 the velocity field at the longitudinal and cross-section planes for a stratified oil-water flow. The mean axial and radial velocities, streamwise and normal velocity fluctuations, and Reynolds stress are represented. It can be noticed a parabolic trend in the oil phase's mean axial velocity profile (u_{mean}) with a maximum velocity near the pipe center once the oil phase flows in the laminar regime. At the same time, the water phase velocity profile is relatively flat, which resembles a turbulent velocity profile. The mean vertical velocity profile (v_{mean}) indicates that water and oil flow downwards and upwards from the liquid-liquid interface, respectively. This suggests the presence of secondary flow. Axial velocity fluctuations peaks are observed in regions close to the pipe wall and the liquid-liquid interface. One can notice that the water phase has greater axial velocity fluctuation (u_{rms}) than the oil phase due to turbulent effects in the water's flow. The vertical fluctuations (v_{rms}) for both phases are quite reduced toward zero. The maximum Reynolds stress (τ) is observed in the water phase near the pipe wall.

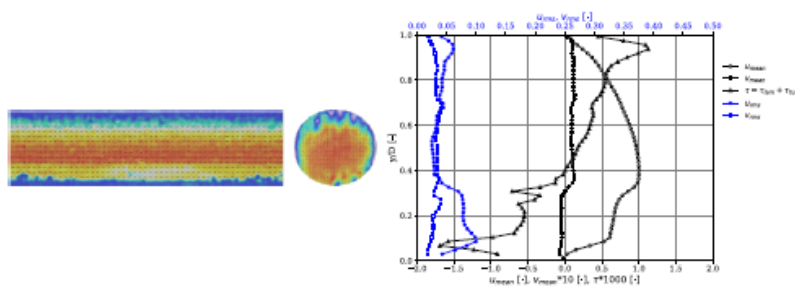


Figure 3: Longitudinal and cross-section field velocities of a horizontal stratified oil-water flow via the PIV technique. Mean axial and vertical velocity profiles and turbulence statistics. $J_m = 0.20$ m/s and $C_w = 0.32$, $Re_w = 2,611$ and $Re_o = 1,758$. Eötvös number of 4.2.

CONCLUSION

The effect of capillary instability on the transition of the stratified liquid-liquid flow is studied experimentally using the 2-D PIV-PLIF techniques. The aim is to quantify the destabilizing effect of the interfacial-tension term and the secondary flow. One can expect that the larger the interface's cross-section curvature, the stronger their effect are.

REFERENCES

Rodriguez, O.M. and Castro, M.S. Interfacial-tension-force model for the wavy-stratified liquid-liquid flow pattern transition. *Int. J. Multiphase Flow*, Vol. 58, pp. 114–126 (2014).

Analysis of the wave characteristics for stratified-wavy flow during in-tube convective condensation

Neumeister, R. F.¹, Kohlmann, A. L. G.¹, Moreira, T. A.² and Ribatski, G.^{1*}

¹Heat Transfer Research Group, São Carlos School of Engineering, University of São Paulo.

²Department of Mechanical Engineering, University of Wisconsin Madison, Madison, USA.

ABSTRACT

Stratified wavy flows present distinct wave patterns according to the duct geometry and flow parameters. The study of wave characteristics is important to determine the flow pattern transition mechanisms and identify their nature. The study of waves during condensation and evaporation is not as explored as waves in non phase change two phase flows. Focusing on filling this gap in the literature, the present study concerns an experimental analysis of the wave patterns and their main frequencies for stratified flow conditions during condensation, including purely stratified flows and intermittent flows characterized by long flow lengths of stratified wavy flow followed by short liquid plugs. Convective condensation experiments were performed for R600a, R1270, R290, and R134a in a horizontal tube with a 9.43 mm internal diameter. Data were obtained for the wave characterization from flow images recorded for mass velocities from 50 to 200 kg/m²s and a saturation temperature of 35°C. The wave frequencies were determined by applying Fast Fourier Transform (FFT) and the wave patterns are classified based on the wave shape and height. The results showed that the wave patterns can be classified as 3D waves, for low liquid superficial velocities, and disturbance waves which appear as the two phase velocity increases. The main wave frequencies were observed between 9Hz and 31Hz, reducing their value for high mass velocities. The Strouhal number decreased as the Lockhart Martinelli parameter increased.

KEYWORDS

Stratified flow, condensation, disturbance waves, wave patterns, flow patterns.

INTRODUCTION

The stratified wavy flow is characterized by the segregation of the liquid and gas phases by a wavy interface, with the liquid flowing in the bottom of the tube and the gas in its upper part. Moreover, it can be considered a transitional flow pattern between stratified and intermittent flows. In this sense, characteristics of the waves such as amplitude, frequency, slope, and velocity are associated with the flow pattern transition promoted by the wave crest achieving the top region of the tube wall. The frequency, wave amplitude, and wavelength can be used to characterize the flow and identify features that can lead to the transition.

The wave patterns were classified into four types by Chen et al. (1997), based on the wave's characteristics: 2D waves, 3D waves, roll waves, and entrained droplet flow. The 3D waves are characterized by some liquid climbing up the pipe wall due to the wave spreading effect, and a curvature occurs at the interface near the pipe wall. The roll waves, also defined as disturbance waves (Bae et al. 2017), present more liquid climbing up the pipe wall compared to 3D waves, and significant concave down curvature occurs at the gas liquid interface. The analysis of void fraction, liquid film height, and wetted wall perimeter was investigated by Aydin et al. (2015) and they observed the decrease of these parameters with the increase in the superficial gas velocity. In their study, interface height fluctuations occurring at a frequency range of 10 Hz < f < 40 Hz were observed independent of the experimental condition. At low superficial gas velocities, the disturbance wave topology is stretched toward the sides of the pipe. Moreover, an increase in the gas flow rate showed,

in the wave topology analysis, the occurrence of oscillations in phase at different locations. Wave frequency, height, velocity, and slope were also experimentally investigated by Bae et al. (2017) in a rectangular channel. They found that the frequency, height, and slope of the interfacial waves do not present clear tendencies with varying gas and liquid Reynolds numbers, however, these dimensionless parameters affect the waves' coalescence and their breakup.

Another aspect studied in the literature that has been the focus of several researchers in this field is the void fraction due to its impact on pressure drop, heat transfer, and refrigerant inventory. Therefore, several models for its predictions were developed over the years (Thome et al., 2003), but improvements in models for specific flow patterns remain necessary. Concerning hydrocarbons, the main focus of the present study, Milkie et al. (2016) presented flow regimes and void fractions results during convective condensation of propane and proposed a new model to predict void fractions for stratified wavy and annular flows.

In this context, the main goal of the present study is to identify the wave patterns and main frequencies of stratified wavy flows during condensation by analyzing interface liquid height temporal signals obtained from flow images.

METHOD

The experimental tests presented in this study were performed in an apparatus available at the Heat Transfer Research Group (HTRG) at EESC USP. The experimental setup is detailed in Moreira et al. (2021) suggested here for further details. The flow images were acquired at a transparent borosilicate glass tube, 140 mm long, positioned downstream of the section responsible for condensing the test fluid and establishing the thermodynamic state of the refrigerant at the visualization section. The inner diameters of the test section and the glass tube were 9.43 mm.

During the experimental procedure, the mass velocity was varied corresponding to liquid Reynolds number from 1,656 to 19,011 and the vapor quality at the visualization section from 0.12 to 0.67. The images of the flow were acquired at the visualization section through a high speed video camera at a full resolution of 24 megapixels and 25000 fps with an exposure time of 1/4000 s (NIKON D5200).

The analysis of the flow image was composed by the following steps: image binarization, interface identification, recording the pixel height of the interface for predefined positions, and conversion of the distances given in the number of pixels to the metric unit (millimeters) using the tube diameter as a reference. The identification of the pixel corresponding to the interface was performed using the binarized image, considering the interface as the pixel at which the color of the image changes from white to black using a code developed in Matlab (2022), this conversion generates an interface height over time.

The frequency analysis was executed by applying an FFT to the liquid height signal evaluated at a fixed position for the acquired images. The Strouhal number is presented versus the Lockhart Martinelli parameter for all the tested conditions, and the results are compared with the model proposed by Bae et al. (2017) developed to predict the frequency of interfacial oscillation for stratified wavy flow. The uncertainties of the measurements were 0.1 mm for the interface liquid height and 18% for the wave frequency.

RESULTS AND DISCUSSIONS

Figure 1 a) show a map characterizing the wave patterns. In this map, the transition straight line was defined based on the wave characteristics of the data obtained in the present study using the wave classification proposed by Chen et al. (1997) and Bae et al. (2017).

According to this figure, 3D waves (markers not filled) occur under conditions of low liquid superficial velocities. Besides, the presence of disturbance waves (markers filled) is associated with the transition to intermittent flow. 3D waves were observed almost only for purely's stratified flows. Disturbance waves were observed in the intermittent flows characterized by long flow lengths of stratified-wavy flow.

Figure 1b) shows the Strouhal Number obtained from the main frequencies in the liquid height time series. The dominant frequencies remain between 9Hz and 31Hz for the tested conditions, these results agree with the observation of Aydin et al. (2015). The analysis of the FFT revealed more than one frequency with a relevant level of energy.

Two K-type thermocouples measured inlet and outlet fluid temperatures, and three K-type thermocouples were lodged in the copper chip below the heated surface, shown in Fig. 1 as T1, T2 and T3, which were used in wall temperature calculations.

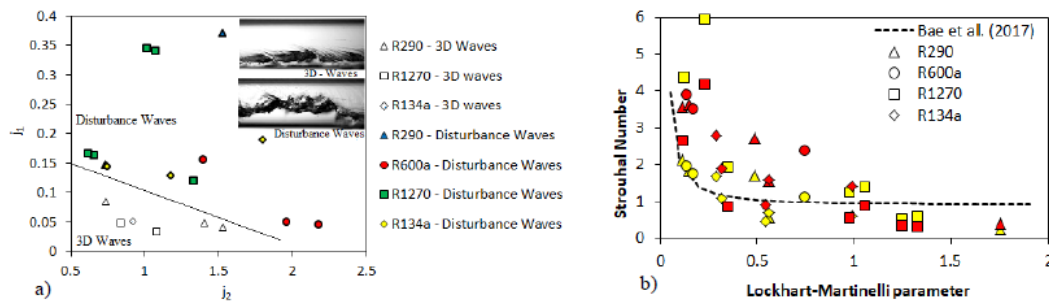


Figure 1. a) Wave patterns map – markers not filled represent 3D waves and markers filled represent disturbance waves. b) Strouhal number versus Lockhart-Martinelli parameter from experimental data – yellow markers represent the lower frequency with high energy in the FFT and red markers represent the second frequency with high energy in the FFT.

CONCLUSION

The results reveal the following wave patterns: 3D waves under low superficial velocity conditions; and disturbance waves under high superficial velocity conditions. The main wave frequencies are observed between 9 Hz and 31 Hz. The Strouhal number decreases with increasing the Lockhart-Martinelli parameter. This behavior is linked to the presence of disturbance waves under conditions of higher liquid superficial velocities.

REFERENCES

- Aydin, T. B., Torres, C. F., Karami, H., Pereyra, E., Sarica, C. "On the characteristics of the roll waves in gas liquid stratified wavy flow: A two dimensional perspective". *Experimental Thermal and Fluid Science*, 65, 90 102, (2015).
- Bae, B., Ahn, T., Jeong, J., Kim, K., and Yun, B. "Characteristics of an interfacial wave in a horizontal air water stratified flow". *International Journal of Multiphase Flow*, 97, 197 205, (2017).
- Chen, X. T., Cal, X. D., and Brill, J. P. "Gas liquid stratified wavy flow in horizontal pipeline". *Journal of Energy Resources Technology*, v.119, 209 216, (1997).
- Matlab. The Mathworks. Inc. Natick MA, USA, (2022).
- Milkie, J. A., Garimella, S., e Macdonald, M. P. "Flow Regimes and Void Fractions during Condensation of Hydrocarbons in Horizontal Smooth Tubes". *International Journal of Heat and Mass Transfer* 92: 252 67, (2016).
- Moreira, T. A., Ayub, Z. H., & Ribatski, G. "Convective condensation of R600a, R290, R1270 and their zeotropic binary mixtures in horizontal tubes. *International Journal of Refrigeration*, 130, 27 43, (2021).
- Thome, J. R., El Hajal, J., & Cavallini, A. Condensation in horizontal tubes, part 2: new heat transfer model based on flow regimes. *International journal of heat and mass transfer*, 46(18), 3365 3387, (2003).

Experimental investigation on upward-vertical adiabatic-inverted annular flow

Edson Orati, Oscar M. H. Rodriguez

University of São Paulo (USP), São Carlos School of Engineering (EESC), Department of Mechanical Engineering, Industrial Multiphase Flow Laboratory (LEMI), Avenida Trabalhador São Carlense, São Carlos, 13566-590, Brazil

Email: orati@usp.br; oscarmhr@sc.usp.br

ABSTRACT

The inverted-annular flow (IAF) pattern has been a research subject for decades due to its importance for safety purpose, since it is commonly observed in the core reflooding step after a loss-of-coolant accident within light water-cooled nuclear reactors. This two-phase flow pattern exhibits a liquid core flowing around the pipe centerline, surrounded by a gas (or vapor) peripheral film under forced convective flow conditions for which a heating source is supplied from the pipe wall. The present research work aims to investigate the possible existence of IAF pattern under adiabatic operating conditions in the upward-vertical direction by the injection of dense-gas and oil. A second objective is to study the onset of liquid jet instabilities caused by the disrupting interaction with the surrounding gas under the flow operating conditions previously described. For the experimental campaign, a new test rig is promptly available at the Industrial Multiphase Flow Laboratory (LEMI) and also the video-recording technique is used with a high-speed camera. Two independent criteria were arbitrarily adopted, namely a thermodynamic one that applies the effective viscosity concept, and one from a hydrodynamic stability analysis that is based on the linear stability theory. Preliminary results pointed out that the adiabatic IAF can likely be attained for moderate liquid superficial velocities and low dense-gas superficial velocities. Under these flow conditions, it has been predicted that a possible oil core flows in laminar regime with Reynolds values between 700 and 1500 while a gas layer streams in turbulent regime into the annulus with Reynolds values ranged from 6500 to 66500. For this research purpose, a proper nozzle will be designed with the aid of which experiments will be carried out to inject the oil into the pipe core region and the dense-gas into the wall region. From a scientific viewpoint, the attempt to experimentally attain the upward-vertical adiabatic IAF with these fluids is original and pioneering.

INTRODUCTION

The inverted-annular flow (IAF) pattern is a film boiling regime beyond the critical wall heat flux in which a liquid jet flows into the core surrounded by a vapor film in the annulus (Miwa & Hibiki 2022). A major application involves accident analyses within light water-cooled nuclear reactors. Experiments were conducted concerning the IAF under adiabatic flow conditions with turbulent water jets issuing downward into a concurrent surrounding gas envelope and the study also focused on jet-core break-up characteristics by changing the gaseous species and, geometrical and operating flow parameters (De Jarlais & Ishii 1983; De Jarlais et al. 1986). The authors' decision to carry out adiabatic experiments was taken due to difficulties in control and measurement of flow parameters under typical film boiling conditions. As a result, those experiments were referred to as a simulated version of the typical IAF pattern conditions. This pioneering scientific work aims to investigate the possible existence of the adiabatic IAF pattern in upward-vertical direction with dense-gas and oil, and also to study the instabilities formation of liquid jet issuing from a properly designed nozzle.

EXPERIMENTAL METHODS

Located in the Industrial Multiphase Flow Laboratory (LEMI), a new test rig (Figure 1) can be readily used to operate with a maximum absolute pressure of 15 bar under a broad range of superficial velocities with mixture of dense-gas (sulfur hexafluoride – SF₆) and turbine mineral oil.

For experiments, a visualization window allows to use a high-speed camera. A properly designed nozzle will be used for the adiabatic IAF experiments and with the aid of which the oil will be injected into the pipe core region while the gas will be introduced into the wall region.



Figure 1: Photograph of the test rig at the LEMI

RESULTS AND DISCUSSION

A hydrodynamic stability analysis (Rodriguez & Bannwart 2008) and a thermodynamic analysis (Joseph et al. 1996) were carried out for an upward-vertical IAF in a 2-inch-id pipe. As shown in Figure 2, one can note that an adiabatic IAF pattern is predicted to occur between the Bubble and Finely Dispersed Bubble flow patterns for moderate oil superficial velocities and low dense-gas superficial velocities. The IAF may be formed by the use of a proper injection nozzle in order to assure that the flow of a possible oil core is laminar under flow conditions for which the predicted ranges of the oil and dense-gas Reynolds numbers values are, respectively, 700–1500 and 6500–66500.

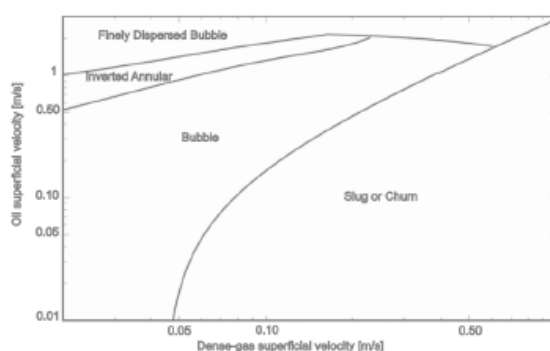


Figure 2: Flow-pattern map obtained for upward-vertical 2-inch-id pipe flows of dense-gas/liquid mixtures

CONCLUSION

From the results, one can conceive that an adiabatic IAF pattern can likely be attained with dense-gas/liquid mixtures for moderate oil superficial velocities and low dense-gas superficial velocities. To achieve the research aim, a proper injection nozzle is to be designed and manufactured at the LEMI.

REFERENCES

- De Jarlais, G. and Ishii, M. Hydrodynamics of adiabatic inverted annular flow – an experimental study. U.S. Nuclear Regulatory Commission, Argonne National Laboratory, Reactor Analysis and Safety Division, pp. 1–15 (1983).
- De Jarlais, G., Ishii, M., Linehan, J. Hydrodynamic stability of inverted annular flow in an adiabatic simulation. *Trans. ASME*, Vol. 108, pp. 84–92 (1986).
- Joseph, D. D., Bannwart, A. C., Liu, Y. J. Stability of annular flow and slugging. *Int. J. Multiphase Flow*, Vol. 22, pp. 1247–1254 (1996).
- Miwa, S. & Hibiki, T. Inverted annular two-phase flow in multiphase flow systems. *Int. J. Heat Mass Transfer*, Vol. 186, pp. 1–15 (2022).
- Rodriguez, O. M. H. & Bannwart, A. C. Stability analysis of core-annular flow and neutral stability wave number. *AIChE Journal*, Vol. 54, pp. 20–31 (2008).

Liquid film behavior regarding pipe diameter on vertical downward annular flow

Ana Luiza B. Santana, Gabriela Kemper de Souza, Eduardo N. dos Santos, Marco J. da Silva, Moisés A. Marcelino Neto, Rigoberto E. M. Morales

Multiphase Research Center (NUEM), Federal University of Technology – Paraná (UTFPR), Curitiba, Brazil

ABSTRACT

In this work, an experimental investigation was conducted to analyze the liquid film properties in downward vertical air-water annular flow using a rig with two different internal diameters, 26 mm, and 50 mm, with a 14 m long pipe at ambient conditions. Twenty-one annular flow combinations of superficial air and water velocities were investigated for each diameter, ranging from 5 m/s to 15 m/s and 0.05 m/s to 0.25 m/s, respectively. Time series of cross-sectional average liquid thickness obtained by a non-intrusive dual ring-shaped conductance sensor was used to provide the fluid film characterization. Moreover, high-speed visualization was used to contribute to the phenomenological and morphology behavior of the annular flow. The liquid film time series analysis provided features such as the average film thickness, film roughness, velocity, frequency, amplitude, length, and appearance of the disturbance waves. The results showed differences in the liquid thickness-to-diameter ratio (h/D) and geometrical characteristics of the disturbance waves by quantitative comparison between the two diameters.

INTRODUCTION

The annular two-phase flow is characterized by a gas core with dispersed droplets and a liquid film wetting the pipe wall. The liquid film presents structures on the gas-liquid interface of the flow, classified into disturbance waves and ripples. The smoothies portion of the liquid film in contact with the pipe wall is identified as substrate or base film. These waves are affected by the high interfacial shear stress between the phases and the gas-liquid flow rate variation.

The disturbance waves are interfacial structures that play a role in influencing the parameters of the flow, such as pressure drop, liquid entrainment, transfer of momentum, mass, and heat. The knowledge of these flow behavior is essential to optimize models and contribute to the progress of the monitoring processes in the industry. In this context, experiments were carried out to investigate the effect of pipe diameter on liquid film properties of vertical downward air-water annular flow.

METHOD

The experimental tests were conducted at the Multiphase Flow Research Center (NUEM) of the Federal University of Technology – Paraná (UTFPR). An apparatus was designed to realize measurements in vertical downward annular flow. The rig has a 26-mm ID and 50-mm ID with a 14-m long test section made of transparent Plexiglas. Special care was taken to obtain the test section alignment (90°) using a professional digital inclinometer with an accuracy of $\pm 0.05^\circ$. The working fluids used in the tests were air and tap water under room conditions. The experimental evaluation comprises twenty-one (21) combinations (C#) of gas (J_g) and liquid (J_l) superficial velocities ranging from 0 m/s to 15 m/s and 0.05 m/s to 0.25 m/s, respectively. All twenty-one flow conditions are investigated for both pipe diameters studied. The liquid film is investigated in a test section placed at 335D and 205D from the flow inlet, for the $D=26$ mm and $D=50$ mm inner pipe diameter, respectively. A non-intrusive dual ring-shaped conductance sensor and a gauge pressure transducer are deployed in the test section. For each superficial phase combination evaluated in this work, the sensor data acquisition frequency was 10 kHz with a sampling time of 30 s and 100 s for 26-mm ID and 50-mm ID, respectively. A high-speed camera was deployed in the test section to flow visualization and provide qualitative information to corroborate the liquid film characterization. The flow snapshots were acquired at a frame rate of 300 Hz and 10 s of record.

RESULTS

Figure 1 shows the averaged liquid thickness for both diameters analyzed as a function of superficial phase velocities for all flow conditions investigated. The average liquid thickness has a well-defined trend regarding the superficial phase velocities, increasing with the superficial liquid velocity (J_L) while J_G remains constant. Moreover, in the opposite effect, the average liquid thickness reduction was observed with the superficial gas velocity increase.

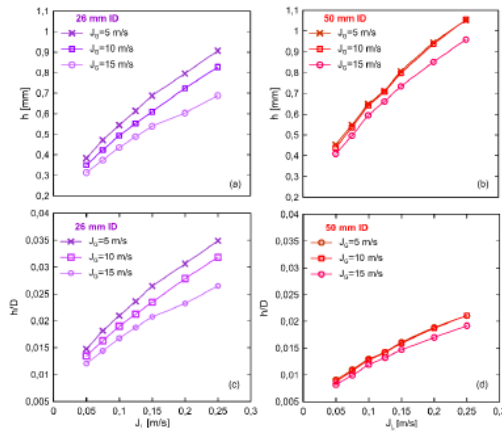


Figure 1 – Averaged liquid film thickness (h) and non-dimensional averaged liquid film thickness as a function of superficial phase velocities for both pipe diameters analyzed.

CONCLUSION

In this work, an investigation of downward vertical air–water annular flows was carried out to evaluate the effect of pipe diameter on features of the disturbance waves. The liquid film analysis was conducted by measurements using a non-intrusive conductance sensor and visualization with a high-speed camera in a 26-mm ID and 50-mm ID, 14-m long pipe. In summary, the significant findings of this work are that the pipe diameter affect the disturbance wave shape when analyzed for the same flow condition of superficial phase velocities. Furthermore, a larger diameter needs a higher shear interaction because of the increasing gas–liquid interface in the circumferential direction.

Characterization of horizontal oil–water core–annular flow using particle image velocimetry (PIV) and planar laser induced fluorescence (PLIF) techniques

Jorge E. Arrollo–Caballero^{1*}, P. J. Miranda–Lugo¹ and O. M. H. Rodriguez¹

¹University of São Paulo (USP), São Carlos School of Engineering (EESC), Mechanical Engineering Department, Industrial Multiphase Flow Laboratory (LEMI), Av. Trab. São Carlense, 400 – Parque Arnold Schimidt, São Carlos – SP, 13566–590, Brazil

Email: jorgearrollo@usp.br*, pjosemiranda@usp.br, oscarmhr@sc.usp.br

KEYWORDS

Core–annular flow, oil–water flow, PIV, PLIF, velocity profile.

ABSTRACT

The interaction of non–miscible liquids is common in the petroleum, food, and chemical industries. Those fluids adopt several spatial configurations when flowing inside a pipe. One configuration is the core–annular flow pattern, in which the more viscous fluid is in the core of the pipe, while the less one forms a ring around the core and is in contact with the pipe wall. Maintaining such a flow pattern in a pipeline is attractive because it reduces pressure loss in oil transportation or production applications. This study aims to classify waves and obtain horizontal oil–water core–annular flow velocity profiles using particle image velocimetry and planar laser–induced fluorescence. The experimental data is collected at the longitudinal section of the pipe. The lower liquid–liquid interface of the core–annular flow is identified using the PLIF technique and classified considering wavelength, period, and amplitude data. Local axial and radial velocities and turbulence statistics are measured in the lower aqueous region of the core–annular flow. Such analysis is expected to shed light on the core–annular flow dynamics and phenomena that may promote the destabilization of the oil core.

INTRODUCTION

Multiphase flows are present in many engineering applications, for instance, refrigeration systems, nuclear power plants, and chemical processing systems. Studying two–phase flows is challenging due to the complexity of the interaction between the phases, which makes flow dynamics predictions difficult. Furthermore, theories on flow pattern transitions are still an open issue.

According to the literature, liquid–liquid flow patterns are classified into dispersed, intermittent, and separated. The latter includes the well–known core–annular flow, which is a spatial arrangement where the more viscous fluid is in the core of the pipe, while the less viscous fluid forms a ring around the core and is in contact with the pipe wall, where the more viscous fluid is in the core of the pipe, while the less viscous fluid forms a ring around the core and is in contact with the pipe wall (Rodriguez and Bannwart, 2008; Rodriguez and Castro, 2014).

Moreover, the liquid–liquid flow transition could be associated with the presence of secondary flow. However, to the best of the authors' knowledge, no experimental study quantifies this effect. This study classifies interfacial waves and obtains velocity profiles in an oil–water annular pipe flow using the PLIF and PIV.

EXPERIMENTAL SETUP

Figure 1 is a diagram of the new test apparatus designed and built up to study the dynamics of liquid–liquid flows. There are two independent supply lines, one for water and another for oil, made of borosilicate–glass pipes with lengths (L_p) of 4.5 and 7.5 m and internal diameters (i.d.) of 9.7 and 20.5 mm, respectively. The fluid distribution system is driven by pumping (C and K) from water and oil reservoirs (A and I). The liquids are injected into the test section through flow straighteners (D, E, L, and M) and a specially designed inlet section (F and N). Both flow lines have an array of liquid

flow-meters (1, 2, 4, 5), thermo-couples type K (3, 6, 7, 8), and differential/gauge pressure transducers (9, 10, 11). The two-phase mixture from the test section is transferred to an oil-water separator (Q). Each fluid is driven to its respective reservoirs completing the test loop. the interface is identified via the PLIF technique. An image processing algorithm identifies the lower oil-water interface and estimates the wavelength, amplitude, and period of the longwave, waves, and ripples. The water's velocity profile is measured with the 2D-PIV technique.

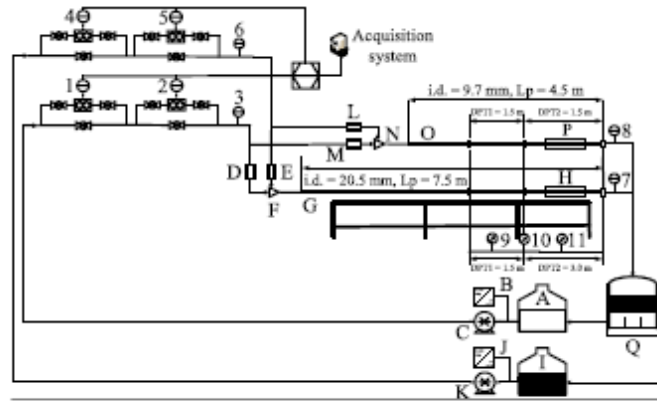


Figure 1: Schematic representation of the new liquid-liquid test apparatus at LEMI.

PRELIMINARY RESULTS

It is well known that core-annular flow still has gaps that need to be studied, some of the expected results of this research is the collection of data that will help to investigate some topics such as the transition of flow patterns and the effects of secondary flows on the hydrodynamics of these patterns.

Figure 2(a) shows the original core-annular flow image, which was processed to identify the interface curvature figure 2(b) Once the liquid-liquid interface is known, one can locate the interface's maximum and minimal local points, as indicated in Fig. 2(c).

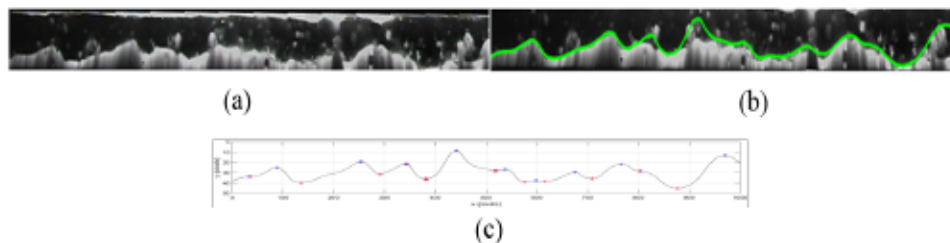


Figure 2: (a) Raw image, (b) Interface identification, and (c) maximum and minimum local points of the interface. The color white represents the water phase, while the color black indicates the oil phase.

CONCLUSION

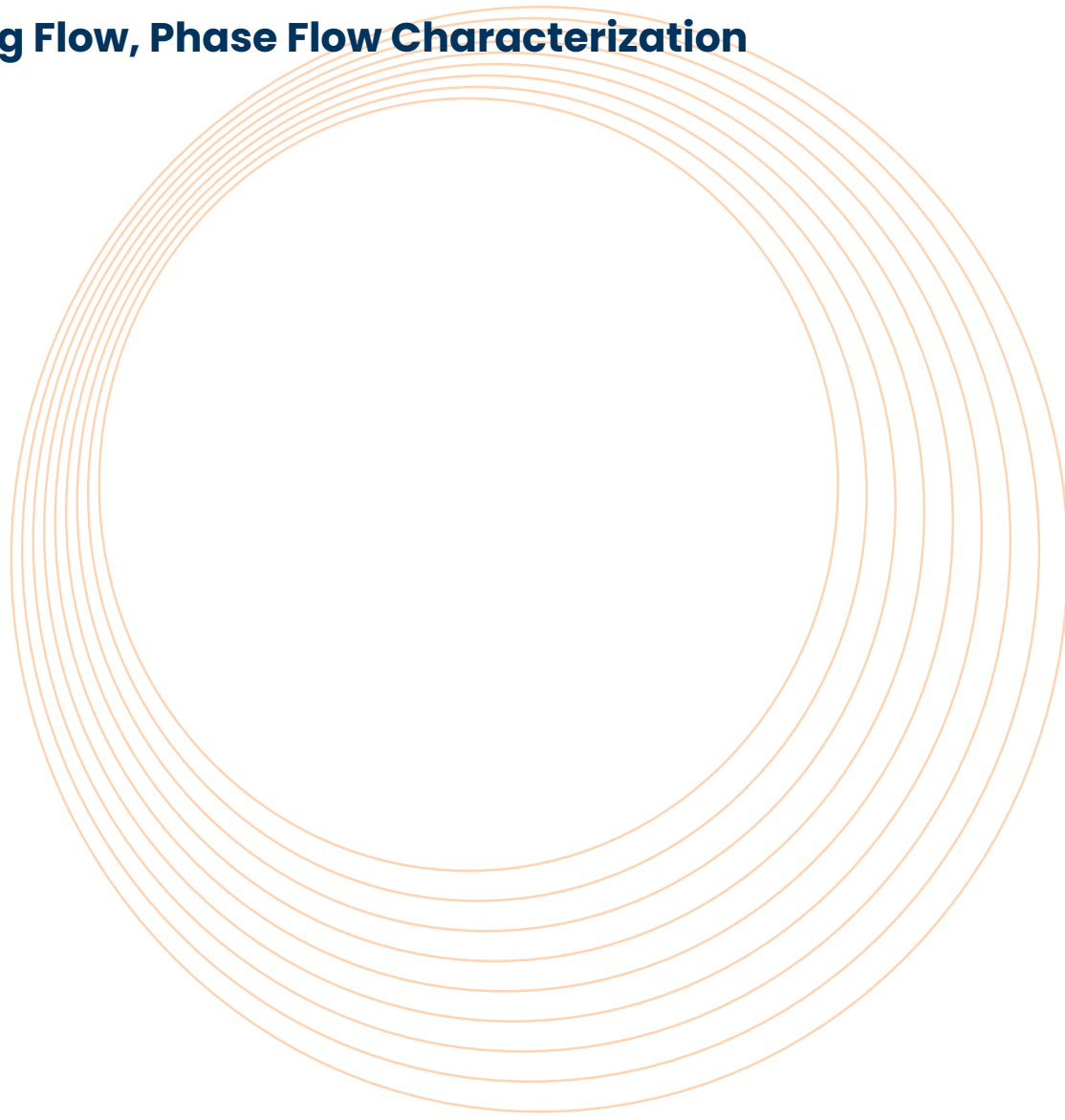
The characterization of oil-water core-annular flow in horizontal pipe provides useful data for future studies, such as the study of the transition of the core-annular flow pattern and the existence of streamwise vortices at the bottom of the liquid-liquid interface. It is expected to identify a mean interface curvature representative of the entire mean velocity field with the processing of the data provided by both techniques.

REFERENCES

Rodriguez, O.M. and Bannwart, A.C. Stability analysis of core-annular flow and neutral stability wave number. *AIChE Journal*, Vol. 54, No. 1, pp. 20–31 (2008).

Rodriguez, O.M., Castro, M.S. Interfacial-tension-force model for the wavy-stratified liquid-liquid flow pattern transition. *Int. J. Multiphase Flow*, Vol. 58, pp. 114–126 (2014).

4 – Slug Flow, Phase Flow Characterization



Influence of the Flow Loop Configuration on the Slug Flow Characteristic Parameters in Vertical Pipes

Carolina Cimarelli Rodrigues¹, Paul Adrian Delgado Maldonado, Eduardo Nunes dos Santos, Moises Alves Marcelino Neto, Rigoberto E. M. Morales – ¹crodrigues@alunos.utfpr.edu.br | Multiphase Flow Research Center – NUEM Federal Technological University of Parana – Av. Deputado Heitor Alencar Furtado, 5000, Curitiba, PR, Brazil

ABSTRACT

Multiphase slug flow is found in pipes and process equipment in the oil & gas industry. Air-water slug flow is usually defined as the alternate passage of two structures: a liquid slug and Taylor bubble. This type of flow occurs intermittently and the passage of all bubbles and liquid slugs have different lengths and velocities. Therefore, the knowledge of the flow evolution and not only of its average behavior is essential to the design of offshore equipment. In this sense, this work aims to evaluate the influence of the flow loop configuration on the evolution of the characteristic parameters of slug flow (Taylor bubble velocity, elongated bubble and liquid slug lengths, void fraction, and slug frequency). The experimental study was carried out in two facilities a horizontal-to-vertical and a vertical flow loop, with a 50-mm ID and air and water as working fluids. To evaluate the flow, pressure transmitters and conductive and capacitive phase detection sensors were used. High speed camera were used to analyze the flow qualitatively. Frequency and lengths of Taylor bubble and liquid slug were influenced by the flow loop configuration, smaller structures and higher frequencies were observed for the vertical tests.

KEYWORDS

vertical slug flow, evolution of air-water slug flow, diameter influence in slug flow.

INTRODUCTION

Slug flow frequently occurs in the petroleum industry during the production and transportation of oil-gas mixtures. This flow pattern is composed by the alternated passage of the elongated bubble (or Taylor bubble) and the liquid slug with dispersed bubbles. As this intermittence is not periodic in time or space (stochastic process), mean values are insufficient to describe the flow hydrodynamics and to assure the reliable design of separators. Therefore, experiments employing recent measurement techniques were performed to investigate with more detail the flow evolution.

The evolution of slug flow along a pipeline strongly depends on the relative velocities between the elongated bubbles. At short distances, trailing elongated bubbles accelerate and eventually merge with the leading ones (Talvy et al., 2000). During the merging process, both the liquid slug and the elongated bubble lengths increase. This coalescence process may occur until the liquid velocity profiles at the back of the liquid slug are fully developed. In this work, the study of the flow evolution and the statistical distribution of the characteristic parameters have been evaluated comparing the flow loop configuration.

METHODS

Two facilities were used: the horizontal-to-vertical flow loop (H-V) and the vertical flow loop (V) as shown in Fig. 1, both of them with a 50-mm ID and air and water as working fluids. The H-V configuration consists of a 10.7-m long horizontal line, followed by a 90°-curve and a 14-m high vertical line, the mixer is a 50-mm ID pipe with a 5-mm hole on the upper part to inject the air, promoting a stratified flow. The V configuration is 12-m high vertical line, with an annular mixer where the gas enters radially in the 50-mm ID pipe through eighty (80) 1-mm holes.

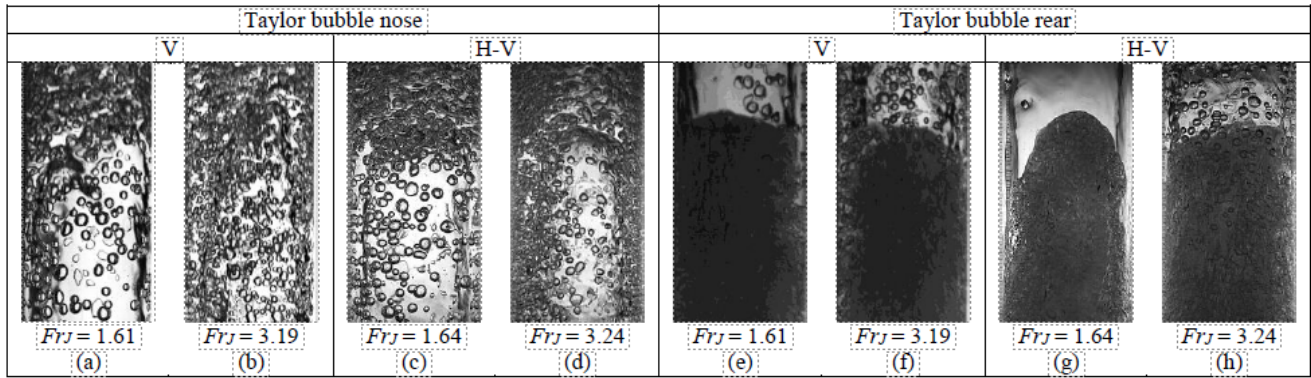


Figure 2 – Taylor bubble nose and rear as a function of Froude number and J_G/J_L ratio, comparing the images for the vertical (V) with the horizontal-to-vertical (H–V) tests configuration. $J_G = 0.4$ and $J_L = 0.6$ m/s for (a, c, e, g) and $J_G = 0.7$ and $J_L = 1.3$ m/s for (b, d, f, h).

The velocity of the Taylor bubble nose is one of the essential parameters in slug flow modeling. In Fig 3(a), the Bendiksen model (1984) for the Taylor bubble translational velocity is compared with the average experiments results obtained from the WMS and conductive sensors. The experimental results have a good agreement with those of the model, showing a mean relative error of 4%, with maximum errors of up to 10% approximately.

The slug frequency is a parameter that indicates the number of unit cells that flow through a system over a unit of time, thereby reflecting the flow intermittency and relating directly with the Taylor bubble and liquid slug lengths. Figure 3(b,c) shows a comparison between the experimental data and the correlations from Legius (1997) and Kaji (2009), respectively. From those images it is possible to recognize a considerable influence of the flow loop inlet as the Legius correlation described well the H-V tests, whereas the Kaji correlation presented a better description of the V tests. This was expected as Kaji experimental facilities were purely vertical with a constant diameter (ID = 51.2 mm). Legius experimental facilities were also purely vertical, but with a contraction, from 80 to 50–mm ID after 7-m height.

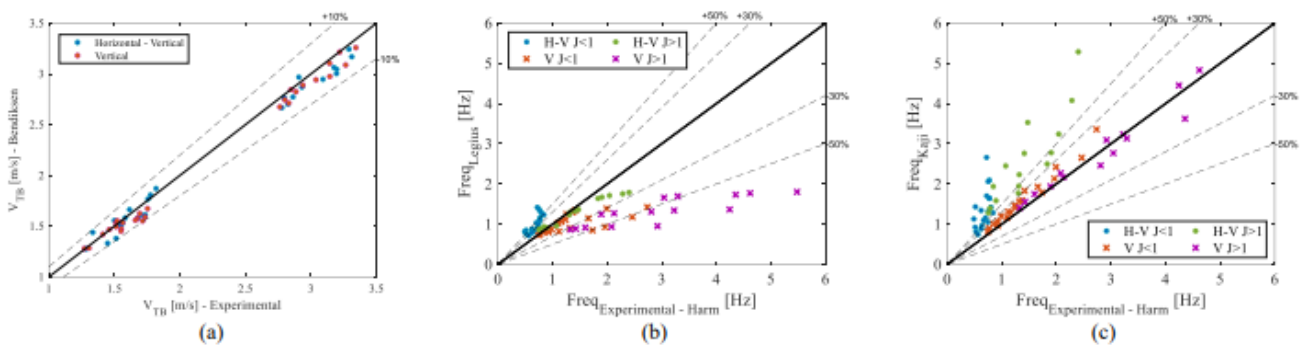


Figure 3 – (a) Comparison of experimental data with Bendiksen model (1984) for the Taylor bubble average velocity (V_{TB}); Comparison of (b) Legius (1997) and (c) Kaji (2009) correlations with experimental data for the slug frequency. The flow loop configuration tests are Horizontal-vertical (H-V) and vertical (V).

CONCLUSION

The results obtained by the experiments herein presented showed great worth to understand the evolution of the vertical slug flow. From the visualization of the images obtained with the high-speed camera, an influence of the J_G/J_L ratio as well as an influence of the Froude number on the Taylor bubble shape (nose, rear and ripples in the bubble body) were noticed, in agreement with the observations reported in the literature on slug flow. In addition, the influence on the disperse bubbles (size, shape and population) was also noticed. From the experiments, it is possible to notice no influence of the flow configuration on the Taylor bubble translational velocity. However an influence can be noticed on the frequency, there is a difference in the flow evolution that depends on the flow loop configuration.

REFERENCES

- Bendiksen, K.H. An experimental investigation of the motion of long bubbles in inclined tubes. *International Journal of Multiphase Flow*, Vol. 10, pp. 467-483, 1984.
- Kaji, R., Azzopardi B.J., Lucas, D. Investigation of flow development of co-current gas-liquid vertical slug flow. *International Journal of Multiphase Flow*, vol. 35, 335-348, 2009.
- Legius, H.J.W.M., Van den Akker, H.E.A. Measurements on wave propagation and bubble and slug velocities in co-current upward two-phase flow. *Experimental Thermal and Fluid Science*, vol. 15, 267-278, 1997.
- Maldonado, P.A.D., Rodrigues, C.C., Santos, E.N., Fonseca Jr, R., Marcelino, M.A., Silva, M.J., Morales, R.E.M. Detailed Analysis of the Diameter Influence on Air-Water Slug Flow Characteristics in Upward Vertical Flow. In: *SPE Flow Assurance Technology Congress, Rio de Janeiro. SPE Flow Assurance Technology Congress, 2022.*
- Taitel, Y., Barnea, D. Dukler, A.E. Modelling flow pattern transitions for steady upward gas-liquid flow in vertical tubes. *AIChE Journal*, vol. 26, 345-354, 1980.
- Talvy, C. A., Shemer, L., Barnea, D. On the interaction between two consecutive elongated bubbles in a vertical pipe. *International Journal of Multiphase Flow*, vol. 26(12), 1905-1923, 2000.
- Acknowledgments This study was financed by the Human Resource Program of The Brazilian National Agency for Petroleum, Natural Gas, and Biofuels - PRH-ANP-FINEP Management, contractual instrument nº 0119024000, Ref 0431/19 - PRH21-UTFPR.

Slug Flows of Gas and Shear-Thinning Fluids in Horizontal Pipes

R. Baungartner², G. F. N. Gonçalves^{1,2}, J. B. R. Loureiro^{1,2}, A. P. Silva Freire^{1,2}
¹Interdisciplinary Center for Fluid Dynamics (NIDF/UFRJ),
R. Moniz Aragão 360, 21941-594, Rio de Janeiro, Brazil
²Mechanical Engineering Program (PEM/COPPE/UFRJ),
C.P. 68503, 21941-972, Rio de Janeiro, Brazil.

ABSTRACT

Experiments on slug flow are carried out with air and three solutions of carboxymethylcellulose (CMC) (0.05, 0.1 and 0.2% w/w) in a 44.2 mm ID horizontal pipe. The lengths, velocities and frequency of passage of the large bubbles are obtained through a high-speed digital camera. The gas fraction and length of liquid slugs are also estimated. Pressure changes are measured with a differential pressure transducer. Particle Image Velocimetry is used to obtain the mean velocity of the continuous liquid field in the film and slug regions. The combination of tested gas and liquid superficial velocities and of distinct fluid rheology results in 48 different experimental conditions. The flow behaviour is found to be strongly dependent on the rheological properties of the continuous phase. In particular, the gas volume fraction within the liquid slug ($\alpha = 1 - R_s$), the passage frequency of the large bubbles (V_t) and the pressure changes are increased. New expressions are proposed for α and V_t to account for the rheology of the liquid phase. Predictions of the flow parameters obtained through two modified mechanistic models are compared to the experimental data. The friction coefficient expression proposed by Anbarlooei et al. (Phys. Rev. E, 92(6), 5--9, 2015) is also tested. The impact of the proposed modifications on the calculated properties of slug flow is assessed; typical RMS-errors of less than 15% are obtained for parameter predictions.

Experimental Investigation of Horizontal Two-Phase Slug Flow with High Density Gases

Bruna P. Naidek¹, Matheus V. R. Pereira¹, Isabela S. Veiga¹, Eduardo M. Baggio¹, Pedro L. N. Machado¹, Roberto da Fonseca Junior², Moisés A. Marcelino Neto¹, Rigoberto E. M. Morales^{1*}

¹Multiphase Flow Research Center (NUEM), Federal University of Technology – Paraná (UTFPR), Curitiba/PR, Brasil

²CENPES/PDIEP/EE Petrobras, Rio de Janeiro – RJ – Brasil

*Corresponding author: rmorales@utfpr.edu.br

ABSTRACT

During the offshore production of oil and gas, it is commonly observed multiphase flow. In this scenario, the gas phase is often of high density with similar magnitude to the liquid phase. This condition greatly differs from the regularly studied system of water and air, where the gas phase is of a much smaller density than the liquid one. Consequently, it is of great interest to investigate how the high gas density will affect the slug flow parameters. Therefore, this study aims to evaluate experimentally the liquid-gas two-phase slug flow for cases with density ratios between 2.3 and 142, using mineral oil and sulfur hexafluoride (SF₆). The pressures ranged from 1 to 35 bar and temperatures from 5°C to 45°C. For each case, several phase velocities were applied and the slug flow parameters and the pressure gradient were obtained. The experimental loop consisted of 60-m long circuit with a 26-mm I.D., with 5 measuring stations and one visualization windows along the pipe. In each measuring station was installed two capacitive sensors that allows measuring slug flow parameters such as bubble velocity, slug frequency, liquid holdup and slug and bubble lengths.

KEYWORDS

experimental analysis, slug flow two phase flow, influence of gas density.

Characterization of two-phase flow pattern for qualitative flow induced vibration analysis in subsea Xmas tree.

Oliveira, M C. – CRN Engenharia, Brazil (matheus@crn.eng.br),
Palladino, L.L – CRN Engenharia, Brazil (palladino@crn.eng.br),
Griffo, S. T. – CRN Engenharia, Brazil (sergio@crn.eng.br)

ABSTRACT

Flow-induced vibration (FIV) is a common physical phenomenon in the engineering field that results from turbulence in the process fluid. This turbulence occurs due to major flow discontinuities such as bends, tees, and partially closed valves. High levels of broadband kinetic energy are created downstream of these sources, concentrated at low frequencies, generally less than 100 Hz. This can lead to the excitation of vibration modes of the piping. In subsea pre-salt wells with significant gas content, FIV of subsea piping may become a structural integrity concern. In the case of multiphase flow, there is uncertainty about the type and mechanisms of excitation. No widely accepted O&G industry standard exists for designing and screening piping for FIV. This work is based on a commonly used approach from The Energy Institute Guidelines, which provides qualitative guidance for screening a process pipeline for potential vibration problems using a Likelihood of Failure (LOF) index. Multiphase flow characterization is based on the Duns and Ross model and confirmed through Computational Fluid Dynamics (CFD) analysis.

KEYWORDS

Flow-induced vibration. Subsea. Two-phase flow. Slug flow. Fluid-structure interaction.

INTRODUCTION

Flow-induced vibration in subsea pipeline and production equipment is a common issue that can lead to significant damage or failure if not addressed properly. Subsea pipelines are subject to FIV when fluid flows through them, and this can lead to fatigue damage or even structural failure over time. It can occur due to a range of factors, including changes in the fluid velocity, flow direction, or pressure, as well as the presence of obstacles or bends in the pipeline. To avoid FIV in subsea production systems, several design and operational measures can be taken. These may include optimizing the pipeline design, reducing the fluid velocity, installing vibration clamps or supports, and using materials with high fatigue resistance. Additionally, regular inspection and maintenance of subsea flowlines can help to identify any potential issues and how to avoid or mitigate them.

METHODOLOGY

Type III empirical correlations considering slip ratio and differences between flow patterns is used to specify the flow pattern. These correlation methods differ from each other by the way that each one predicts the flow pattern and how they calculate the hold-up of liquid, the friction factor, and the interference component of the pressure gradient. To assure the flow pattern, CFD numerical simulations were performed using the Siemens Simcenter STAR-CCM+ software. The simulation was based on the finite volume technique in three-dimensions, using a non-homogeneous model (i.e. gas-liquid slip ratio can be different than 1). The viscosity model chosen was the $k-\epsilon$ (Launder and Spalding, 1974). The input data in terms of flow was based on the oil and natural gas production bulletin provided by the Brazilian regulatory agency ANP (National Agency of Petroleum, Natural Gas and Biofuels) for the year 2023. Among the Type III methods, high-lights: Duns & Ros; Orkiszewski [I]; Begs & Brill; Aziz Govier Fogarasi [III] and Mukherjee & Brill [IV]. Equations (1) and (2) were obtained using the Duns & Ros method for characterization of the flow pattern. Figure 1 illustrate different flow regimes as described by Duns & Ros (1963) and adapted from Lyons (2010).

QUALITATIVE FLOW-INDUCED VIBRATION ANALYSIS

The Energy Institute Guideline on Subsea FIV provides a methodology for assessing the LoF in subsea piping systems. The guideline uses a combination of engineering analysis, operational experience, and test data to estimate the probability of FIV-induced failure. The methodology outlined in the guideline involves several considerations, but this work has focused on the qualification of FIV likelihood through the LoF index for the pipeline. The guideline defines an acceptance criteria of $LoF < 0.3$ for the mainlines and $LoF < 0.4$ for the valves.

RESULTS AND DISCUSSION

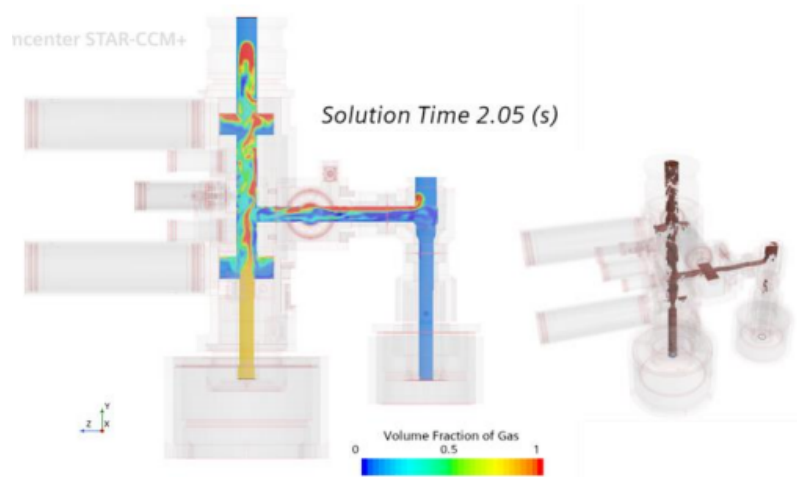


Figure 2 Volume Fraction of Gas

Figure 2 shows a slug flow pattern for main line, with the characteristic Taylor bubble. According to the guideline, a $LoF = 1$ should be considered due to the slug flow pattern, which means that there is a high structural risk and possibility of damage. This multiphase flow pattern is considered as a major concern in the design of pipelines. For this reason, the guideline suggests that the mainline should be redesigned, re-supported, or analyzed numerically.

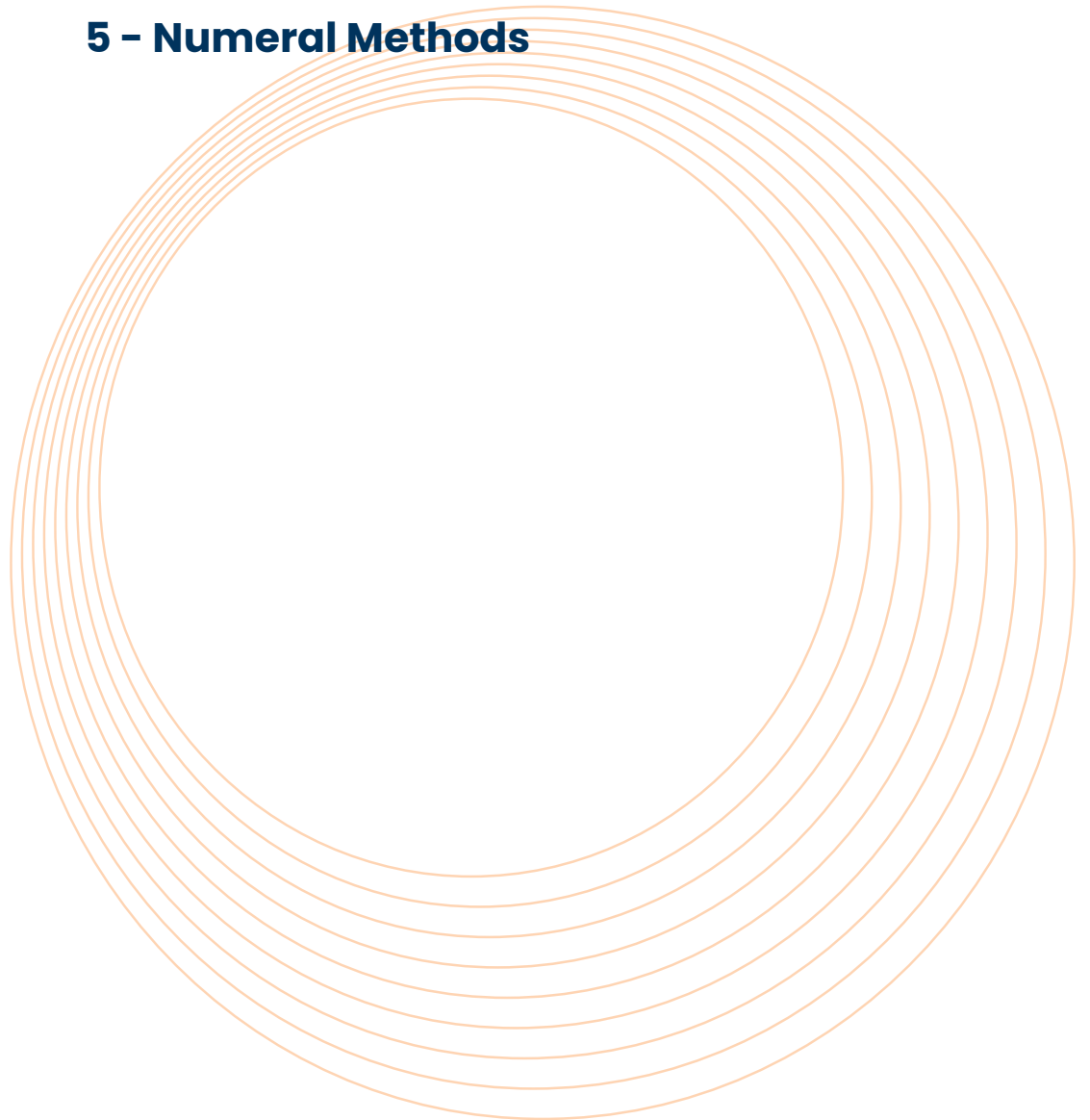
CONCLUSIONS

The possibility of FIV phenomenon in a subsea XMAS Tree was verified through qualitative analysis from the Energy Institute based on the multiphase flow pattern. A numerical CFD simulation was performed to assure the flow pattern identified through the Duns & Ros (1963) method. The results confirm the slug flow pattern, which leads to a LoF index higher than the maximum allowed for the mainlines. Although, the LoF index is considered as a very conservative approach for a FIV analysis Ref. [VIII], this criteria warns about possible problems associated with fatigue due to vibration and recommends more detailed studies, such as Fluid-Structure Interaction (FSI) analysis considering RMS displacement acceptance criteria. For future work, it is recommended to simulate more cases and accomplish FSI analysis for detailed fatigue life assessment for subsea production systems.

REFERENCES

- I. Energy Institute (org.). Guidance for the Avoidance of Vibration-Induced Fatigue Failure in Subsea Systems. 2018.
- II. Orkiszewski, J.: Predicting Two-Phase Pressure Drops in Vertical Pipes. JPT (June 1967) 829, Trans., AIME, 240.
- III. Aziz, K., Govier, G.W., and Fogarasi, M.: Pressure Drop in Wells Producing Oil and Gas. J. Cdn. Pet. Tech. (July-September 1972), 11, 38.
- IV. Mukherjee, H. and Brill, J.P.: Pressure Drop Correlations for Inclined Two-Phase Flow. J. Energy Res. Tech. (December 1985), 107, 549.
- V. STAR-CCM+ User guide. Siemens, Release 2302 (2019).
- VI. Barton, N., Parry, A. Using CFD to Understand Multiphase and Wet Gas Measurement, Institute of Measurement and Control, UK, Volume 46, Issue 2, 2013.
- VII. Launder, B.E., Spalding, D.B. The numerical computation of turbulent flows, Computer Methods in Applied Mechanics and Engineering, Volume 3, Issue 2, Pages 269-289, 1974.
- VIII. Gharaibah, OTC-26844-MS. Flow Induced Vibration for Design and Operation of Subsea Systems. GE Oil & Gas – Subsea / Flow Assurance. 2016

5 - Numeral Methods



Three dimensional two-phase finite element simulation using a front-tracking method

Daniel B. V. Santos¹ and Gustavo R. Anjos²

1 Universidade Federal do Rio de Janeiro/Coppe

2 Universidade Federal do Rio de Janeiro/Coppe

Email: daniel.barbedo@coppe.ufrj.br, gustavo.rabello@coppe.ufrj.br

INTRODUCTION

The numerical modeling of two-phase flow is of interest in many applications, such as oil extraction and refining, chemical engineering, nuclear engineering, and others [3]. It allows engineers to predict and optimize the behavior of two-phase flow applications.

This work proposes a methodology for three-dimensional two-phase simulation, extending the uncoupled formulation described in [1] for 3-dimensional flows. In this methodology, the finite element method is applied to the solution of the Navier-Stokes equations, where the fluid phases are separated by an unstructured three-dimensional surface mesh geometrically uncoupled to the fluid mesh.

METHODOLOGY

The proposed methodology employs the finite element method to numerically solve a single set of Navier-Stokes equations written to account for varying fluid properties. The fluid phases can be distinguished by their distinct properties. The equations are presented below:

$$\nabla \cdot \mathbf{v} = 0 \quad (1)$$

$$\rho(\mathbf{x}) \left(\frac{\partial \mathbf{v}}{\partial t} + \mathbf{v} \cdot \nabla \mathbf{v} \right) = -\nabla p + \frac{1}{Re} \nabla \cdot \mu(\mathbf{x}) [\nabla \mathbf{v} + (\nabla \mathbf{v})^T] + \frac{1}{Fr^2} \mathbf{g} + \frac{1}{We} \mathbf{f} \quad (2)$$

The finite element discretization is done using the mini element [4], in order to respect the LBB condition. The discretization of the non-linear advective term of the Navier-Stokes equations is done through a first-order semi-Lagrangian method [2]. The semi-Lagrangian method is unconditionally stable and conserves the stiffness matrix symmetry.

The surface tension term is calculated through a finite element discretization of the Laplace-Beltrami operator applied to the interface mesh and transformed into a body force through the continuum surface force method [5].

A Heaviside function is used to distinguish the fluid phases, and smooth properties across the fluid interfaces, and its gradient serves as a Dirac delta function. It is given by

$$H(\mathbf{x}) = \begin{cases} 1, & \text{if } d(\mathbf{x}) > \epsilon \\ 0, & \text{if } d(\mathbf{x}) < -\epsilon \\ 1 - 0.5 \left[1 + \frac{d(\mathbf{x})}{\epsilon} + \frac{1}{\pi} \sin(\pi d(\mathbf{x})/\epsilon) \right], & \text{otherwise} \end{cases} \quad (3)$$

and the fluid properties are calculated by

$$\rho(\mathbf{x}) = \rho_1 H(\mathbf{x}) + \rho_2 (1 - H(\mathbf{x})) \quad \mu(\mathbf{x}) = \mu_1 H(\mathbf{x}) + \mu_2 (1 - H(\mathbf{x})) \quad (4)$$

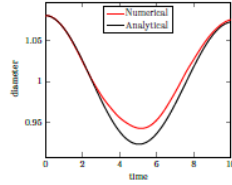
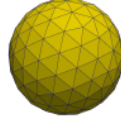
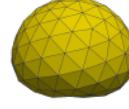


Figure 1: Oscillating Droplet results, compared to exact data. The test was executed with $Re = 500$, $We = 125$, over 10000 time steps with a time step value of $\nabla t = 0.001$.



(a) Initial Bubble Geometry



(b) Bubble Geometry at time step 400

Figure 2: Bubble from the Rising Bubble test case, (a) initial geometry and (b) at time step $i = 400$, with the mesh represented. A remeshing algorithm is executed every other iteration, accompanied by a mass preservation method. The obtained shape is very close to the expected result.

RESULTS

In order to verify the accuracy of the proposed methodology several test cases are executed and the results obtained are compared to existing data. The first test case is the static droplet.

A spherical droplet of dense fluid inside the less dense fluid is simulated, in the absence of gravity force and with null velocity fields. This test should present a balance between the surface tension force and the pressure gradient, with no velocity present. The simulation results for the velocity fields should be as close as possible to zero. The maximum velocity value found in this test case can be found in Tab. 1 for several interface meshes, with Reynolds = Weber = 1, and is in order with values found in the literature.

Interface Edge (h)	v_{max}	Δp_{error}
0.16	6×10^{-1}	0.408%
0.12	1.9×10^{-2}	0.118%
0.085	1.2×10^{-2}	0.102%
0.06	4×10^{-3}	0.061%
0.03	4.2×10^{-1}	18.4%
0.02	366	1223.1%

Table 1: Spurious velocity intensity and pressure error for the static droplet test case. The simulation appears to degrade when the interface mesh average edge length is smaller than the fluid mesh average edge length, optimal values are obtained with close average edge lengths.

The second test case is the oscillating droplet, where an ellipsoidal droplet of dense fluid is simulated inside the less dense fluid, in absence of gravity force. The ellipsoidal shape is a perturbation of the spherical shape, and the surface tension force makes the droplet oscillate around its equilibrium radius, towards a spherical shape. The oscillation frequency and radius values are known, and the comparison between the exact values and the simulation values, with $Re = 500$ and $We = 125$ can be observed in fig. 1.

Lastly, the rising bubble test case was executed. The test consists of a bubble inside a channel, subjected to gravity force. The bubble ascends in the background fluid and changes shape as it rises. The bubble shape after 400 iterations can be observed in fig. 2, and it is consistent with the literature results, presenting an ellipsoidal bubble cap shape. Reynolds number is $Re = 10$ and Weber number $We = 35$.

CONCLUSION

The static droplet and the rising bubble test cases presented accurate results, in line with results found in the literature. The intensity of the spurious velocities in the static droplet case decreased after the initial time steps, the results are presented in Tab. 1 being the worst-case scenario. The oscillating droplet presents some inaccuracy, and it overshoots the diameter value after one period. This result might be improved by adjusting simulation parameters such as domain size and time step value. Overall, the proposed methodology is sufficiently accurate with improvements being currently researched.

REFERENCES

- [1] G.R. Anjos. Moving mesh methods for two-phase flow systems: Assessment, comparison and analysis. *Computers & Fluids*, 228:105053, October 2021.
- [2] Gustavo R. Anjos, Gustavo P. Oliveira, Norberto Mangiavacchi, and John R. Thome. One-and two-step semi-Lagrangian integrators for arbitrary Lagrangian-Eulerian-finite element two-phase flow simulations. *International Journal for Numerical Methods in Fluids*, 94(6):632–654, June 2022.
- [3] Issam Mudawar Chirag R. Kharangate. Review of computational studies on boiling and condensation. *International Journal of Heat and Mass Transfer*, 108:1164–1196, 2017.
- [4] M. Fortin D. N. Arnold, F. Brezzi. A stable finite element for the stokes equations. *Estrato da Calcolo*, XXI(IV):337–344, oct 1984.
- [5] C. Zemach J. U. Brackbill, D. B. Kothe. A continuum method for modelling surface tension. *Journal of Computational Physics*, 100:335–354, 1992.

Simplified lattice Boltzmann implementation of the Brinkman equation with applications in the viscous fingering instability

Hugo Saraiva Tavares

Universidade Federal do Rio de Janeiro (UFRJ), Rio de Janeiro, RJ, Brazil.

E-mail: hugoczpb@gmail.com

KEYWORDS

Lattice Boltzmann method; Brinkman equation; viscous fingering instability.

ABSTRACT

In this work, a novel approach for the lattice Boltzmann method for two-phase flows in porous media is discussed. In this approach, a different analysis of the Chapman-Enskog multiscale expansion provides a simplification of the classical collision-propagation scheme for the lattice Boltzmann equation. This simplification provides a significant improvement in terms of computational memory management and stability of the simulations in comparison with the classical algorithms, while maintaining almost the same accuracy. An extension of this simplified approach, first proposed for Navier-Stokes equation, is now proposed as a numerical solution of the Brinkman equation, which is used to describe low-Reynoldsnumber flow in porous media. Some results with the appearance of the viscous fingering phenomenon are analysed, including verification of benchmarks and the analysis of the energy budget of the system. Some configurations involving surface tension effects are also discussed.

INTRODUCTION

Viscous fingering is a phenomenon that occurs when a less viscous fluid displaces a more viscous fluid in a porous medium. This can occur in many different types of porous media, such as oil reservoirs, groundwater aquifers, and soil. The process of viscous fingering is driven by the differences in viscosity and interfacial tension between the two fluids, as well as the structure of the porous medium itself. Viscous fingering can have important practical implications for the recovery of oil and gas from reservoirs, as well as the management of groundwater resources.

Understanding the mechanisms behind this phenomenon can help in the development of better strategies for controlling the flow of fluids in porous media [7].

The problem with numerical simulation of viscous fingering arises due to the complex nature of the flow, which involves the interaction of several physical phenomena such as multiphase flow, mass transfer and interfacial dynamics. A recent numerical approach for the simulation of this phenomenon is the lattice Boltzmann method [3, 5].

In this work, we considered a simplified lattice Boltzmann approach based on the algorithms developed in [2, 4], where we also introduce an entropically damped form of artificial compressibility [1] that helps in a efficient control of the compressible waves that sometimes are observed in LBM simulations. As a consequence, a better verification of the incompressibility condition is obtained. A careful study of this conditions is not considered in the previous studies about the same theme in the LBM literature [5, 6]. The proposed framework also allows a very natural introduction of surface tension effects, whose influence in the evolution of the viscous fingering instability is also discussed.

METHODOLOGY

We consider an adequate scale where global variables such as the permeability of the porous medium is well defined. The Brinkman equation adds a drag force to the Stokes equations as [6],

$$\nabla p = -\frac{\mu}{K}u + \nabla \cdot \{\mu_e(\nabla u + (\nabla u)^T)\}, \quad \nabla \cdot u = 0. \quad (1)$$

where p is the pressure, K is the permeability of the medium, u is the fluid velocity, and μ_e is the effective viscosity. The viscous fingering instability occurs when a less viscous fluid invades a more viscous fluid. Some important dimensionless parameters that have strong influence in this phenomenon are the log-viscosity ratio and the Péclet number given respectively by

$$R = \ln\left(\frac{\mu_2}{\mu_1}\right), \quad Pe = \frac{UL_{ref}}{D} \quad (2)$$

where U is the injected velocity and L_{ref} is the reference length. The viscosity of the mixture is a function of the concentration assuming an Arrhenius-like exponential dependence given by

$$\mu(c) = \mu_2 \exp(-cR) = \mu_2 \left(\frac{\mu_1}{\mu_2}\right)^c, \quad (3)$$

where c is the concentration of the injected component satisfying the following advection-diffusion equation

$$\frac{\partial c}{\partial t} + u \cdot \nabla c = D\Delta c. \quad (4)$$

The equations (1) and (4) are solved with a new lattice Boltzmann algorithm based on the methods developed in [2, 4]. This algorithm allows efficient computational simulations of the viscous fingering instability with viscosity ratio and Péclet number up to at least $\mu_1/\mu_2 = 100$ and $Pe = 4000$, respectively.

RESULTS

We investigate the evolution of the viscous fingering instability with many different configurations using the proposed simplified LBM algorithm. The results are validated with the verification of some classic benchmarks and the analysis of the energy balance of the system.

One of the results is shown in Figure 1, where the results of a simulation of the viscous fingering solution in a computational grid with size $L_x \times L_y = 1000 \times 2000$, $Pe = 4000$ and $R = \ln 100$ are shown.

CONCLUSIONS

A new simplified lattice Boltzmann implementation of the Brinkman equation for porous media is obtained. In this new method, we consider an entropically damped form of artificial compressibility that allows much better control of compressible wave effects, while maintaining the simplicity and locality characteristic of LBM algorithms. With this improvements, simulations of the viscous fingering instability with viscosity ratio up to 100 are obtained. The same framework also allows an easy implementation of surface tension effects.

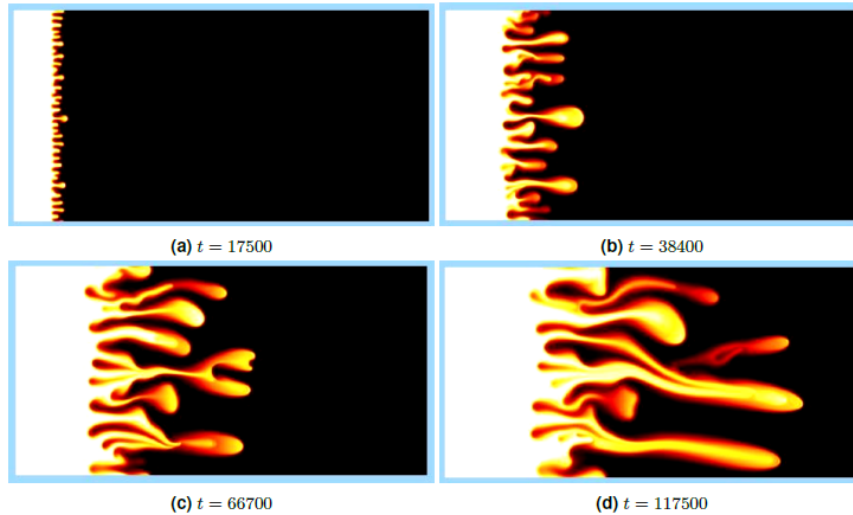


Figure 1: Simulation of the viscous fingering instability by solving the Brinkman equation using the lattice-Boltzmann method. The computational grid has the size 1000×2000 . The pictures are taken in four different times, with Péclet number $Pe = 4000$ and viscosity ratio equal to 100. The time is measured in lattice Boltzmann units (l.b.u.).

REFERENCES

- [1] J. R. Clausen. Entropically damped form of artificial compressibility for explicit simulation of incompressible flow. *Physical Review E*, 87(1):013309, 2013.
- [2] A. Delgado-Gutiérrez, P. Marzocca, D. Cárdenas, and O. Probst. A single-step and simplified graphics processing unit lattice boltzmann method for high turbulent flows. *International Journal for Numerical Methods in Fluids*, 93(7):2339–2361, 2021.
- [3] T. Krüger, H. Kusumaatmaja, A. Kuzmin, O. Shardt, G. Silva, and E. M. Viggen. The lattice Boltzmann method. Springer International Publishing, 10:978–3, 2017.
- [4] H. S. Tavares, B. Magacho, L. Moriconi, and J. B. Loureiro. A simplified lattice boltzmann implementation of the quasi-static approximation in pipe flows under the presence of nonuniform magnetic fields. *arXiv preprint arXiv:2211.09370*, 2022.
- [5] L. Vienne and S. Marié. Lattice boltzmann study of miscible viscous fingering for binary and ternary mixtures. *Physical Review Fluids*, 6(5):053904, 2021.
- [6] L. Vienne, S. Marie, and F. Grasso. Simulation of viscous fingering instability by the lattice boltzmann method. In *AIAA Aviation 2019 Forum*, page 3432, 2019.
- [7] L. Xia. Morphology of flow patterns generated by viscous fingering from miscible fluids. *arXiv preprint arXiv:1809.09460*, 2018.

Numerical simulation of a multiphase flow inside a diesel particulate filter

Felipe Feres Ferreira, Gustavo Rabello dos Anjos
Universidade Federal do Rio de Janeiro (UFRJ), Rio de Janeiro, RJ, Brazil

ABSTRACT

Nowadays, air pollution is one of the greatest problems that humankind is trying to mitigate. Since vehicle emissions are a main source of air pollution main causes, many efforts have been made to control this problem. A specific case is vehicles with diesel engines, which use a device called Diesel Particulate Filter, or just DPF, to control the exhausted particulates. It is important to study the behavior of air and particulates inside this device to better understand the problem's physics, making it possible to improve it. Then, one way to achieve that effectively is by carrying out numerical simulations. In this scenario, this work aims to develop a computational code that can accurately calculate the particulates' behavior along with the flow. In order to do that, this case, which is a multiphase flow problem with air and particulates, is modeled in such a way that the air is treated from an Eulerian point of view through the Navier–Stokes equations while the particulates are treated in a Lagrangian way by using Newton's second law. Finally, the developed code is used to simulate a case found in the literature, allowing the results obtained in this work to be compared with the literature ones, making it possible to verify the code's reliability.

INTRODUCTION

Until now, the only device that is capable to control the diesel engine's particulate emission in an effective way is the Diesel Particulate Filter, or just DPF (GUAN et al., 2015). The DPF has two functions: to capture the particulates and eliminate them safely (KHAIR, 2003). Then, it is important to understand the behavior of the flow inside it and numerical simulation is an important tool to be used in complex cases such as this, a multiphase flow constituted by air and the particulates exhausted by the engine, which is a solid-gas flow.

METHODS

The continuous phase, constituted by air, is treated from an Eulerian point of view using a modified version of the Navier–Stokes equation, which consists of the original one with the inclusion of terms related to Darcy's law and Forchheimer equation to account for the porous effects that exist in the porous wall inside the device (CIMOLIN e DISCACCIATI, 2013). The dimensionless form is presented where \mathbf{U} is the velocity vector, T the time, P the pressure, Re the Reynolds number, Fr the Froud number, \mathbf{g} the gravity vector, μ the viscosity, ρ the density, K the permeability coefficient, C_f the inertial resistance coefficient, L_c the characteristic length, U_c the characteristic velocity, \mathcal{E} the penalty coefficient which is equal to zero outside the porous wall and equal to one inside it, and the superscript ` refers to the variable's dimensionless form. These equations are numerically solved by the Finite Element Method and modeled as follows:

$$\nabla \cdot \mathbf{u}' = 0 \quad (1)$$

$$\frac{D\mathbf{u}'}{Dt'} = -\nabla P' + \frac{1}{Re} \nabla^2 \mathbf{u}' + \frac{1}{Fr^2} \mathbf{g}' - \left(\frac{\mu L_c}{\rho K U_c} \mathbf{u}' - \frac{L_c C_f}{\sqrt{K}} |\mathbf{u}'| \mathbf{u}' \right) \mathcal{E} \quad (2)$$

The carrier phase, constituted by the particulates, is treated from a Lagrangian point of view using Newton's 2nd law. Since both biodiesel and diesel particulates are in the sub-micrometer range (SOUZA, 2021), the main forces actuating on the particles are the drag and Brownian force (SBRIZZAI, FARALDI e SOLDATI, 2005). Furthermore, this work also considers the gravity force.

Then, the particulate's motion equation is presented as follows where \mathbf{v} is the velocity vector, d the particle diameter, C_c the Stokes-Cunningham slip correction, P_p the spectral intensity of the noise, Δt the difference between time steps, and \mathbf{G} is a vector containing a different zero-mean independent Gaussian random number of unit variance for each direction at each time step. This equation is numerically solved by the Runge-Kutta method.

$$\frac{d\mathbf{v}'}{dt'} = \frac{1}{Fr^2} \mathbf{g}' + \frac{18\mu L_C}{d^2 C_c \rho_p U_C} (\mathbf{u}' - \mathbf{v}') + \frac{\mathbf{G}}{U_C} \sqrt{\frac{L_C \pi S_0}{U_C \Delta t'}} \quad (3)$$

RESULTS

It was simulated the same case that was studied at the work of SBRIZZAI, FARALDI AND SOLDATI (2005) but modelling the device as 2D and the results were compared. Figure 1 presents the results for the flowrate through the porous wall and for the particles concentration at the porous wall along the channel and it is possible to see a good agreement between them with some difference that can be explained by 3D effects that were not considered in this work.

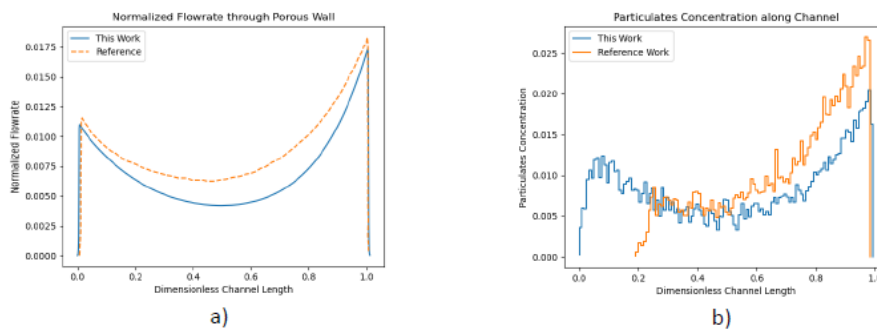


Figure 1: Comparison between results of this and reference works along the channel for a) normalized flowrate through porous wall b) particulates concentration.

CONCLUSION

It was presented a methodology to solve the flow inside a DPF. It was used to simulate a case found in the literature and the work's results have shown a good agreement with the literature's ones. Then, it is possible to conclude that this methodology is reliable, but some improvement can be made on it, like the adjustment to a 3D case which would be even closer to real conditions.

REFERENCES

- CIMOLIN, F.; DISCACCIATI, M. Navier–Stokes/Forchheimer models for filtration through porous media. *Applied Numerical Mathematics*, v. 72, p. 205–224, Julho 2013.
- GUAN, B. et al. Review of the state-of-the-art of exhaust particulate filter technology in internal combustion engines. *Journal of Environmental Management*, v. 154, p. 25–258, Março 2015.
- KHAIR, M. K. A Review of Diesel Particulate Filter Technologies. SAE Technical Paper. [S.l.]. 2003. (2003-01-2303).
- SBRIZZAI, F.; FARALDI, P.; SOLDATI, A. Appraisal of three-dimensional numerical simulation for sub-micron particle deposition in a micro-porous ceramic filter. *Chemical Engineering Science*, v. 60, n. 23, p. 6551–6563, Dezembro 2005.
- SOUZA, J. P. I. Particle-Laden Multiphase Flows: A Finite Element Analysis on Biofuel Particle Emissions. COPPE, Universidade Federal do Rio de Janeiro. Rio de Janeiro. 2021.

Simulation of multiphase flow and analysis of droplet formation patterns in a microchannel

Kevin Lima Pinto¹, Víctor Lênnin Porto Amorin¹, Raquel Jahara Lobosco¹, Edmundo Guimarães de Araújo Costa², Guilherme Barbosa Lopes Junior³

¹Poli, Universidade Federal do Rio de Janeiro, ²COPPE, Universidade Federal do Rio de Janeiro, ³Universidade Federal de Pernambuco

E-mail: rlobosco@macae.ufrj.br, edmundo_costa@coc.ufrj.br, guilherme.lopes@ufpe.br

ABSTRACT

In the last decades, the development of technologies involving micro- and nano-devices has emerged as a new branch in fluid mechanics. The main components of these devices are the microchannels, which handle with single-phase and multi-phase fluid flow. Previous studies have demonstrated that the use of these components can provide energy-efficient systems due to its high thermal performance. Therefore, within this context, the present work has as a goal to investigate the behavior of micro-scale fluids by means of numerical simulations for a better understanding of the operational processes of these microchannels and thus to enhance their energy efficiency.

The open software OpenFoam version 8 was used to discretize the conservation equations of fluid mechanics, to create the numerical model, to describe the physical properties of the fluids and to establish boundary conditions necessary to represent the different flow regimes in the computational scope. The chosen solver was the interFoam, suitable for cases involving two incompressible, isothermal and immiscible fluids, making use of the VOF (Volume of Fluid) method for the calculations of a phase-fraction based interface capturing approach.

In this work, an analysis for classification of flow regimes was performed as a result of the numerical simulations, allowing observing the patterns of droplet formation created by the detachment of one of the phases along the main channel of the structure. These simulations can be seen in Fig. 1, as proposed in [1, 2].

A frequency analysis was also performed, allowing evaluating the numerical residual for the processed cases, in which these drops are generated. The results of this analysis can be seen in Tab. 1 and in Fig. 2.

Table 1 – Relative time between the detachment of two consecutive drops and frequency of droplet formation (F) for the velocity pair of each of the nine cases.

Cases	1	2	3	4	5	6	7	8	9
T(s)	0,0330	0,0210	0,0175	0.0135	0,0055	0,0055	0.0050	0.0025	0.0020
F(Hz)	30,30	48,78	57,14	74,07	181,82	181,82	200,00	400,00	500.00

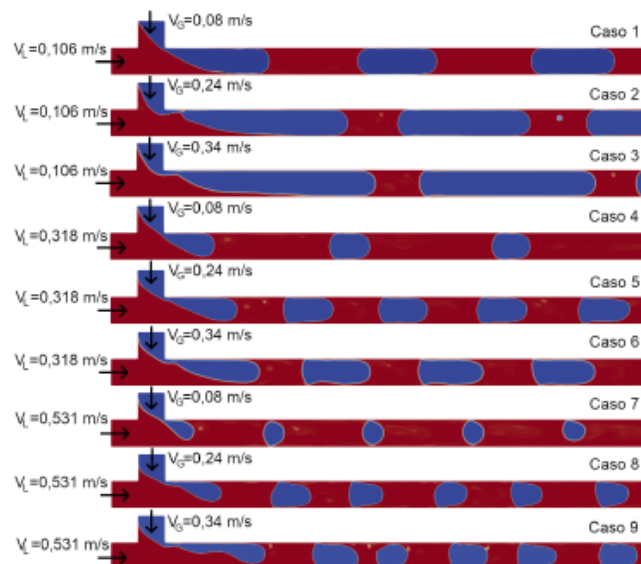


Figure 1 – Moment of drop rupture for the nine cases analyzed with the liquid phase represented in red and the gaseous phase in blue.

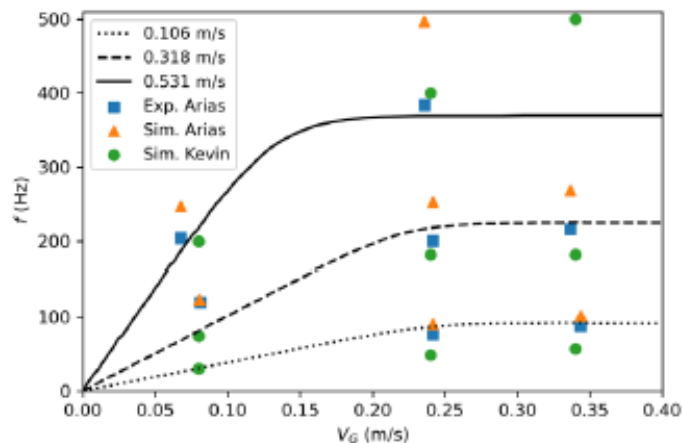


Figure 2 – Frequency analysis for droplet generation.

Fig. 2 displays the experimental and numerical results obtained for the droplet generation frequency as a function of the dispersed phase velocity (V_G) for different values of continuous phase velocity (V_L). From this figure, it becomes clear that the results obtained numerically are in good concordance with those provided in [1]. It can also be seen that as the values of V_G decrease the results trend to be closer to the data obtained experimentally, revealing a good convergence of the proposed methodology, particularly when a dispersed phase velocity equal to 0.08 m/s is considered.

REFERENCES

- [1] Arias, S.; Legendre, D.; González-Cinca, R. Numerical simulation of bubble generation in a T-junction, *Computers and Fluids*, v. 56, pp. 49–60, 2012.
- [2] Guimarães, G.M., Pinto, K.L., Lobosco, R.J., Comparative Analysis of Multiphase Flow in a T Type Micro Junction, *Smart Innovation, Systems and Technologies*, v. 233, pp. 723–731, 2021.

A semi-Lagrangian finite element method for two-phase flows

Gustavo Rabello dos Anjos, Rafael Araujo Vidal

Department of Mechanical Engineering, Federal University of Rio de Janeiro, Brazil

E-mail: gustavo.rabello@coppe.ufrj.br, vidal@mecanica.coppe.ufrj.br

ABSTRACT

This work aims to present a computational approach to study two-phase flows using direct numerical simulation. The flows are modeled by the two-dimensional incompressible Navier-Stokes equations, which are approximated by the Finite Element Method. The Galerkin formulation is used to discretize the Navier-Stokes equations in the spatial domain and the semi-Lagrangian method is used to discretize the material derivative in the temporal domain. A static unstructured triangular mesh is defined in the whole spatial domain. In order to satisfy the Ladyzhenskaya-Babuška-Brezzi condition, the mini and the quadratic elements are used, with pressure and velocity fields being calculated on different sets of the triangular mesh points. The interface is modeled by an adaptive moving one-dimensional mesh, according to a fronttracking method, in which connected marker points are moved with the imposed velocity of the triangular mesh. The interfacial tension is calculated using the interface curvature and a Heaviside function gradient, and included in the Navier-Stokes equations as a volume force. In order to stabilize the simulation results, a smooth transition between fluid properties is defined on the interface region. Several benchmark tests, such as the rising bubble and the oscillating drop, have been carried out to validate the proposed approach and the obtained results have matched analytical solutions and results found in literature. Therefore, the presented approach is validated to provide an accurate description of diverse two-phase flow phenomena.

KEYWORDS

Two-phase flows, Finite Element Method, semi-Lagrangian, front-tracking.

INTRODUCTION

Classically, two distinct approaches are used to describe a system of particles: the Eulerian and the Lagrangian. Let $\varphi(x, t)$ be a passive scalar to be advected by a velocity field. In the Eulerian interpretation, the spatial points remain static, and the scalar field φ , at each instant of time, is defined from the positions of the moving particles. The Lagrangian interpretation, on the other hand, considers the movement of spatial points together with the particles.

The semi-Lagrangian method combines the characteristics of an Eulerian interpretation with those of a Lagrangian interpretation. Although the scalar field is defined with respect to fixed spatial points, a particle movement is considered to define a virtual position of these points at the previous instant, at each instant of time. This method was first described in 1959, gaining notable relevance in the field of meteorology, mainly due to two of its characteristics: unconditional stability and the possibility of using higher temporal steps. Nowadays, however, the semi-Lagrangian method is not restricted to this application, being used for a wide variety of simulations with different levels of complexity.

Motivated by the expansion of the application of the semi-Lagrangian method to different areas of knowledge, this work proposes to present the use of this approach in a front-tracking methodology for the simulation of two-phase flows.

METHODOLOGY

In this work, the two-phase flows are modeled by the two-dimensional incompressible Navier–Stokes equations, shown in (1) and (2).

$$\rho \left[\frac{\partial \mathbf{v}}{\partial t} + \mathbf{v} \cdot \nabla \mathbf{v} \right] = -\nabla p + \frac{1}{Re} \nabla \cdot [\mu (\nabla \mathbf{v} + \nabla \mathbf{v}^T)] + \frac{1}{Fr^2} \rho \mathbf{g} + \frac{1}{We} \mathbf{f} \quad (1)$$

$$\nabla \cdot \mathbf{v} = 0 \quad (2)$$

These equations are then approximated by the Finite Element Method. The Galerkin formulation is used to discretize them in the spatial domain and the semi-Lagrangian method is used to discretize the material derivative in the temporal domain, achieving the formulation given by (3) and (4).

$$M_p \left(\frac{\mathbf{v}^{n+1} - \mathbf{v}_d^n}{\Delta t} \right) + \frac{1}{Re} K \mathbf{v}^{n+1} - G p^{n+1} - \frac{1}{Fr^2} M_p \mathbf{g}^n - \frac{1}{We} M \mathbf{f}^n = 0 \quad (3)$$

$$D \mathbf{v}^{n+1} = 0 \quad (4)$$

A static unstructured triangular mesh is defined in the whole spatial domain. In order to satisfy the Ladyzhenskaya–Babuška–Brezzi condition, the mini and the quadratic elements are used, with pressure and velocity fields being calculated on different sets of the triangular mesh points. The interface is modeled by an adaptive moving one-dimensional mesh, according to a front-tracking method, in which connected marker points are moved with the imposed velocity of the triangular mesh. The interfacial tension is calculated using the interface curvature and a Heaviside function gradient, and included in the Navier–Stokes equations as a volume force. In order to stabilize the simulation results, a smooth transition between fluid properties is defined on the interface region.

RESULTS

The figures below show the results obtained to a rising bubble flow, with a geometry considering a bubble with diameter $D = 0,5$ in a 1×2 rectangular domain. The simulation has considered a Reynolds number $Re = 35$ and a Weber number $We = 10$. The metrics considered for the evaluation of the results were: the evolution of the vertical position of the bubble centroid throughout the simulation; the evolution of the circularity of the bubble throughout the simulation; and the geometry of the interface at time $t = 3$ of the simulation. The reference values for all these metrics were published by Hysing et al. (2009), in an article which is frequently referenced in the validations of later works in the field of two-phase flows.

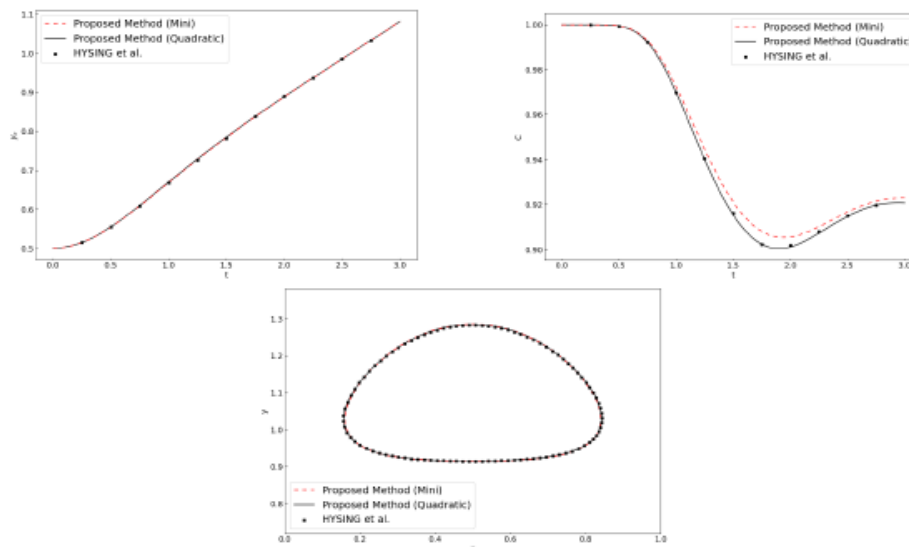
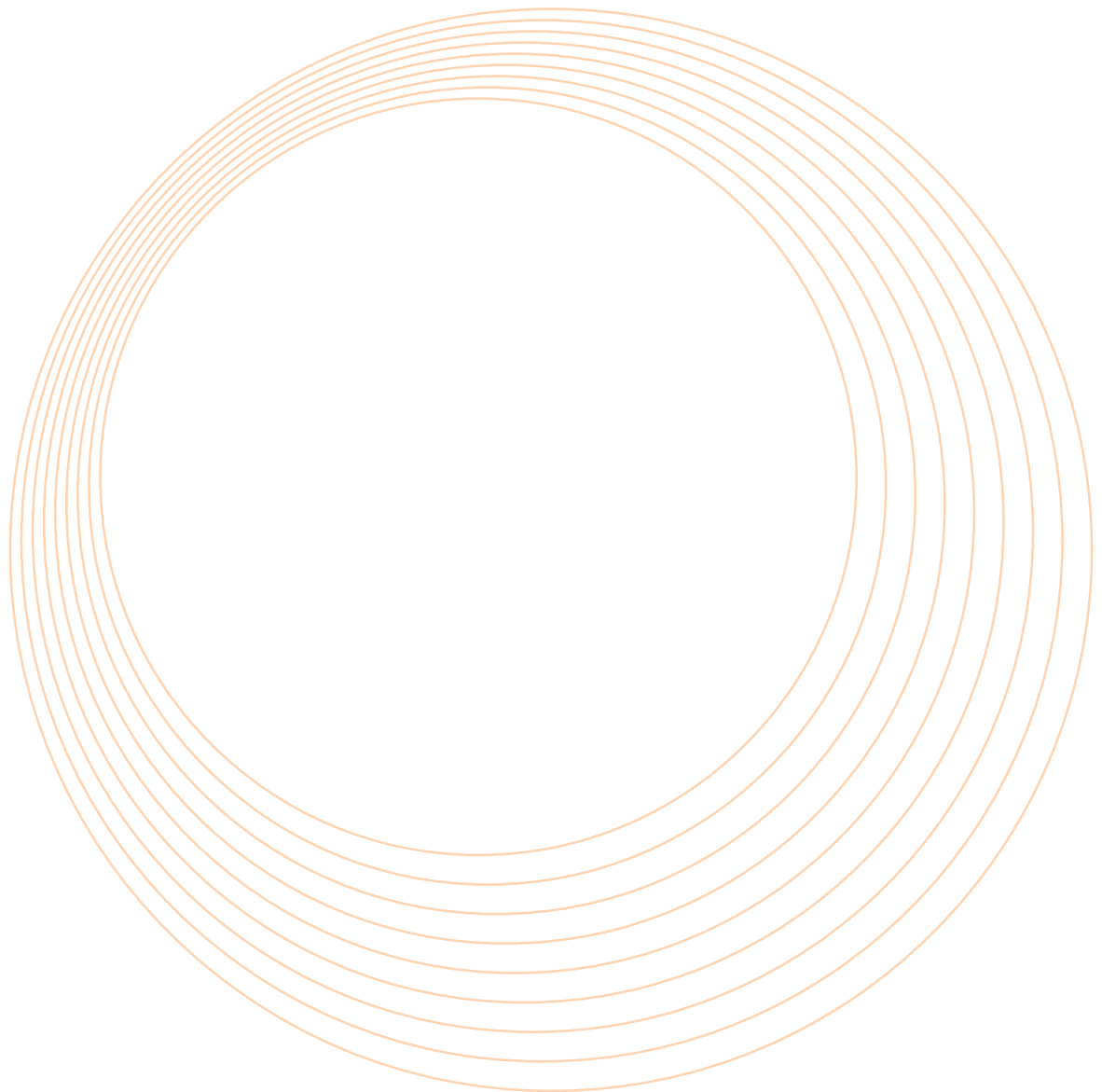
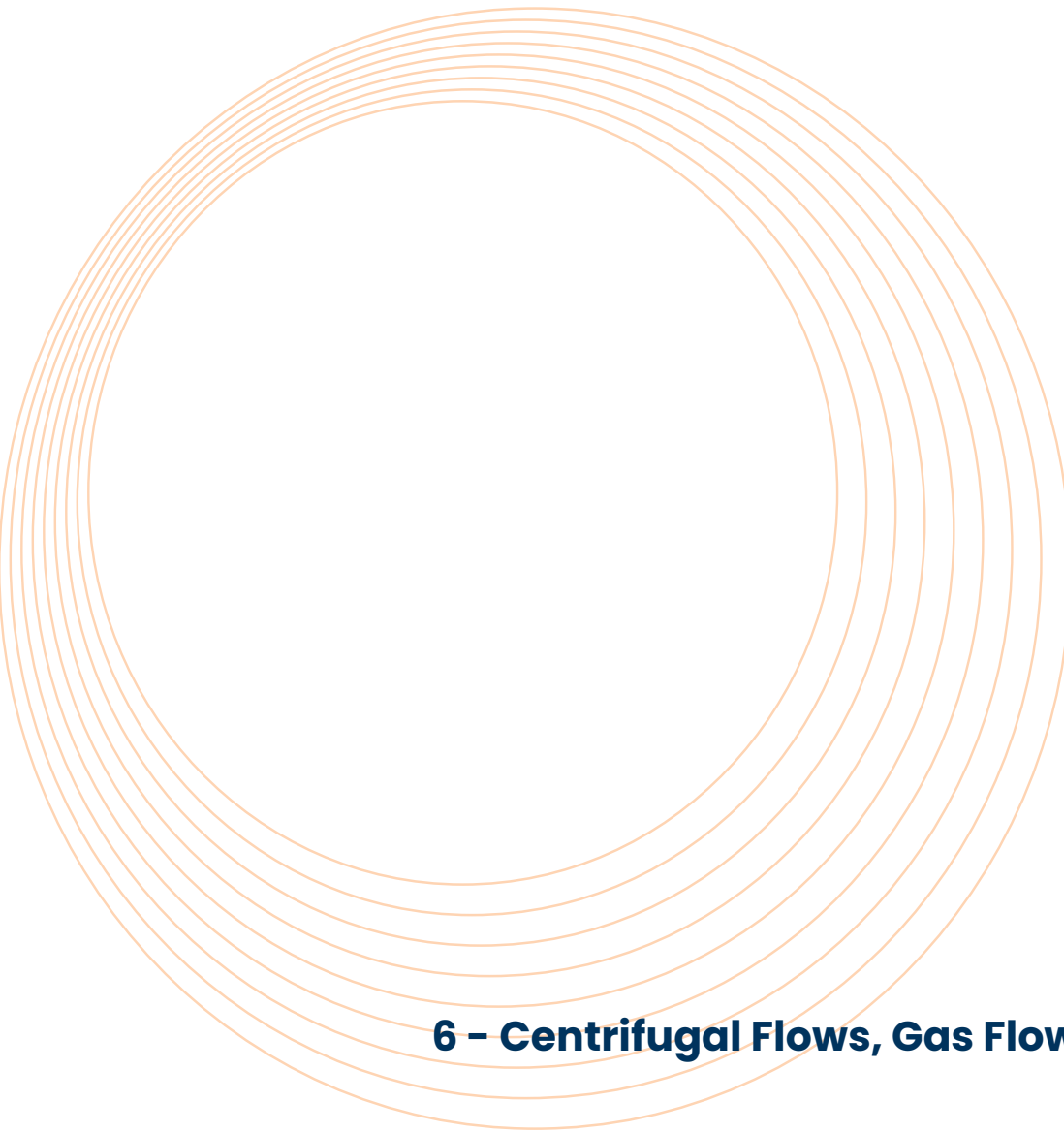


Figure 1. (1) The evolution of the vertical position of the bubble centroid throughout the simulation; (2) the evolution of the circularity of the bubble throughout the simulation; and (3) the geometry of the interface at time $t = 3$ of the simulation.

CONCLUSION

The obtained results have shown good agreement with results found in literature. Therefore, the proposed methodology is validated to provide an accurate description of two-phase flow phenomena.





6 - Centrifugal Flows, Gas Flow

Using electrical submersible pump mechanical vibrations and Fourier convolution neural network to estimate the water cut in two-phase liquid-liquid flows

Felipe de Castro Teixeira Carvalho*, Alberto Luiz Serpa†

School of Mechanical Engineering, University of Campinas, Campinas, Brazil

Email: *felipecastrotc@gmail.com, †alserpa@unicamp.br

ABSTRACT

In oil exploitation, water in the production is common and increases with the field life. For oil production to be economically feasible, artificial lifting techniques may be required. In this context, electrical submersible pumps have been widely used to provide energy to the fluid for decades. Despite the recent development on ESP vibration signal usage, most studies use the vibration signal for fault diagnosis algorithm development. On the other hand, the water cut is essential to obtain several volumetric variables, such as the flow rate of each phase, the effective viscosity, and the pressure drop. This study aims to obtain an artificial neural network that correlates the ESP mechanical vibrations with the water-liquid ratio of an oil-water two-phase flow. The artificial neural network uses a Fourier convolution neural network architecture, where the convolutions are performed in the frequency domain rather than the time domain. The experimental data obtained resulted in a non-uniform dataset on different spatial projection, which significantly affected the data-driven technique performance. Then, by filtering out spaced experimental points and using only the samples inside the sample convex hull, it was possible to successfully obtain a regression between the ESP vibration spectrum and the water cut. The results showed that data filtering and selection were crucial for the artificial neural network performance.

INTRODUCTION

Oil exploitation often involves water production which increases with the field lifespan, requiring artificial lifting techniques for economically feasible production. Multistage centrifugal pumps have been widely used to provide energy to the fluid to overcome pressure losses in such scenarios, and electrical submersible pumps (ESP) have been used for decades. However, the literature on the ESP behavior when operating on liquid-liquid mixtures is still missing [9].

Several studies have focused on developing data-based algorithms for ESP fault diagnosis using different techniques such as Bayesian belief networks as in Rauber et al. [6], extreme learning machines, support vector machines, K-nearest neighbor, decision trees, and random forests in de Assis Boldt et al. [2] and Rauber et al. [7], and adaptive neuro-fuzzy systems in Moosavian et al. [5]. ESP vibration has been studied to determine its condition, and according to Durham et al. [3], the high radial vibration amplitudes are the primary cause of ESP failure.

Recent developments in ESP vibration comprehension include modal analysis, in Minette et al. [4] and Castillo et al. [1], wear condition identification in Zhu et al. [11], and the study of interstage pressure difference and pressure pulsation in Yang et al. [10], which are associated with ESP vibration. Later, Reges et al. [8], based on the invariance of the ESP vibration orbit shape proposed a technique to determine the maximum radial amplitude more accurately.

This work is arranged in sections, where in Section II it is presented the experimental facility, and the experimental procedure. In Section III, the results for the Fourier Convolution Neural Network (FCNN) training procedure and the test dataset are presented. Finally, Section IV presents the conclusion of this work.

METHODS

A. Experimental apparatus

The experimental process was carried out using an experimental assembly in the Experimental Laboratory of Petroleum Kelsen Valente Serra (LABPETRO) of the Center for Energy and Petroleum Studies (CEPETRO) at the University of Campinas. The schematics of the experimental equipment are shown in the Figure 1. There are three separate flow lines in the experimental setup, a mineral oil line, a water line, and a two-phase line. The primary component is an eight-stage ESP with blades that has a diameter of 108mm and 7 blades. The assembly also includes a centrifugal pump (for the pumping of water), a two-screw pump (for the pumping of oil), variable speed drives (VSD), a heat exchange circuit, a remotely controlled valve, auxiliary manual valves, and monitoring. At the ESP intake, a triaxial accelerometer (A1) measures the vibration.

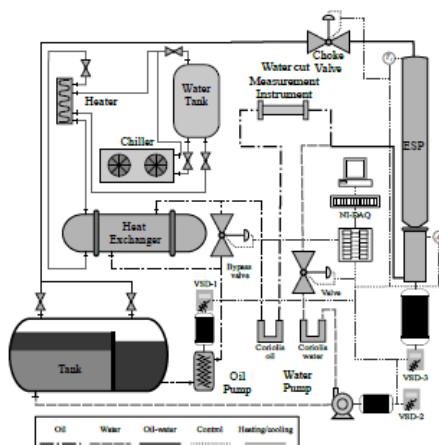


Fig. 1: Experimental assembly layout.

RESULTS AND DISCUSSION

During the manual hyperparameter optimization, we observed that after approximately 300 epochs, the rootmean-square error (RMSE) stagnated. Then, the best architecture found presented a coefficient of determination (R^2) of 0.9980 for the training dataset. For a better analysis, the Figure 2 presents the water cut predicted by the FCNN as a function of measured water cut. Thus, the results of an ideal predictor would be the red dashed line. Then, evaluating the FCNN performance on a dataset not used on the training step similarly to the training dataset, we have the Figure 3

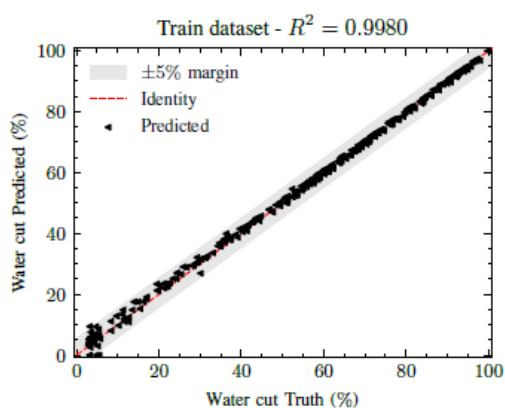


Fig. 2. Predicted water cut using the train dataset.

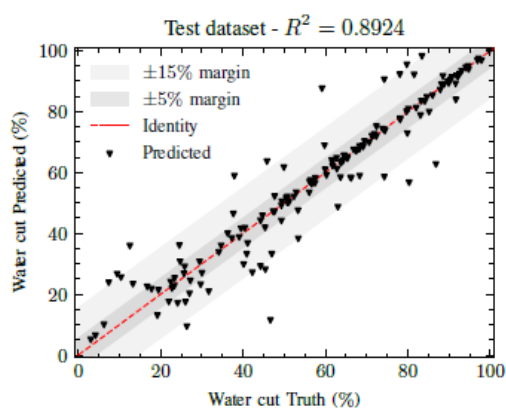


Fig. 3. Predicted water cut using the validation dataset.

It is observable in Figure 2 that most of the predicted points would fall inside a $\pm 5\%$ band, depicted as a gray area. For the validation dataset the coefficient of determination (R^2) dropped to 0.8924, and most of the points fall inside a $\pm 5\%$ error band, approximately 68.8% of the experimental points.

CONCLUSION

Most of the experimental points falls inside a $\pm 5\%$ error band. Also, it was not noticeable a worse performance in a particular water cut range. The errors were evenly distributed, with the majority of points with a low percentage error. The manual hyperparameter optimization was successful in finding a reasonable architecture. However, a more comprehensive hyperparameter space exploration is still lacking.

ACKNOWLEDGMENT

We gratefully acknowledge the support of the Energy Production Innovation Center (EPIC) at the University of Campinas (UNICAMP) and the financing by the São Paulo Research Foundation (FAPESP, process 2019/14597-5). We acknowledge the support of Brazil's National Oil, Natural Gas, and Bio-fuels Agency (ANP) through the R&D levy regulation. Acknowledgments are extended to the Center for Petroleum Studies (CEPETRO), School of Mechanical Engineering (FEM), and Artificial Lift and Flow Assurance Research Group (ALFA).

REFERENCES

- [1] M. A. Castillo, R. H. R. Gutiérrez, U. A. Monteiro, R. S. Minette, and L. A. Vaz, "Modal parameters estimation of an electrical submersible pump installed in a test well using numerical and experimental analysis," *Ocean Engineering*, pp. 1–7, 2019.
- [2] F. de Assis Boldt, T. W. Rauber, F. M. Varejao, and M. P. Ribeiro, "Performance analysis of extreme learning machine for automatic diagnosis of electrical submersible pump conditions," in *2014 12th IEEE International Conference on Industrial Informatics (INDIN)*, IEEE, 2014, pp. 67–72.
- [3] M. O. Durham, J. H. Williams, and D. J. Goldman, "Effect of vibration on electric-submersible-pump failures," *Journal of Petroleum Technology*, no. 2, pp. 186–190, 1990.
- [4] R. S. Minette, S. F. Silva Neto, L. A. Vaz, and U. A. Monteiro, "Experimental modal analysis of electrical submersible pumps," *Ocean Engineering*, pp. 168–179, 2016.
- [5] A. Moosavian, M. Khazaei, H. Ahmadi, M. Khazaei, and G. Najafi, "Fault diagnosis and classification of water pump using adaptive neuro-fuzzy inference system based on vibration signals," *Structural Health Monitoring*, no. 5, pp. 402–410, 2015.
- [6] T. W. Rauber, F. M. Varejão, F. Fabris, A. Rodrigues, and M. P. Ribeiro, "Automatic diagnosis of submersible motor pump conditions in offshore oil exploration," in *IECON 2013 - 39th Annual Conference of the IEEE Industrial Electronics Society*, 2013, pp. 5537–5542.
- [7] T. W. Rauber, T. Oliveira-Santos, F. de Assis Boldt, A. Rodrigues, F. M. Varejao, and M. P. Ribeiro, "Kernel and random extreme learning machine applied to submersible motor pump fault diagnosis," in *2017 International Joint Conference on Neural Networks (IJCNN)*, 2017, pp. 3347–3354.
- [8] G. Reges, M. Fontana, E. Costa, A. Lima, M. Ribeiro, and L. Schnitman, "A new method for the vibration amplitude assessment of the esp systems considering the vibration orbit," *Journal of Petroleum Science and Engineering*, no. January, p. 110 214, 2022.
- [9] G. Takács, *Electrical Submersible Pumps Manual: Design, Operations, and Maintenance*, Second edition. Cambridge, MA: Gulf Professional Publishing, 2018, 564 pp.
- [10] Y. Yang, L. Zhou, W. Shi, Z. He, Y. Han, and Y. Xiao, "Interstage difference of pressure pulsation in a three-stage electrical submersible pump," *Journal of Petroleum Science and Engineering*, p. 107 653, 2021.
- [11] H. Zhu et al., "Experimental study of sand erosion in multistage electrical submersible pump esp: Performance degradation, wear and vibration," *International Petroleum Technology Conference 2019, IPTC 2019*, pp. 1–15, 2019.

Surging parametrization for gas-liquid centrifugal pumps

L. E. M. Carneiro¹, G. S. O. Martins¹, C. M. P. Rosero², J. B. R. Loureiro^{1,2}, A. P. Silva Freire^{1,2}

¹Interdisciplinary Center for Fluid Dynamics (NIDF/UFRJ), R. Moniz Aragão 360, 21941-594, Rio de Janeiro, Brazil

²Mechanical Engineering Program (PEM/COPPE/UFRJ), C.P. 68503, 21941-972, Rio de Janeiro, Brazil

ABSTRACT

The present work investigates the dimensional and similarity representation of two-phase flows in centrifugal pumps. A new parametrization scheme is advanced for the capacity $\varphi = Q/(\omega D^3)$ and head $(\varphi = gH/(\omega^2 D^2))$ coefficients, in terms of the non-dimensional parameters β (no-slip volume gas fraction) and $\Omega (= \omega D/UM, UM = \text{mixture velocity in the inlet pipe})$. The new parametrization yields universal performance curves that capture the positions of performance degradation (φ_{cr} and φ_{max}) and the appearance of surging. The new expressions are supported by a comprehensive set of experiments, carried out for volume gas fractions up to 12% and four rotational speeds. The experimental conditions cover the four different flow patterns commonly described in the literature. The experiments are conducted for water and air and employ the Shadow Sizer Technique for optical measurements. The experiments characterize the flow patterns in the inlet and outlet regions of the centrifugal pump through global and local parameters (pressures, velocities, bubble diameter distributions). The work confirms the rotation speed as a relevant parameter in the performance determination of gas-liquid systems and shows its relation to bubble breakup and the definition of the four observed flow patterns. The particularly introduced parametrization equations are limited to the geometry of pump that is tested. The developed methodology, however, is expected to be extendable to pumps of different geometries.

A coupled PIV/PTV framework for the determination and assessment of interfacial momentum closure in dispersed two-phase rotating flows

William D. P. Fonseca¹, Rafael F. L. Cerqueira², Rodolfo M. Perissinotto², William Monte Verde², Marcelo S. Castro^{1,2} and Erick M. Franklin¹

¹School of Mechanical Engineering, University of Campinas, Brazil

²Center for Energy and Petroleum Studies, University of Campinas, Brazil

INTRODUCTION

Centrifugal pumps are widely used in engineering applications. In certain situations, they must operate in out-of-design conditions, such as in two-phase liquid-liquid dispersed flows. In these cases, it is interesting to understand the drops' dynamics and kinematics for accurate CFD modelling [1], in particular for better understanding in unstable water/oil emulsion operations [2].

The present work describes an experimental framework for determining and assessing interfacial momentum closure in dispersed two-phase rotating flows. A transparent acrylic pump prototype was designed and installed to enable the use of Particle Tracking Velocimetry (PTV) and Particle Image Velocimetry (PIV) techniques for dispersed liquid-liquid flow characterization. A set of deep-learning image processing techniques were developed and applied in the raw PIV acquisitions to distinguish the tracer particles and the oil drops in a single-camera PIV setup.

EXPERIMENTAL SETUP

The experimental setup consists of a water line, an oil line, a booster pump, and instruments to measure flow rate, pressure, and temperature. The test section is a transparent centrifugal pump which enables the flow visualisation by the PIV technique in the impeller and volute.

The present work aims to describe a coupled PIV/PTV framework for determining and assessing interfacial momentum closure in dispersed two-phase rotating flows using a single camera.

Therefore, the oil drops need to be visible in the raw PIV acquisitions. Hence, an optimal white dye concentration had to be added to the oil phase to enable the drops' visualisation. A small dye concentration would result in poor drop visualisation, while a high concentration disrupted the laser sheet illumination, resulting in shadows and poor visualisation of the PIV tracer particles. By doing controlled tests, a small white dye concentration (0.5 grams per litre) was found, in which the oil drops were visible without disrupting the laser sheet illumination.

Figure 1 presents a raw image acquired during a PIV acquisition. As observed the oil drops and tracer particles are visible and distinguishable from the dark background.

IMAGE PROCESSING

The application of the PIV technique is not straightforward in two-phase flows, since the dispersed phase may be visible in the PIV images. In these situations, it is necessary to remove its contribution to the image since, otherwise, the computed velocity field will return corrupted values [3].

For this purpose, a dynamic masking method is employed to mask out the oil drops from the PIV image. The technique was described in Cerqueira et al. [3] to remove the gas bubbles in the PIV raw images. The masking is based on the development and training of a U-Net convolutional neural network, which generates a binary mask that can then be used to remove the oil drops from the image.

The same U-Net mask is also used to identify the oil drops in the PIV images. A PTV algorithm could be developed by identifying the oil drops in each PIV frame, resulting in a coupled PIV/PTV framework. The identification of the oil drops in the PIV image is performed by a CNN (Convolutional Neural Network) and after, the oil drop velocity is calculated. The entire approach, including the segmentation, identification and velocity calculation, is carefully detailed in Cerqueira et al. [3].

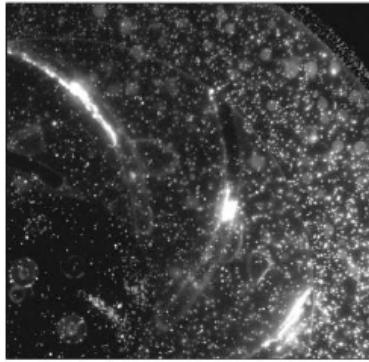


Figure 1: Raw image acquired during a PIV acquisition.

RESULTS AND DISCUSSION

A typical instantaneous velocity field obtained with the coupled PIV/PTV framework can be seen in Fig. 2, where the oil drops are highlighted in the PIV raw image with their instantaneous velocity vectors. By rewriting the equations of motion of a single oil drop, knowing the dispersed and continuous instantaneous velocity and acceleration, it is possible to assess classical drag and lift relations from the literature [4] and, if necessary, propose corrections for the rotational flow found within the impeller channels.

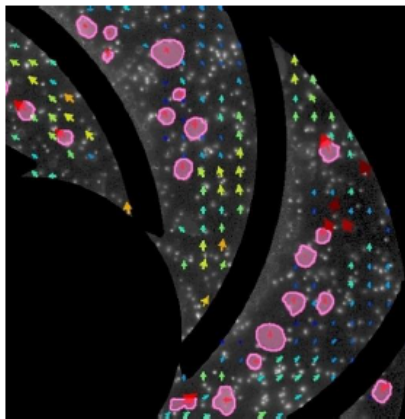


Figure 2: Example of a typical instantaneous velocity field obtained with coupled PIV/PTV framework.

REFERENCES

- [1] Perissinotto R. M., Monte Verde W., Gallassi M., Gonçalves G. F. N., Castro M. S., Carneiro J., Biazussi J. L. and Bannwart A. C. 2019. "Experimental and numerical study of oil drop motion within an esp impeller". *Journal of Petroleum Science and Engineering*, 175:881–895.
- [2] Bulgarelli N. A. V., Biazussi J. L., Monte Verde W., Perles C. E., Castro M. S. and Bannwart A. C. 2021. "Experimental investigation on the performance of electrical submersible pump (esp) operating with unstable water/oil emulsions". *Journal of Petroleum Science and Engineering*, 197:107900.
- [3] Cerqueira R. F. L., Paladino E. E., Ynumaru B. K. and Maliska C.R. 2018. "Image processing techniques for the measurement of two-phase bubbly pipe flows using particle image and tracking velocimetry (piv/ptv)". *Chemical Engineering Science*, 189: 1–23.
- [4] Crowe C. T., Schwarzkopf J. D., Sommerfeld M. and Tsuji Y. 2011. "Multiphase Flows with Droplets and Particles". CRC Press.

Experimental methodology to simulate leaks in dense-gas/liquid pipe flow

C. M. Ruiz-Díaz, C. E. Alvarez-Pacheco, M. da Silva Carr, and Oscar M. H. Rodriguez
Industrial Multiphase Flow Laboratory (LEMI), Mechanical Engineering Department, São Carlos School of Engineering (ESSC), University of São Paulo (USP), Brazil.

Email: carlosruiz978@usp.br, cristhianeap@usp.br, marcus_carr@usp.br, oscarmhr@sc.usp.br

KEYWORDS

Leakage, dense gas, two-phase flow, pressure drop, flow-pattern classification, abnormal event

ABSTRACT

The oil and gas industry invests significant resources to eliminate risks generated by unexpected abnormal conditions in production processes. One major risk is leaks, which are in part generated by critical operating conditions of pressure and temperature that pipelines installed in production wells must withstand, as well as the complex natural environment in which all extraction lines are installed. Besides impacting in productivity, leaks also represent environmental problem due to the release of oil and gas into the offshore platforms' surroundings, causing irreparable damage. This research aims to develop an experimental methodology in a laboratory scale to simulate leaks of different sizes typical of hydrocarbon production, using the two-phase flow of dense gas and mineral oil as working fluids in an inclinable pipe. Various operating conditions will be tested to obtain detailed information on the dynamics of the leaking phenomenon. The study will also establish techniques for measuring flow pressure gradients and volumetric fractions, along with flow pattern visualization techniques.

INTRODUCTION

In hydrocarbon production, it is common to encounter multiphase flows involving gases, liquids, and other substances such as resins and sands. The industry invests significant resources in monitoring production lines to reduce the probability of failures (Vargas et al., 2019), Temperature (Guo et al., 2021), pressure (Kang et al., 2021), and high-resolution flow sensors are installed at critical positions to eliminate the risks generated by unexpected abnormal conditions in production processes due to degradation of the system components (Khan et al., 2006). Methodologies have been developed with industrial applications in monitoring multiphase flow transportation, focused on increasing process safety (Aljaroudi et al., 2015). These methodologies are based on mathematical models and simulations but lack abundant real data for validation and optimization. This research study proposes an experimental methodology for a laboratory environment with controlled operational variations, aimed at simulating leaks of different sizes using the two-phase flow of dense gas and mineral oil as working fluids (Quintino, 2022). The fluids flow inside an inclinable pipeline for which there are no existing records in the literature available for leakage simulation in this configuration. Additionally, techniques and procedures will be proposed to perform correct measurements of pressure differentials, volumetric fractions, and adequate identification of flow patterns. All procedures will be developed to ensure adaptability through dynamic similarity to real systems installed on offshore platforms.

EXPERIMENTAL APPARATUS

The methodology will be developed considering the devices installed in the new experimental apparatus of the Industrial Multiphase Flow Laboratory (LEMI) at the University of São Paulo on the São Carlos campus. A schematic representation of the installation is presented in Figure 1, referring to the high-pressure line installed.

This laboratory's apparatus that will be used has its specifications described in Table 1. It is capable of working with two-phase flow through its 30 [m] long U-shaped pipe, which is subdivided into two sections, each of 15 [m], one upstream and one downstream that goes directly to the separator tanks. A separate 1-inch i.d. pipe for the leak outlet is installed too. The apparatus includes a test section equipped with various components, including a visualization segment, a high-speed camera, pressure, temperature and flowmeter sensors, and pneumatically controlled quick-closing directional valves.

To generate novel insights, we will develop a unique methodology that utilizes dense gas and mineral oil as working fluids under specific pressure and temperature conditions. The properties of the substances are presented in Table 2.

Table 1. Experimental apparatus capabilities.

Parameter	Measurement	Units
Inclination	- 90 to 90	deg
Internal diameter	50.8	mm
L/d	459 – 918	-
Max. Oil Volumetric flow rate	40	m ³ /h
Max. SF ₆ Volumetric flow rate	3062	kg/h
Temperature range	15 – 50	°C
Absolute inner pressure	15	bar

Table 2. Physical properties of the fluids used at 15 bar and 25°C.

Phase	Fluid	Density [Kg/m ³]	Viscosity [cP]
Oil	Turbine 22	867,1	22
Dense-gas	Sulfur hexafluoride – SF ₆	110,1	0,015

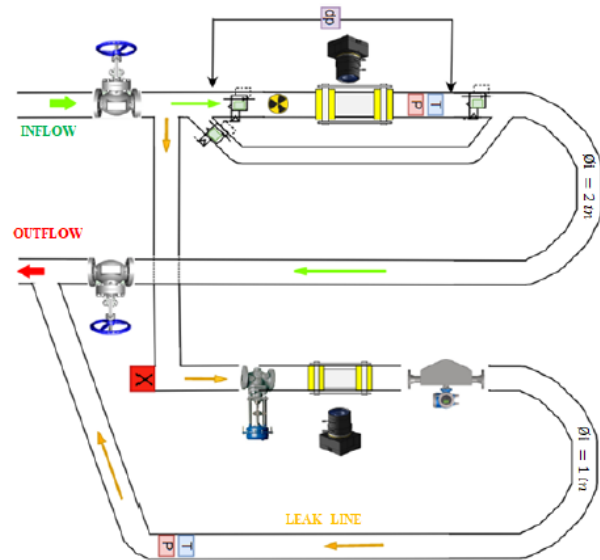


Figure 1. Schematic representation of the experimental loop.

EXPECTED RESULTS AND CONCLUSION

This study aims to develop an experimental methodology for simulating leaks of various sizes using the measurement and control devices installed in the experimental apparatus at LEMI. By generating changes in the operational conditions of the system, we will employ advanced techniques to measure pressure gradients, volumetric fractions, and identify patterns of dense gas and mineral oil two-phase flow through pipelines with varying inclinations. The expected results will provide valuable insights not previously available in the literature.

ACKNOWLEDGMENTS

We would like to thank the Industrial Multiphase Flow Laboratory (LEMI) at the São Carlos School of Engineering (EESC), University of São Paulo (USP), for their assistance with this study.

REFERENCES

- Aljaroudi, A., Khan, F., Akinturk, A., Haddara, M., & Thodi, P. (2015). Risk assessment of offshore crude oil pipeline failure. *Journal of Loss Prevention in the Process Industries*, 37, 101–109. <https://doi.org/10.1016/j.jlp.2015.07.004>
- Guo, W., Liu, C., & Wang, L. (2021). Temperature fluctuation on pipe wall induced by gas–liquid flow and its application in flow pattern identification. *Chemical Engineering Science*, 237, 116568. <https://doi.org/10.1016/j.ces.2021.116568>
- Kang, J., Zhang, X., Zhang, D., & Liu, Y. (2021). Pressure drops and mixture friction factor for gas–liquid two–phase transitional flows in a horizontal pipe at low gas flow rates. *Chemical Engineering Science*, 246, 117011. <https://doi.org/10.1016/j.ces.2021.117011>
- Khan, F. I., Haddara, M. M., & Bhattacharya, S. K. (2006). Risk–based integrity and inspection modeling (RBIIM) of process components/system. *Risk Analysis : An Official Publication of the Society for Risk Analysis*, 26(1), 203–221. <https://doi.org/10.1111/j.1539-6924.2006.00705.x>
- Quintino, A. M. (2022). Phenomenological , heuristic and experimental study of liquid / dense–gas two–phase pipe flow. São Carlos School of Engineering, University of São Paulo, São Carlos – SP, 2022.
- Vargas, R. E. V., Munaro, C. J., Ciarelli, P. M., Medeiros, A. G., Amaral, B. G. do, Barrionuevo, D. C., Araújo, J. C. D. de, Ribeiro, J. L., & Magalhães, L. P. (2019). A realistic and public dataset with rare undesirable real events in oil wells. *Journal of Petroleum Science and Engineering*, 181(June), 106223. <https://doi.org/10.1016/j.petrol.2019.106223>

Influence of the Slip parameter in pressure wave propagation in wet gas flow

Johann E. C. Bolívar, Oscar M. H. Rodríguez

Industrial Multiphase Flow Laboratory (LEMI), São Carlos School of Engineering (EESC), University of São Paulo (USP), Av. João Dagnone 1100, São Carlos, 13568-250, Brasil

Email: johanncastro@usp.br; oscarmhr@usp.br

ABSTRACT

Acoustic properties of two-phase flow are of interest to industrial and gas transportation in the petroleum industry. In this study, the influence of the Lockhart-Martinelli parameter on acoustic wave pressure propagation in wet gas in pipes is investigated. Wet gas flows, however, frequently occur in gas-flare systems and affect the performance of flow metering devices such as differential pressure meters and ultrasonic flows meters. This promotes erroneous measurements of these devices. Therefore, the no-slip model cannot accurately predict the amount of water present in the gas phase. Therefore, it is suggested that the Chilsom slip parameter should be used to correct the gas volumetric and void fraction of the mixture. Hence, of 20% is observed when the slip is considered in the prevision of the sound propagation velocity..

KEYWORDS

Wavelength; gas-liquid flow; water-drops; slip; sound propagation, acoustics

INTRODUCTION

In the oil and gas industry, the presence of a wet gas is a common matter due to the water content and the condensation of heavier components of the flow on the line. On the other hand, wet gas flow is a particular case of multiphase flows present in food, chemical and even, in oil and gas industry; moreover, there is a further discussion on the definition of a wet gas as can be seen in Hall et al. (2007), where it is defined as a two-phase flow with a gas volumetric fraction (GVF) above of 90%. However, based on the Lockhart and Martinelli parameter, the Norwegian Society for Oil and Gas Measurement, API and ASME, define the wet gas as a flow with a $X_{LM} < 0,3$, where the flow is dominated by the gas inertia, and it shows well accepted by the multiphase flow community (Steven, 2000). On the other hand, the measurement of the flow rates in gas-flare systems are essential to industry, depending on the definition used to the wet gas, the gas volumetric fraction can be overestimated and providing an erroneous reading of the flow meters used with this purpose (Hall, Graffin, & Steven, 2007; Steven, 2000). Hence, the influence of the slip parameter between the phase are investigated and analyzed for a new experimental long-wavelength acoustic technique of flow rate measurement in wet gas flow with a gas volumetric fraction of 97%.

The results of the inclusion of the slip parameter shows a variation of 12% on the predictions of the gas volumetric fraction, and a 20% variation on the sound velocity predictions when the slip parameter is included on the model.

METHODOLOGY

In this section a simplified modeling of the slip parameter to predict the gas volumetric fraction and the void fraction is presented, based on the work of Hall et al. (2007).

The gas volumetric fraction (GVF) is defined as relation between the gas volume flow rate (Q_g) to the total volume flow rate (Q_{TP}) of the two-phase mixture. As can be seen in Eq. (1):

$$GVF = \frac{Q_g}{Q_{tp}} = \frac{Q_g}{Q_w + Q_g} \quad (1)$$

On the other hand, introducing the Chilsom (1985) slip parameter $K = \frac{U_g}{U_l} = \left(\frac{\rho_l}{\rho_g}\right)^{0.25}$, we obtain an expression to calculate the gas void fraction (α_g) of the wet gas flow see Eq (2):

$$\alpha_g = \frac{1}{1 + K \left(\frac{1}{GVF} - 1\right)} \quad (2)$$

Therefore, this expression is used to calculate the pressure wave propagation velocity based on the Wallis (1969) model. The results are shown in the next section.

RESULTS

The model presented in Eq (2) is compared with the no-slip model (Eq 1) and the result is presented in figure 1. From figure is possible to see that when the slip between the phase is considered, a limited band of the gas fraction is predicted under the same conditions of water injection (we consider $Q_1=1,5 L_{PM}$). On the other hand, when the slip parameter is used, the gas fraction can be varied from 97% to 99,6%, showing a strong difference on the previsions of the models. Also, it is seen that the pressure wave speed decrease from 300 M/S/ to 75 M/S when the no slip model is used, but it can be varied from 200 M/S to 50 M/S because the distribution of the water dispersed phase is not uniform along the radial direction of the pipe, being larger near the wall and smaller in the center.

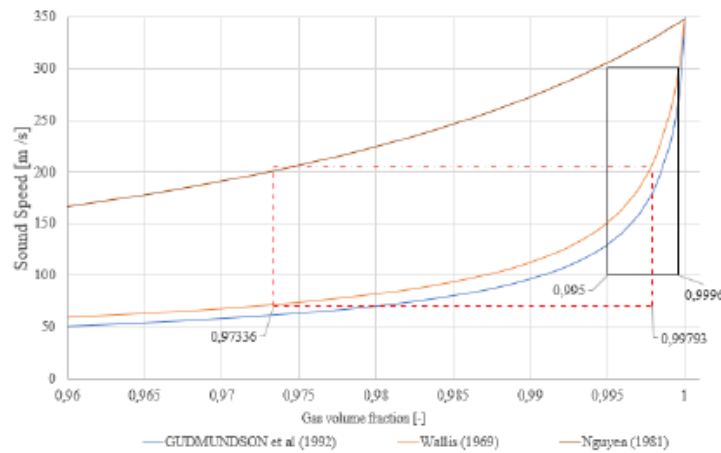


Figure 1. Pressure wave propagation in wet gas flow: influence of the Chilsom parameter on the sound velocity and void fraction.

CONCLUSION

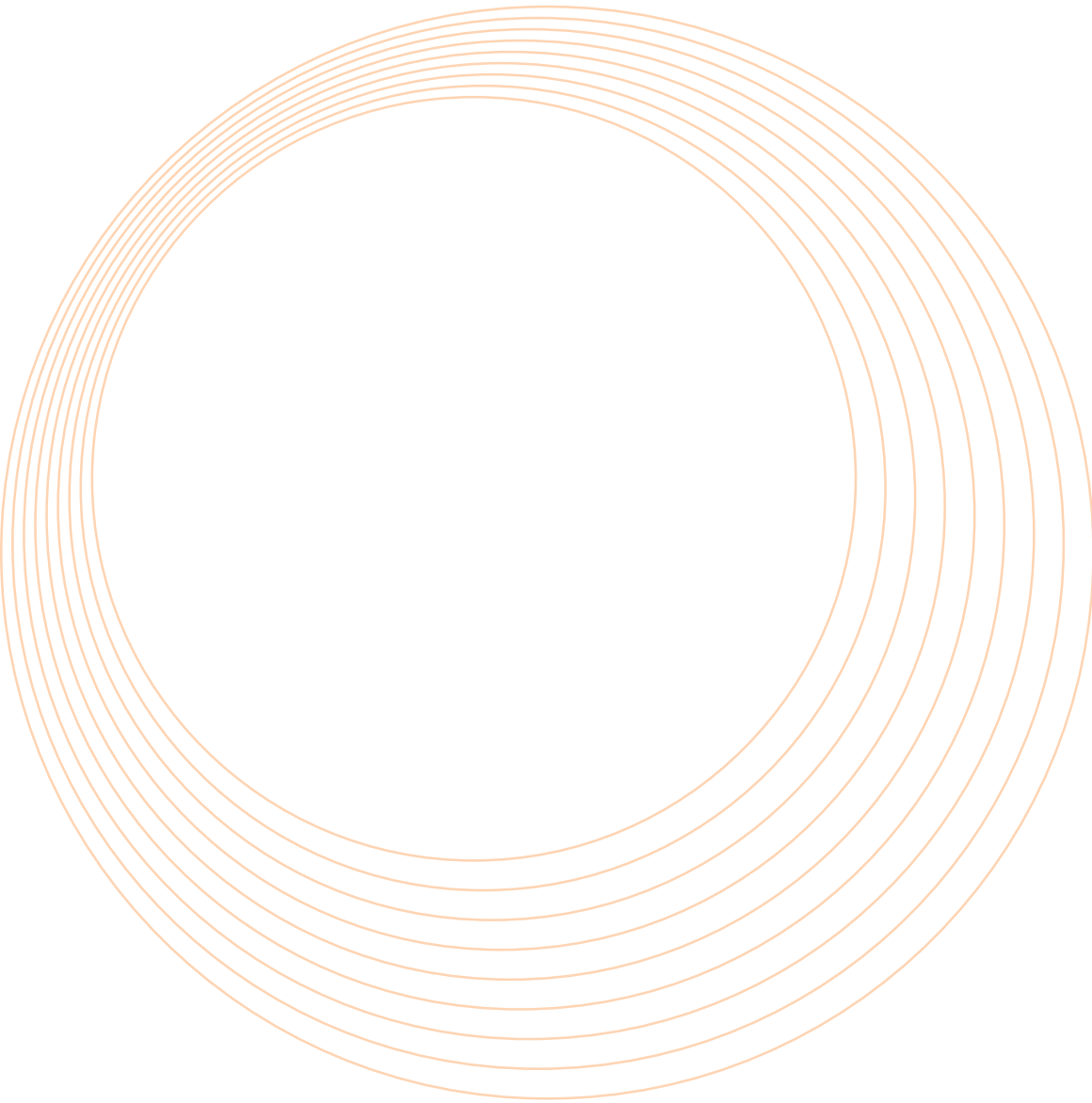
There is strong influence on the slip parameter on the gas fraction predictions and hence, on the sound propagation velocity, due to the variation of the concentration of the drops along the radial direction, this causes variations of 70% on pressure wave propagation. The next step is collecting experimental data and correlates to the two-phase flow rates and the to the pressure wave velocity.

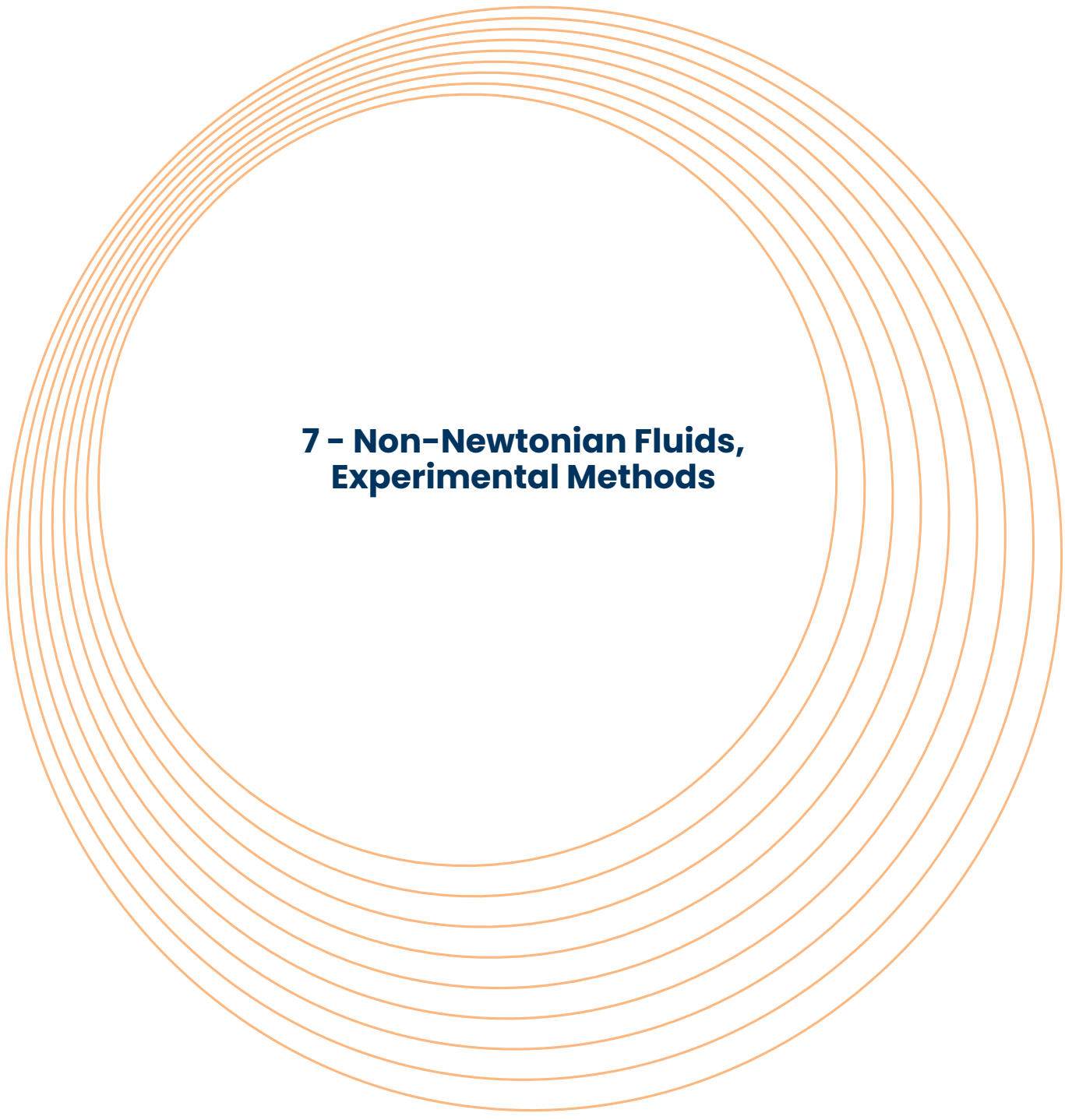
REFERENCES

Chilsom, D. (1985). Two-phase Flow in Heat Exchangers and Pipelines. Heat Transfer Engineering, p. 11.

Hall, A., Graffin, D., & Steven, R. (2007). A Discussion on Wet Gas Flow Parameter Definitions. p. 25.

Steven, R. (4-8 de June de 2000). Wet Gas Metering with a Horizontally Installed Venturi Meter. IMEKO TC9 Conference, p. 11.





**7 - Non-Newtonian Fluids,
Experimental Methods**

Effect of drag reducing polymer on flow patterns of horizontal air–water flow

Pedro B. P. Panisset, Igor B. de Paula, Luis Fernando Azevedo

Pontifical Catholic University of Rio de Janeiro (PUC–Rio)

Rua Marquês de São Vicente, 225, Gávea – Rio de Janeiro, RJ – Brazil – 22451-900

Emails: dvmarinc@unl.edu.co, pl_panisset@hotmail.com, igordepaula@puc-rio.br, Lfaa@puc-rio.br

ABSTRACT

Polymers additive have been used to reduce friction losses in single-phase pipe flows since 1940. Several studies confirm the benefits of using drag reducer polymers (DRP), but diverge on the basic mechanisms responsible for the effect of polymers on the friction losses. The recent interest of the oil and gas industry to use drag reducing polymers to increase multiphase oil production rates has raised additional questions on the basic mechanisms for this complex flow. Researches on the use of DRP in multiphase flows, especially in gas/liquid flow, have not yet been able to elucidate all questions regarding the influence of these agents on certain characteristics of two-phase flows. In this work, an experimental study was carried out to investigate the influence of a guar gum polymer on the air/water flow patterns in a horizontal 40-mm diameter acrylic pipe. Three flow regimes (stratified, elongated bubble and slug) were investigated in a range of gas and liquid surface velocities equal to $0.2 < j_g < 4\text{m/s}$ and $0.1 < j_l < 0.9\text{m/s}$, respectively. During the tests, the rate of polymer degradation was also measured. The tests were performed in a closed circuit loop instrumented with pressure transducers, a capacitive void fraction sensor, to characterize the flow pattern; and a fast camera for flow visualization. In the intermittent flow regime, bubble mean velocity, bubble frequency and void fraction was analyzed. Preliminary results suggest that the drag reducer polymer is capable of reducing the pressure drop in intermittent flow in addition to promoting modifications in the flow pattern.

KEYWORDS

two-phase flow, drag reducer polymer, intermittent flow

INTRODUCTION

Drag reducer agents (DRA) like fibers, surfactants and polymers have become more important in the oil/gas industries over the years because of the capability of increasing oil production rate and transportation. Many researches have focused on characterize long chain polymers with high molecular weights because of its high effectiveness only with a few parts per million of the material. For example, Al-Sarkhi and Hanratty (2001a) reported a DR of 48% using 10 ppm of polymers solution in air/water horizontal flow. Effects of geometry, surface roughness, molecular weight, chain flexibility, pH, temperature and others on drag reducer polymers (DRP) response were studied along the years and summarized by A. Abubakar (2014) for single and multiphase flows. In the literature is well accepted that drag reduction effect needs a turbulent regime to be detected (Virk, 1975) because it is necessary a certain amount of flow shear stress for trigger the polymer solution damping. The drag reduction can be increased by incrementing polymer concentration and/or the Reynold number until reaches a maximum value. Beyond this maximum point there is no advantage in increase theses parameters. White and Mungal (2008) showed that there is, in a single phase flow, a maximum drag reduction trend achieved by increasing polymer solution for a fixed Reynolds number or increasing the Reynolds number and fixing the concentration, Fig. 1. The author called this trend as maximum drag reduction asymptote.

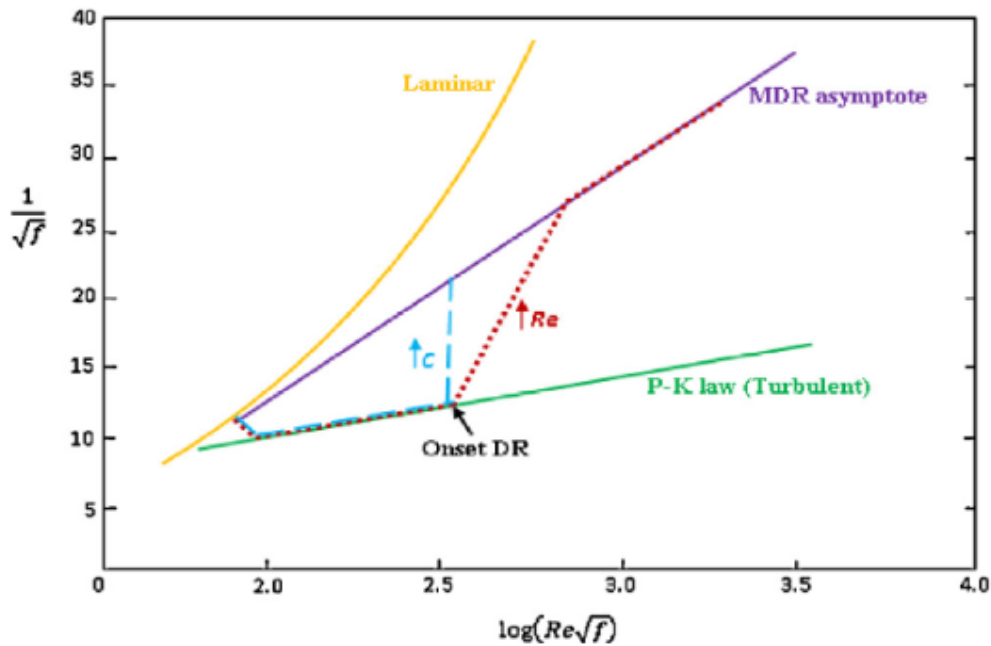


Figure 1: A schematic illustration of onset and different trajectories of polymer drag reduction. The dashed line represents the case in which Re is fixed (at the value when the onset of drag reduction is first observed) and polymer concentration, C , is increased. The dotted line represents the case in which C is fixed and Re is increased (White and Mungal, 2008).

In a multiphase flow, specially in gas/liquid flow, there are different flow patterns appearance, such as: stratified flow, intermittent flow, annular flow and bubbly flow. Intermittent flows are typically characterized by pressure drop and statistical analysis of the slug length, frequency, translational velocity, void fraction and liquid holdup. First studies concerning the influence of DRP in two phase flows targeted pressure drop measurements. One of the first investigation of drag reduction polymers in two-phase flow was made by Greskovich and Shrier (1971). The authors measured DR in a horizontal air-water flow and reported a drag reduction of 40-50% in slug flow regime.

Findings of Rosehart et al (1972) showed that, similarly to the single-phase flows, exists an asymptote limiting the maximum drag reduction effect in two-phase flows. Interesting results from earlier Scott and Rhodes (1972) research showed that two-phase flow drag reduction, in an air-water horizontal flow, can reach higher values than single-phase flow. N.D. Sylvester et al (1980) suggested that drag reduction have not only a relationship with shear stress but also with a liquid/gas ratio. According them, drag reduction decreased rapidly as the liquid/gas ratio approached zero. Their findings agree well with the Otten and Fayed (1976) research. Kang and Jepson (1998) investigate the effect of drag reducer agents in single and three phase flows. According the authors, DRA was effective in reducing pressure gradient in all single and multiphase flows reaching up to 81% of pressure drop reduction using only 75 ppm of DRA. Some researches shed light on the effect of DRP on flow patterns diagrams because as DRP reduce pressure drop, eventually, may alter the two phase flow regime. Kang and Jepson (2000) used amounts of 50 ppm to investigate flow patterns modifications in a large diameter pipeline, oil-gas horizontal flow. They noted that slug flow can change to stratified flow and achieved an average pressure drop reduction up to 82%. Soleimani 2002 observed another aspect focusing on investigate stratified to slug flow transition at high gas velocities. Polymers addition to stratified flow increased the critical liquid holdup and critical superficial liquid velocity needed to transition happens. In other paper from Soleimani (2004), the authors reported a more pronounced effect of DRP on stratified to annular transition than stratified to slug transition, which effect is better detected in terms of slug frequency.

Al Sarkhi (2013) carried out an experimental research about the influence of DRP on the slug frequency, pressure drop and liquid holdup for a range of superficial liquid velocities from 0.2 to 0.8 m/s and the superficial gas velocities from 1 to 7 m/s. The experiments cover stratified and transition to slug flow regimes. The frequency of slugging appears to increase with increasing the superficial liquid velocity but the increasing frequency with DRP was much less than without DRP mainly for high superficial gas velocities. Pressure drop results showed that the drag reduction is seen for superficial liquid velocities higher than 0.05 m/s, at this point they measured a 67% of drag reduction. Finally, the liquid holdup with DRP was larger than that for air-water flow without DRP. The author conclude that exist a threshold under which the flows lacks the existence of disturbances waves or turbulent liquid flow and the drag reduction is not observed, agreeing with some observations made by Soleimani (2002, 2004). Most of works have been looking for pressure drop measurements, flow maps observations and liquid holdup measurements. Even today there is a lack of information about changes in two phase flow statistics and predicted friction factor due to the use of drag reducer polymers. The objective of this work is measure the effect of guar gum drag reducer on slug frequency, length, slug velocity and pressure drop in a horizontal pipe air-water flow. Additionally, a modified Lockhart-Martelli friction factor is proposed to estimate drag reduction in two-phase flow.

REFERENCES

- IAI-Sarkhi, A., Hanratty, T.J., 2001a. Effect of drag-reducing polymers on annular gas-liquid flow in a horizontal pipe. *International Journal of Multiphase Flow* 27, 1151-1162.
- A. Al-sarkhi, A. Soleimani, 2004. Effect of Drag Reducing Polymers on Two-Phase Gas-Liquid Flows in a Horizontal Pipe, *Chemical Engineering Research and Design*, 82, 1583-1588.
- Al-Sarkhi, A. Effects of Drag-Reducing Polymers on Stratified and Slug Gas-Liquid Flows in a Horizontal Pipe. *Arab J Sci Eng* 38, 699-704 (2013)
- A.Abubakar, T. Al-Wahaibi, Y. Al-Wahaibi, A.R. Al-Hashmi, A. Al-Ajmi, 2014. Roles of drag reducing polymers in single- and multi-phase flows. *Chemical Engineering Research and Design*, 92, 2153-2181.
- Fossa, M.; Guglielmini, G.; Marchitto, A. Intermittent flow parameters from void fraction analysis. *Flow measurement and instrumentation*, v. 14, n. 4-5, p. 161-168, 2003.
- Greskovich, E.J., Shrier, A.L., 1971. Drag reduction in two-phase flows. *Industrial & Engineering Chemistry Fundamentals* 10, 646-648.
- Kang, C., Kerr, H., Vancko, R.M., Green, A.S., Jepson, W.P., 1998. Effect of drag-reducing agents in multi-phase flow pipelines. *Journal of Energy Resources Technology* 120, 15-19.
- Kang, C., Jepson, W.P., 2000. Effect of drag-reducing agents in multiphase, oil/gas horizontal flow. *Society of Petroleum Engineers* 58976, 1-7.
- Nydal, O. J.; Pintus, Sandro; Andreusii, Paolo. Statistical characterization of slug flow in horizontal pipes. *International journal of multiphase flow*, v. 18, n. 3, p. 439-453, 1992.

The 7th Multiphase Flow Journey

Otten, L., Fayed, A.S., 1976. Pressure drop and drag reduction in two-phase non-Newtonian slug flow. *Canadian Journal of Chemical Engineering* 54, 111–114.

Rosehart, R.G., Scott, D., Rhodes, E., 1972. Gas-liquid slug flow with drag-reducing polymer solutions. *AIChE Journal* 18 (4), 744–750.

Scott, D., Rhodes, E., 1972. Gas-liquid slug flow with drag reducing polymer solutions. *AIChE Journal* 18, 744–750.

Sylvester, N.D., Dowling, R.H., Brill, J.P., 1980. Drag reductions in concurrent horizontal natural gas-hexane pipe flow. *Polymer Engineering & Science* 20, 485.

Soleimani, A., Al-Sarkhi, A., Hanratty, T.J., 2002. Effect of drag-reducing polymers on pseudo-slugs—interfacial drag and transition to slug flow. *International Journal of Multiphase Flow* 28, 1911–1927.

Virk, P.S., 1975. Drag reduction fundamentals. *AIChE Journal* 21, 625–656.

White, C.M., Mungal, M.G., 2008. Mechanics and prediction of turbulent drag reduction with polymer additives. *Annual Review of Fluid Mechanics* 40, 235–256.

Numerical study of capillary thinning dynamics with FENE-P model

Rafael A. Figueiredo, Cassio M. Oishi and Alexandre M. Afonso

ABSTRACT

The influence of oil combined with the non-Newtonian properties of the viscoelastic fluid presents an interesting challenge in Computational Rheology. In this work, we numerically investigated this type of interaction using a rheometer known as CaBER. This study is an extension of our previous work [1], now considering the FENE-P model. We presented the impact of the extensibility parameter on the viscoelastic filament stretching dynamics for two outer fluid conditions. As the viscoelastic extensibility parameter decreases, the finite time breakup filament is anticipated, which is consistent with results in the literature.

FLOW PROBLEM DESCRIPTION

This work focuses on the flow of a viscoelastic filament stretching between two parallel plates, a configuration commonly found in extensional rheometry. To simplify numerical modeling, we assumed stationary top and bottom boundaries and initialized the interface with a predetermined shape given by $\frac{R(z)}{R_p} = 1 - \left(1 - \frac{R_0}{R_p}\right) \cos\left(\frac{\pi z}{L_z}\right)$. An axisymmetric system with the same computational mesh

as in a previous work [1] was adopted. We performed a numerical study to investigate the influence of the oil bath and the FENE-P extensibility parameter, following an experimental proposal to mitigate the effects of inertia and beads-on-a-string (BOAS) structures.

GOVERNING EQUATIONS

In order to simulate the micro-scale extensional flow with FENE-P model, we consider the following set of governing equations:

$$\begin{aligned} \nabla \cdot \mathbf{u} &= 0, \\ \rho \left(\frac{\partial \mathbf{u}}{\partial t} + \mathbf{u} \cdot \nabla \mathbf{u} \right) &= \nabla \cdot (-p\mathbf{I} + \boldsymbol{\tau} + 2\mu_s \mathbf{D}) + \mathbf{F}, \\ \lambda \overset{\nabla}{\mathbf{A}} &= - \left(\left(\frac{L^2}{L^2 - Tr(\mathbf{A})} \right) \mathbf{A} - \left(\frac{L^2}{L^2 - 3} \right) \mathbf{I} \right) \\ \frac{\partial f}{\partial t} + \nabla \cdot (f\mathbf{u}) &= 0, \end{aligned}$$

where \mathbf{u} is the velocity field, t is the time, ρ is the fluid density, μ_s is the Newtonian solvent viscosity, p is the pressure, \mathbf{F} is the surface tension contribution, \mathbf{D} is the rate of deformation tensor, $\boldsymbol{\tau}$ is the polymeric extra-stress tensor, λ is the relaxation time, μ_p is the polymer viscosity coefficient, L is the extensibility parameters, \mathbf{A} is the conformation tensor and f is the volume fraction used in the volume-of-fluid method. The dimensionless numbers defined for this problem are the Ohnesorge number, $Oh = \mu_1 / \sqrt{\rho R_p \sigma}$, the solvent viscosity ratio $\beta = \mu_s / \mu_1$ the Deborah number, $De = \lambda / t_c$ where $\mu_1 = \mu_s + \mu_p$ and $t_c = \sqrt{\rho R_p^3 / \sigma}$ is a characteristic time scale. The subscript 1 refers to the viscoelastic fluid while the subscript 2 refers to the Newtonian phase, air or oil. The numerical method is explained in detail in [1], and so it is not repeated here.

RESULTS

The Fig. 1 shows the dynamics of the viscoelastic filament stretching for different values of the extensibility parameter L^2 and two outer fluid conditions. In the case of the external phase being air, the appearance of BOAS was observed, just to $L^2 \geq 10000$. On the other hand, the experiment conducted in an oil bath prevented the formation of BOAS. In the case of air, for values of $L^2 < 10000$ the filament breaks prematurely and the appearance of BOAS did not occur. The time evolution of the filament radius and the finite breakup time are in agreement with theoretical results from the literature.

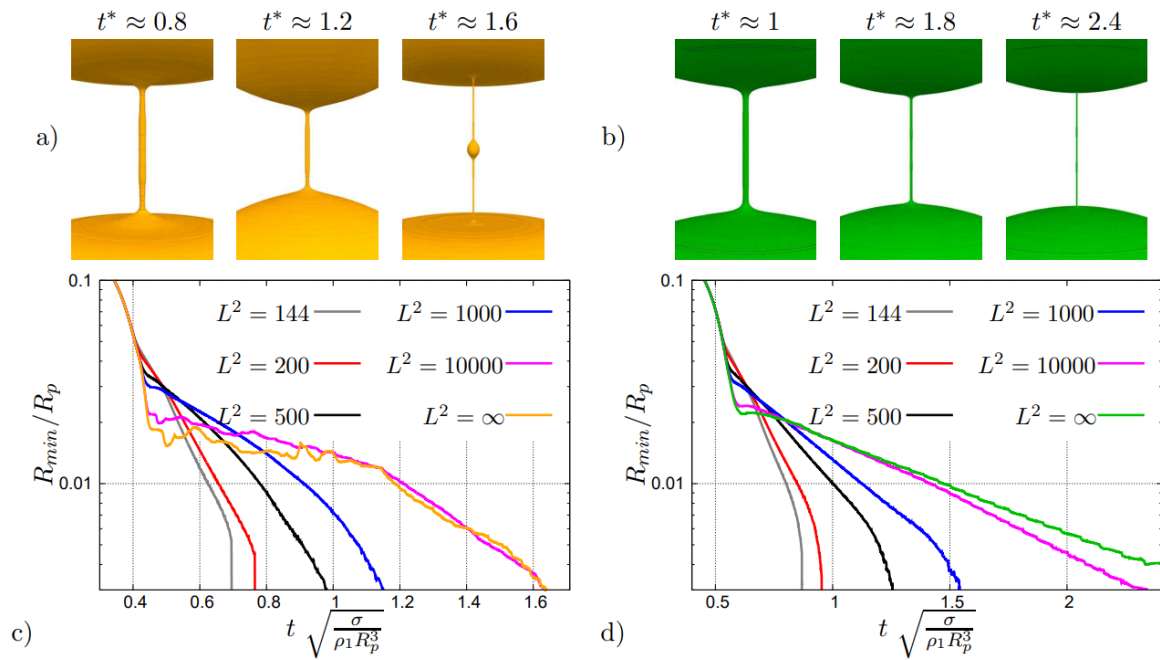


Figure 1: a) and b) show the shape of the filament stretching at different non-dimensional times ($t^* = t/t_c$), with $L^2 = \infty$ and the external phase being air and oil, respectively. In the case of air, we have $Oh = 0.0234$, $De = 0.427$, $\beta = 0.5$, $\mu_1/\mu_2 = 111$ and $\rho_1/\rho_2 \approx 813$, while in the case of oil, $Oh = 0.0316$, $De = 0.316$, $\beta = 0.5$, $\mu_1/\mu_2 = 2$ and $\rho_1/\rho_2 \approx 1.18$. c) and d) show the transient computation of the minimum filament radius with the FENE-P model, surrounded by a Newtonian fluid, air and oil, respectively.

CONCLUSIONS

The numerical study of capillary thinning dynamics of FENE-P model with different external newtonian fluids presented agreement with experimental results from the literature [2]. Furthermore, we presented the influence of the extensibility parameter with a weakly viscoelastic polymer solution. As far as we know, such flow types with more complex viscoelastic models have not been reported in previous numerical studies.

REFERENCES

- [1] R.A. Figueiredo, C.M. Oishi, A.M. Afonso, M.A. Alves, Numerical study on micro-scale extensional viscoelastic flows, J. Non-Newton. Fluid, 276, (2020), pp. 104219, 10.1016/j.jnnfm.2019.104219.
- [2] P.C. Sousa, E.J. Vega, R.G. Sousa, J.M. Montanero, M.A. Alves, Measurement of relaxation times in extensional flow of weakly viscoelastic polymer solutions, Rheol. Acta, 56 (2017), pp. 11–20, 10.1007/s00397-016-0980-1.

ACKNOWLEDGMENTS

The authors acknowledge the financial support of the FAPEMIG Grants APQ-01925-21 and the computational support provided by the FCT/UNESP Numerical Simulation Laboratory.

Mesurement System for the airflow of an EA211 1.0 MPI Volkswagen engine

F.Frejat, F Lisboa

ABSTRACT

This work aims to implement a measurement system for the airflow of an EA211 1.0 MPI Volkswagen engine. Based on the theoretical basis of mass flow calculation, a system was implemented in the laboratory that allowed obtaining, through the difference in pressure and air velocity and using ways to calibrate the measuring nozzle, the discharge coefficient of the entire system. From these data, it was possible to obtain the theoretical and absolute values of the mass flow of air entering the engine. With these results, it was possible to conclude that any sensor that measures pressure or flow must, considering experimental errors, coincide with the mass flow value obtained through the implemented system.

INTRODUCTION

Based on the idea of replacing fossil fuels such as gasoline and diesel with renewable sources, the Biogás project seeks to operate a commercial engine fueled by Biomethane from biodigestion processes. Several mechanical and engine control changes are necessary for the operation of this type of engine, as the instrumentation and measurement of gaseous and mass flow are the targets of this project.

Thus, it is necessary to know the parameters of the engine, understand its correct operation, and calculate the measurement values correctly. With a very detailed knowledge, applying biogas and obtaining its mass flow rate is vital for the project to be presented in a way that explains its efficiency and performance.

For correct air flow calculations, it used devices such as a pulse damping box, calibrated orifice plate, instruments for measuring the differential pressure, and software for acquiring and recording the measured values. Based on the measured quantities, verifying the engine's operating parameters, and calculating its efficiency, fundamental indicators for converting the desired fuels were possible.

This work shows the air flow measurement system present in the engine test laboratory of Faculdade Gama, Universidade de Brasília, and its calibration to obtain the discharge coefficient. It was possible to calibrate the entire system in the laboratory using a pulse dampening box, an object with known air mass flow connected to the box, and a differential manometer connected next to the orifice plate on the box. Thus, this system will be applied to the engine under study to obtain the actual mass air flow value and later compare it with the values presented by the flow sensors. The preliminary results refer to the discharge coefficient of the measuring nozzle and the orifice plate belonging to the damper box.

METHODOLOGY

The mass air flow measurement system was installed in the laboratory. It has a pulse dampening box. At one of its ends is an orifice plate and a thin tube next to the plate, which connects to a differential manometer inside the laboratory. At the other end, a duct connects to the engine intake inside the laboratory.

As the objective is to discover the mass flow that enters the engine through this system, it was necessary to calibrate it. The calibration method was to replace the engine with a known airflow apparatus. The device used was a vacuum cleaner.

The vacuum cleaner airflow was obtained using an anemometer to measure the air velocity, a caliper for the vacuum tube diameter, the cross-sectional area equation, and the air density. When connecting it to the system duct and turning it on, the water that filled the manometer suffered a height difference, indicating pressure variation.

Also, by measuring the diameter of the nozzle and the orifice plate, using the pressure difference and the pressure in the nozzle section, it was possible to obtain the mass flow of the aspirator, the nozzle and the plate. With these flows, the discharge coefficient of the system was calculated, nozzle and plate coefficients.

RESULTS AND CONCLUSION

After the system calibration process, some results obtained were preliminary. Despite the measurements being made using experimental error, the error was not propagated because it is a preliminary measurement system analysis.

The main value found was the discharge coefficient. This coefficient is essential as it allows to find the mass flow from it. Knowing its correct value, it is possible to assume that the system is calibrated. When using the Volkswagen EA211 1.0 MPI engine, the mass flow is calculated from the already established discharge coefficient.

Preliminary values help in understanding what should be done for the next steps. These are: the inclusion of errors in the calculations; validation of calculated values, such as discharge coefficient, mass airflow, and transfer function of flow sensors; convergence of the values analyzed experimentally with the values presented by the ECU, acquired by the flow sensor; biofuel mass flow analysis in the engine; and validation of the system so that another bench engine can be tested and be able to measure its mass airflow parameters correctly.

Analysis of velocity fields during Hydrogen production by eletrolysis

Jeferson Diehl de Oliveira, Thomas Willians Leite, Elaine Maria Cardoso, Jacqueline Biancon Copetti

FSG – University Center, Center of Innovation and Technology,

UFRGS – Federal University of Rio Grande do Sul,

UNESP – São Paulo State University, UNISINOS – University of Vale do Rio dos Sinos

*jeferson.oliveira@fsg.edu.br

ABSTRACT

This study is devoted to analyzing hydrodynamic behavior and mass transfer performance in water electrolysis processes in an alkaline solution (30% wt KOH) under different current densities, using vertical electrodes with different gaps between them in an electrolyzer made of glass (200 mm X 296 mm X 200 mm). An optical flow method is implemented to study velocity fields of hydrogen bubbles based on image sequences captured by a CCD camera with a $200\ \mu\text{m}$ /(pixel length) with 120 frames per second. In this case, the influence of current density between 36.5 and 223 A/m^2 was investigated. The experimental results show that the velocity distribution in most regions of the electrolyzer is dominated by two asymmetry bubble buoyancy-induced flow patterns caused by hydrogen and oxygen plumes. The increasing velocity and vorticity fields are observed in regions near the electrolyte's surface, increasing turbulence. However, the vertical velocity component does not present considerable variations in relation to the depth of the electrode wall. Due to the more intense hydrogen generation, the greatest velocity fluctuations are found near the cathode. The average velocity of the hydrogen bubbles increases with increasing the current density up to 136 A/m^2 for a gap between the electrodes equal to 40 mm. However, the average velocity decreases for higher current densities due to increased turbulence zones. Hydrogen production, bubble-driven convection and convective mass transfer increase at higher current densities, but this increase are not linear; the interaction mechanisms are investigated in an electrochemical reaction, mass transfer and bubble effect. Complex structures generated by turbulence considerably affect bubble dynamics. Such results facilitate understanding the transport phenomena of hydrogen bubbles in the electrolyzer.

KEYWORDS

Hydrogen Generation, Renewable Energy, Electrolysis, Velocity Field

INTRODUCTION

Several issues involving the generation and transformation of energy have been the focus of much concern in recent years, especially regarding the environmental consequences. Thus, the need to generate greener forms of energy has drawn attention. Hydrogen generation through water electrolysis processes is a viable alternative using solar panels to supply electrodes (Dincer, 2012). In fact, during water electrolysis, electrons flow through the anode to the cathode, where hydrogen ions incorporate them to form hydrogen gas. In this way, the dissolved gas accumulates until it reaches a critical condition of supersaturated concentration at the electrode surface, initiating bubble nucleation (Van Damme et al., 2010). Several experimental and theoretical investigations have been reported in the literature studying various aspects of water electrolysis, including bubbles' main fluid dynamical characteristics. Abdelouahed et al. (2014) studied the hydrodynamics of gas bubbles during water electrolysis using NaOH as an electrolyte and investigated the distributions of bubble velocities and void fractions in the anode-to-anode space. The effects of the anode gap, current density and cell inclination on the hydrodynamics of the gas phase were followed. Mohammed-Ibrahim and Moussab (2020) summarized the discussion on the use of seawater for hydrogen generation, pointing out important aspects, including competition of chlorine evolution reaction (CIER) with oxygen evolution reaction (OER) on the anode, salinity and temperature of the electrolyte

EXPERIMENTAL FACILITY AND METHODOLOGY

Figure 1 presents the schematic of the experimental setup used to investigate the bubble dynamics. Such a setup consists of a test section that includes a cubic container with 80 mm edge and a DC power supply model Minipa MPL-3305. The working electrodes are made of stainless steel 304 (19% chrome and 9% nickel). The choice of this material is due to its stability in an alkaline medium. Both electrodes have 30 mm wide and 70 mm long, arranged vertically with a 20 mm gap. The experiment was performed at room temperature, i.e., around 20 °C with a 30 %wt KOH aqueous solution in deionized water. Considering the optical flow equation, an optical flow method was implemented to estimate velocity fields.

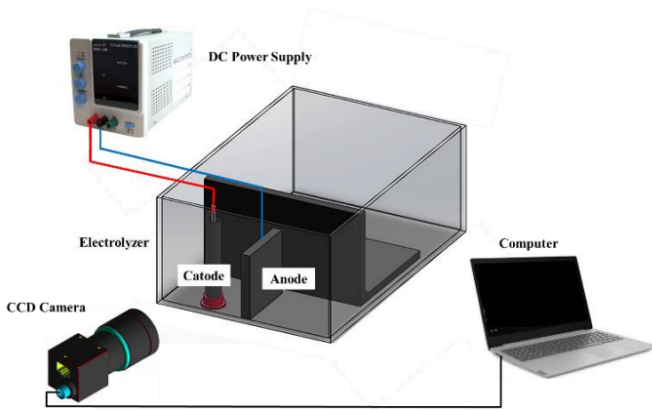


Figure 1 - Experimental setup

Properties and Parameter	Value/Range
<i>Molar mass</i> [mol/l]	5.34
<i>Density of electrolyte</i> [kg/m ³]	1237
<i>Viscosity of electrolyte</i> [kg/(m·s)]	1.731x10 ⁻³
<i>Current density</i> [A/m ²]	190-650

Table 1 - Experimental parameters

RESULTS

Figure 4 presents a sequence of images with respective velocity fields generated by the optical flow method. As expected, velocity fields with greater intensity can be observed in regions over the cathode. The increase in bubble velocity also increases with increasing current density, indicating the greater production of bubbles. Instabilities caused by variations in velocity gradients generate turbulent zones, thus making it challenging to release bubbles through the electrolyte.

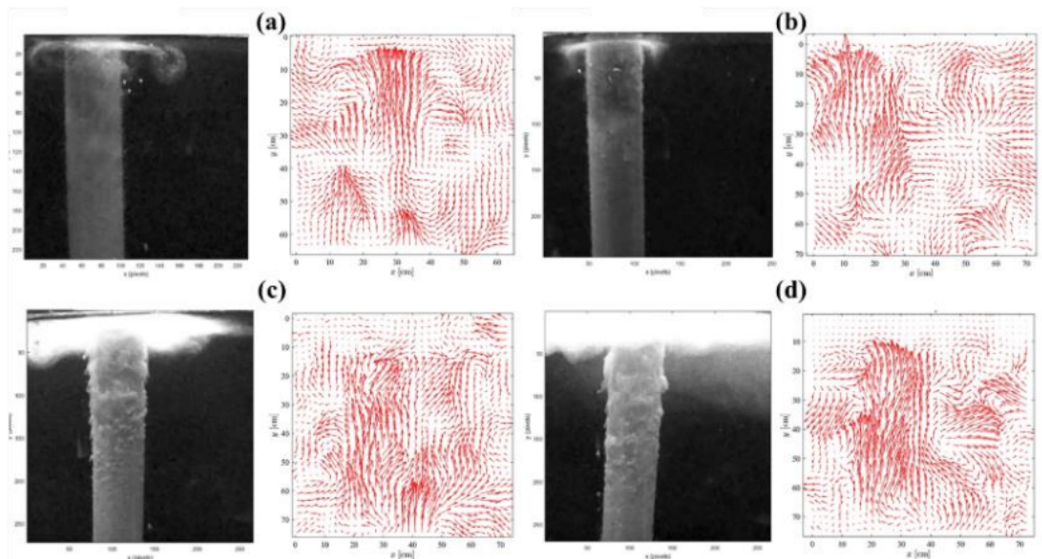
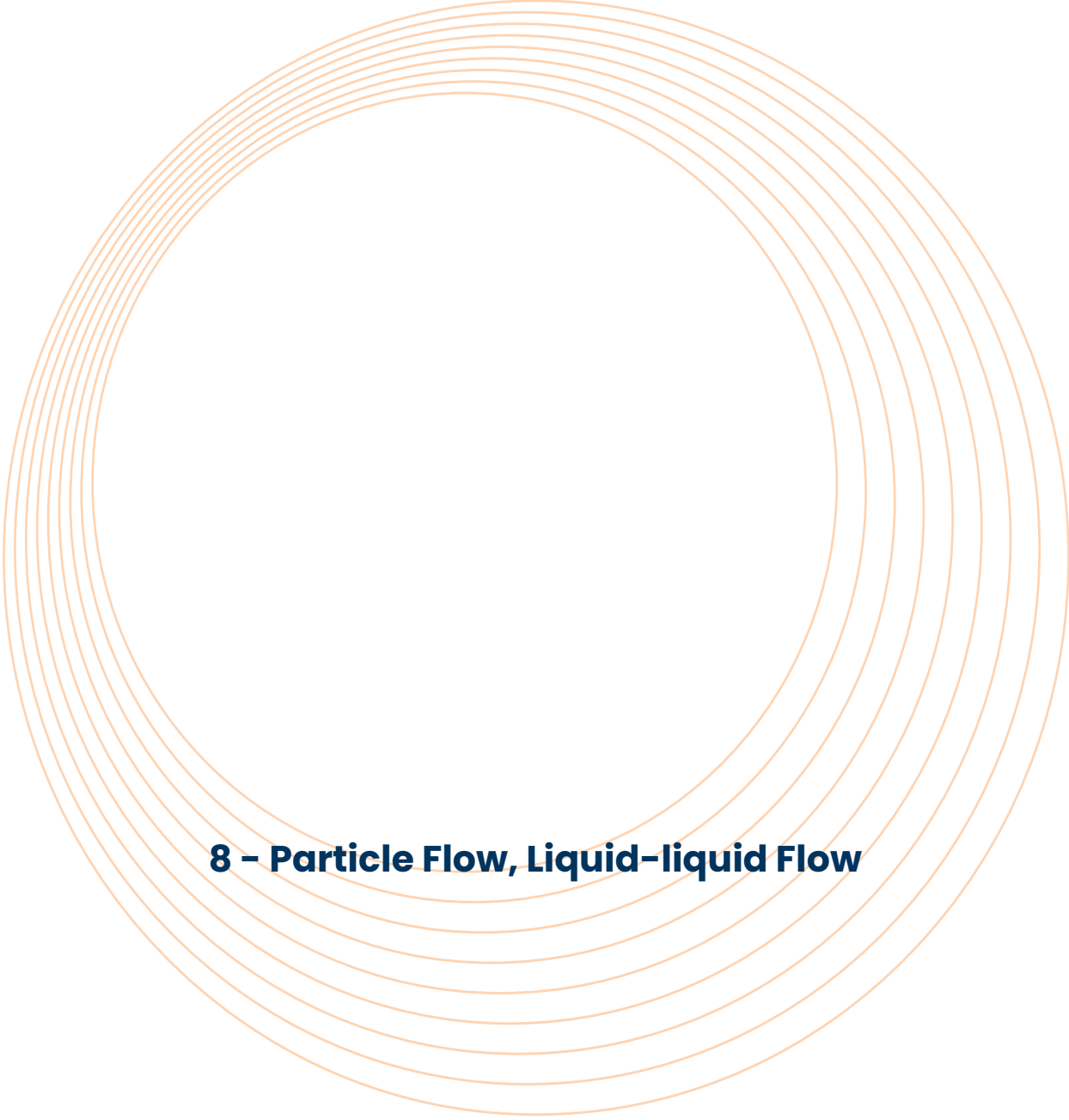


Figure 2 – Images and velocity fields with a gap of 40 mm for (a) 36.5, 91.35, 182.7 and 225.33 A/m².

REFERENCES

- Abdelouahed, L., Hreiz, R., Poncin, S., Valentin, G. and Lopicque, F., 2014. "Hydrodynamics of gas bubbles in the gap of lantern blade electrodes without forced flow of electrolyte: Experiments and CFD modelling". *Chemical Engineering Science*, Vol. 111, p. 255–265.
- Dincer, I., 2012. "Green methods for hydrogen production". *International Journal of Hydrogen Energy*, Vol. 37, p. 1954–1971.
- Mohammed-Ibrahim, J. and Moussab, H., 2020. "Recent advances on hydrogen production through seawater electrolysis". *Materials Science for Energy Technologies*, Vol. 3, p. 780–807.
- Van Damme, S., Maciel, P., Parys, H.V., Deconinck, J., Hubin, A. and Deconinck, H., 2010. "Bubble nucleation algorithm for the simulation of gas evolving electrodes". *Electrochemistry Communications*, Vol. 12, p. 664–667



8 - Particle Flow, Liquid-liquid Flow

Effect of concentration on particle velocity and erosion at T-junctions

A.E. Lima Silva¹, D.A. Silva¹, A. G. Sabino, A.P. Silva Freire¹, C. Potosi¹,
¹Nucleo Interdisciplinar de Dinâmica dos Fluidos (NIDF/UFRJ), Universidade Federal do Rio de Janeiro

INTRODUCTION

Introduction

Erosion by solid particles on equipment in the petroleum industry is a common problem. During oil production, normally the fluids that are extracted from the reservoir and transported to the processing platform are loaded with sand. Solid particles cause abrasive wear in pipes, connections and valves existing in industrial processes, contributing to failure or reduction of life of equipment. Therefore, understanding how erosion works is of great relevance to prevent damage caused by the impact of solid particles on walls, contributing to safer and more effective processes. Tee fittings are crucial elements in oil recovery pipelines and are components susceptible to erosion. One aspect that is not clearly elucidated in the literature is the erosion rate variation and the trajectory behavior of the particles that collide with T as the concentration increases for the same flow conditions. The current study aims to evaluate the degree of erosion and how it develops in tee-junction with a square profile and the behavior of the velocity of solid particles (silicon carbide) as the concentration increases in the continuous medium (water).

METHODOLOGY

Erosive behavior is related to several loading parameters, both in the continuous phase and in the discrete phase. Variables such as velocity, particle shape and dimensions, impact angle, material properties, among others, influence the erosion rate, becoming a complex problem to be studied. Several CFD and experimental studies in the literature evaluate the behavior of the particles in relation to the continuous medium and eroded surfaces for small concentrations of sand.

In the present, closed-circuit experiment, a loading of solid particles with an average diameter of 150 micrometers and concentrations of 0.05 to 1.1% in water was considered. The T geometry was an acrylic closed bifurcation fitted with two aluminum plates, one in the bottom and another on the side of the joint. The experiment lasted 32 hours. Throughout the test, samples were taken to evaluate the concentration and the average diameter of the particles.

Characterizations of eroded aluminum surfaces were obtained through digital optical microscopy and profilometry. The erosion rate was determined by the mass removed during the experiment time. Measurements were performed with PIV to characterize the properties of the continuous and the discrete phases. Particle diameter was measured during the experiment through laser diffraction.

RESULTS AND CONCLUSION

The work shows that for concentrations over 0.1%, the role of particle-to-particle interaction becomes relevant. The characterizations allowed understanding that the side wall of the tee interface has a high erosion rate when uncovering the back wall. It was also possible to evaluate the most eroded areas for each plate, determining the places of greatest erosion for the conditions of the experiment. The PIV measurements allowed evaluating the velocities of particles for concentrations up to 1.1%. Under this condition, the discrete and continuous velocity fields are very different.

Numerical Simulation of Particle Erosion in Slurry Flow in Squared T-Junctions

E. R. David², D. A. Rodrigues², A. P. Silva Freire^{1,2}

¹Mechanical Engineering Program (PEM/COPPE/UFRJ), Rio de Janeiro, Brazil

²Interdisciplinary Center for Fluid Dynamics (NIDF/UFRJ), 21941-972, Rio de Janeiro, Brazil

ABSTRACT

Sand particles are often present in oil and gas production. Their presence can severely damage completion devices by erosion. Thus, erosion prediction in particle-laden flows is a valuable resource. Finnie (1960) was the first to propose a model to predict erosive wear, based on purely mechanistic assumptions. Oka and Yoshida (2005) performed experiments with different combinations of particle and target materials and developed means of finding calibration constants as a function of Vickers hardness. The present work demonstrates how to predict erosion damage using numerical simulations, applied to a squared-T geometry. The free and open source project, OpenFOAM (Greenshields 2022), was used to determine the fluid dynamics of the water phase and perform a one-way coupling with the solid SiC phase. The wall material was Aluminium 5052. The authors developed a numerical code to calculate the erosion predicted by such models for each particle-wall collision, considering the impact velocity and angle.

Representative particle tracks that were calculated are shown in Figure 1. Figure 2 shows the resulting local erosion profile caused by all particles combined. The work compares the magnitude and location of local eroded material in the side and bottom walls. All numerical simulations are compared to experimental data, including the local wall erosion rate. A discussion on particle-to-particle interaction is introduced.

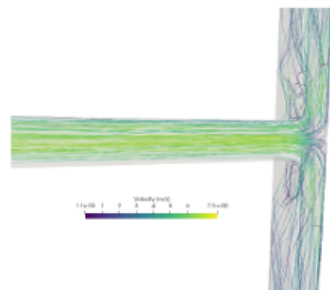


Figure 1. Numerically calculated particle tracks.

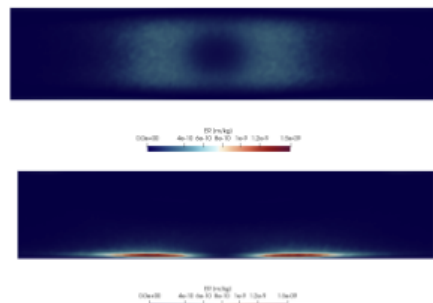


Figure 2. Erosion ratio given by Oka and Yoshida model for the bottom wall (left) and side wall (right)

REFERENCES

FINNIE, I. "Erosion of surfaces by solid particles", *Wear*, v. 3, n. 2, pp. 87-103, 1960.

GREENSHIELDS, C. "OpenFOAM v10 User Guide", 2022.

OKA, Y., YOSHIDA, T., 2005, Practical estimation of erosion damage caused by solid particle impact: Part 2: Mechanical properties of materials directly associated with erosion damage, *Wear*, v. 259, n. 1-6, pp. 102-109.

Experimental investigation of particle-Laden gas-jets impinging on inclined surfaces

J. L. Araujo¹, C. M. P. Rosero^{1,2}, E. R. David², D. A. Rodrigues², A. P. Silva Freire^{1,2}

¹Mechanical Engineering Program (PEM/COPPE/UFRJ), Rio de Janeiro, Brazil

²Interdisciplinary Center for Fluid Dynamics (NIDF/UFRJ), 21941-972, Rio de Janeiro, Brazil

ABSTRACT

Erosion caused by solid particles is a real problem in O&G industry. This phenomenon reduces the life cycle and performance of well components and production systems. There are two critical points to focus: (a) as shown by Parsi (2017) the quantity of parameters involved the understanding of this phenomenon is large and diverse, and (b) most erosion models are developed and calibrated for impinging jet flows. Considering this, the impinging jet geometry is important for the validation of experimental and numerical techniques. In the present work, detailed experiments are carried out for three different Re (28000, 29000, 34000), two particle size distributions (with mean diameters of 40 and 100 μm), four impact angles (30, 45, 60 and 90°) and one type of surface material (AISI 304). A 15Hz 2D-2C PIV system was used to characterize the continuous phase velocity field (Fig.1).

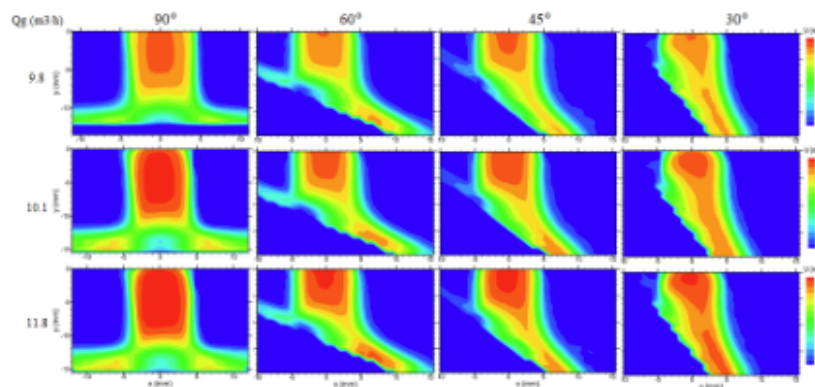


Figure 1. Continuous phase velocity fields for different flow rates and inclination angles. Local 3D erosion profiles were measured with a Profilometer with resolution of 3nm and they are used to validate four different erosion models (Finnie 1960, Oka and Yoshida 2005, Zhang 2007 and Arabnejad 2015). Fig. 2 presents the measured eroded surface profiles compared with results using calibrated models implemented in OpenFOAM.

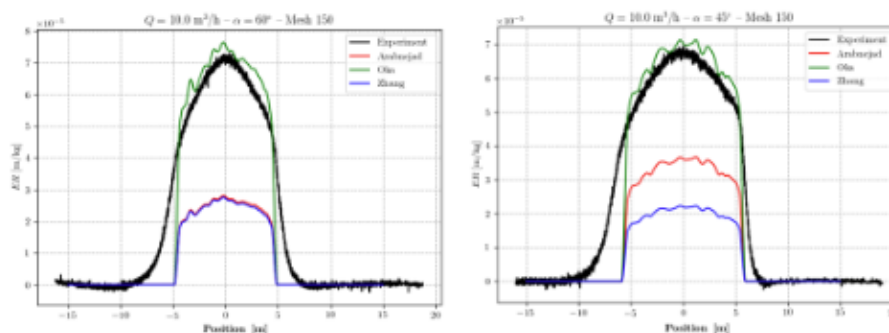


Figure 2. Experimental and numerical erosion profiles comparison.

REFERENCES

REFERENCES

- ARABNEJAD, H., MANSOURI, A., SHIRAZI, S., et al., 2015, Development of mechanistic erosion equation for solid particles, *Wear*, v. 332, pp. 1044-1050.
- FINNIE, I., 1960, Erosion of surfaces by solid particles, *Wear*, v. 3, n. 2, pp. 87-103.
- OKA, Y., YOSHIDA, T., 2005, Practical estimation of erosion damage caused by solid particle impact: Part 2: Mechanical properties of materials directly associated with erosion damage, *Wear*, v. 259, n. 1-6, pp. 102-109.
- Parsi, M., Najmi, K., Najafifard, F., Hassani, S., McLaury, B.S. and Shirazi, S.A., 2014. "A comprehensive review of solid particle erosion modeling for oil and gas wells and pipelines applications". *Journal of Natural Gas Science and Engineering*, Vol. 21, pp. 850-873.
- ZHANG, J. X., BAI, Y. Q., KANG, J., et al., 2017, Failure analysis and erosion prediction of tee junction in fracturing operation, *Journal of Loss Prevention in the Process Industries*, v. 46, pp. 94-107.

Experimental study of water flushed by a mixture of glycerol and water in a horizontal pipe

Elcilane Freitas^{1*}, Murilo Santos¹, Rafaella Silva¹, Marco Conte¹, Eduardo Santos¹, Moisés Neto¹, Rigoberto Morales¹

¹Multiphase Flow Research Center (NUEM), Federal University of Technology – Paraná (UTFPR), Rua Deputado Heitor Alencar Furtado, 5000, Bloco N, CEP 81280-340, Curitiba/PR, Brazil

Email: *elcilaneaf@gmail.com

ABSTRACT

The displacement of a fluid by another is a common technique to cleanse oil and gas pipelines to prevent operational problems such as hydrate blockage and corrosion. This type of operation is called flushing. The optimization of such process, considering the time and volume of fluid spent, demands specific knowledge about the characteristics of the flow so as to enhance the whole process from an economic standpoint. With this scenario in mind, this work presents an experimental study on the flushing of fresh water by a viscous fluid. The viscous fluid was a mixture of water and glycerol with viscosities of 3.5 cP and 8.5 cP. The flow loop consisted of a 8.15-m long, 26-mm ID horizontal pipe, built at the Multiphase Flows Research Center – NUEM, a body of the Federal Technological University of Paraná – UTFPR. Time series of the mixture mass concentration were recorded at two different pipe locations using resistive sensors. Pressure drops between two points were also recorded. The instruments were connected to a data acquisition system and monitored through an interface developed in LabVIEW. The flushing efficiency was analyzed with regard to the viscosity ratios, to the behavior of the pseudo-interface between the fluids and to the required volume of fluid injected to clean the pipe.

INTRODUCTION

Flushing processes used to clean remaining fluids from oil and gas pipelines have been studied over the past years. The characterization of the flow with regard to the difference in viscosities was addressed by some authors. Xu et al. (2011) and (2016) studied the displacement of water by oil in low sections of pipes. They proposed a model to predict the conditions for the onset of water displacement by oil flow from a horizontal section followed by an upward inclined section. They also analyzed the influence of viscosities and densities in the flow. Alba et al. (2013) and Etrati et al. (2018) experimentally investigated the displacement of two miscible fluids, observing the effect of the density ratio on the pseudo-interface instability, the conditions for backflow and the flow displacement efficiency. Schumann et al. (2014) investigated the displacement of oil by tap water concerning the frontal velocity propagation as well as buoyancy and gravitational forces acting in the flow direction. Leuchtenberger et al. (2021) performed a comprehensive analysis on how the displacement of a viscous liquid by a less viscous one occurs in different pipe segments, varying the injection velocity. They suggested a dimensionless group to analyze optimal values for the cleansing time in relation to the flow configuration. As reported above, flushing optimization processes have been analyzed in several ways. Although those analyses describe the behavioral aspects of the flow, they also bring important information such as the influence of the fluid properties and optimal viscosity ratios and measurements of the mixing interface length, allowing the development of models capable of predicting the optimal conditions for the flushing with a low economic cost.

METHODS

In this work two miscible fluids were used: a mixture of tap water and glycerin with two different concentrations resulting in viscosities of 3.5 cP e 8.5cP, and tap water. The experiments were performed in a horizontal flow loop (as shown in Figure 1) of 8.15-m long and 26-mm ID built at NUEM-UTFPR. One camera positioned 5.8 m distant from the pipe inlet captured images of the flow. Time series of the mixture mass concentration were recorded at two different points, 5.135 m and 5.35 m, using resistive sensors. Pressure drops between two points, 2.015 m and 5.335 m, were also recorded. For the experiments with the 3.5-cP injection fluid, the superficial velocities of 0.2, 0.3, 0.4, 0.5 and 1 m/s were tested, whereas for the 8.5-cP injected fluid those velocities were 0.2, 0.5 and 1 m/s. The instruments were connected to a data acquisition system and monitored through an interface developed in LabVIEW.

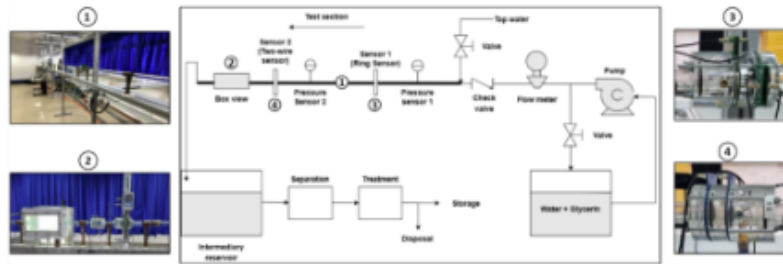


Figure 1: Experimental loop scheme of the test rig and its respective instruments

RESULTS

Figure 2 shows the camera images for the two concentrations used. The difference in the mixing of the phases and consequently in the cleaning efficiency can be clearly seen. The results for the injection fluid of 3.5 cP and lower velocities (0.2 and 0.3 m/s) show a stratified flow pattern, as well as for the 8.5-cP injection fluid(0.2 and 0.5 m/s). For the 3.5-cP fluid and 0.2 m/s, the value of Re is less than 2000 and the flow is laminar, while for 0.3 m/s, $Re \approx 2000$ and it the transition from laminar to turbulent just began. However, a stratified behavior can still be seen. For values of $Re > 2300$, we might already consider transition flow that includes velocities of 0.4, 0.5 and 1 m/s, with flow characteristics similar to plug flow. For a viscosity of 8.5 cP, the appearance of a plug pattern occurs at a velocity of 1 m/s, with a delayed transitional Reynolds range due to the higher viscosity (ABRAHAM et al. 2008). The flushing efficiency will be analyzed with regard to the viscosity ratio, the behavior of the pseudo-interface between the fluids, and the required volume of injected fluid for cleaning the pipeline

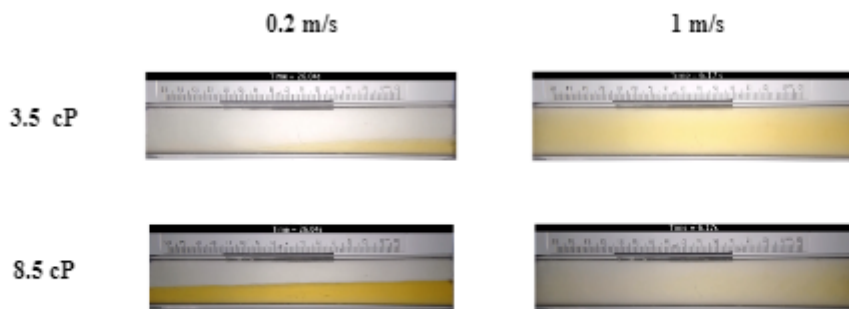


Figure 2: Behavior of the two viscosities in different velocities

CONCLUSIONS

Tests in a horizontal pipe were performed for two different viscosities, in order to flush the water in this pipe. These viscous fluids were injected at different speeds. Cleansing time, flow pattern and viscosity effects will be analyzed and discussed in order to better understand how they influence the flushing process.

REFERENCES

- ABRAHAM, J. P.; SPARROW, E. M.; TONG, J. C. K. Breakdown of laminar pipe flow into transitional intermittency and subsequent attainment of fully developed intermittent or turbulent flow. *Numerical Heat Transfer, Part B: Fundamentals*, v. 54, n. 2, p. 103-115, 2008.
- ETRATI, Ali; ALBA, Kamran; FRIGAARD, Ian A. Two-layer displacement flow of miscible fluids with viscosity ratio: Experiments. *Physics of Fluids*, v. 30, n. 5, p. 052103, 2018.
- ALBA, K.; TAGHAVI, S. M.; FRIGAARD, I. A. Miscible density-unstable displacement flows in inclined tube. *Physics of Fluids*, v. 25, n. 6, p. 067101, 2013.
- LEUCHTENBERGER, Roberto Fernando et al. Experimental Analysis of Water/Oil Displacement Tests in Horizontal Pipe. *SPE Journal*, v. 26, n. 05, p. 2993-3010, 2021.
- SCHUMANN, H. et al. Liquid-liquid displacement in a horizontal and inclined pipe section. In: 9th North American Conference on Multiphase Technology. OnePetro, 2014.
- Xu, G.-l., et al., Trapped water displacement from low sections of oil pipelines. *International Journal of Multiphase Flow*, 2011. 37(1): p. 1-11.
- XU, Guangli et al. Experiments and simulation of water displacement from lower sections of oil pipelines. *Journal of Petroleum Science and Engineering*, v. 147, p. 829-842, 2016.
- SCHUMANN, H. et al. Liquid-liquid displacement in a horizontal and inclined pipe section. In: 9th North American Conference on Multiphase Technology. OnePetro, 2014.

Particle dynamics in wall-bounded turbulence

Bayode Owolabi, Robert Jackel, Luca Moriconi, Juliana Loureiro
Universidade Federal do Rio de Janeiro, NIDF – Rua Moniz Aragao 360, Rio de Janeiro, 21941-594, Brazil

Email: owolabi@ufrj.br

KEYWORDS

Particle-laden-flows, turbulence

ABSTRACT

We investigate particle-turbulence dynamics in a vertical pipe over a parameter space covering a wide range of particle-volume fractions (θ_v), Stokes (St) and Froude (Fr) numbers. First, the effect of inertial particle concentration on the skin friction drag is determined and a correlation for the growth rate of the friction factor with volume fraction of particles is obtained. Using Voronoi diagrams, we examine the motion of dispersed particles to obtain a deeper understanding of particle-wall, particle-particle and particle-turbulence interactions and the competing roles played by inertia and gravitational acceleration.

INTRODUCTION

Turbulent particulate flows are important both in nature and in many industrial applications. Examples include droplets in the clouds, fluidized beds, pharmaceutical sprays, scale formation in pipes among many others. A fundamental physical understanding of these flows is therefore crucial. Due to the compressibility of their velocity field, inertial particles in turbulence exhibit phenomena such as preferential sampling and clustering. Furthermore, in wall-bounded flows, turbophoresis – the migration of particles towards the wall – is observed as a result of the non-homogeneity of the turbulence intensity. The mechanism for these phenomena is not yet fully understood (Balachandar & Eaton, 2010; Brandt & Coletti, 2022).

In this study, we examine the particle-turbulence dynamics in a pipe aligned with the gravitational vector, thus allowing for the investigation of, purely, the influence of turbulence on the wall-normal migration of particles, and obtain data up to the two- and four-way coupling regimes for which there is little information in the literature.

EXPERIMENTAL FACILITY

Experimental measurements were conducted in a rig having a vertical-pipe test section of length 3.45 meters and 44 millimeters in diameter (D). The carrier fluid was recirculated using a positive-displacement pump, the flow direction going from top to bottom. Spherical glass beads having a modal diameter of about 700 microns and a density of approximately 2.5 times that of the carrier fluid were continuously injected into the flow at the top of the pipe but unlike the carrier phase, they were collected at the bottom and not re-circulated. Pressure drop measurements over a length of about $53D$ were conducted using an Endress Hauser differential pressure transducer and high-speed images of particles over a pipe cross-section were obtained at a distance of $57D$ from the inlet. To obtain data over a wide range of Stokes, Froude and Galileo numbers, water, and various glycerol/water mixtures were employed as working fluids.

RESULTS AND DISCUSSION

Pressure drop measurements indicate an increase in the coefficient of skin friction (f) as the volume fraction of particles is increased (see figure 1).

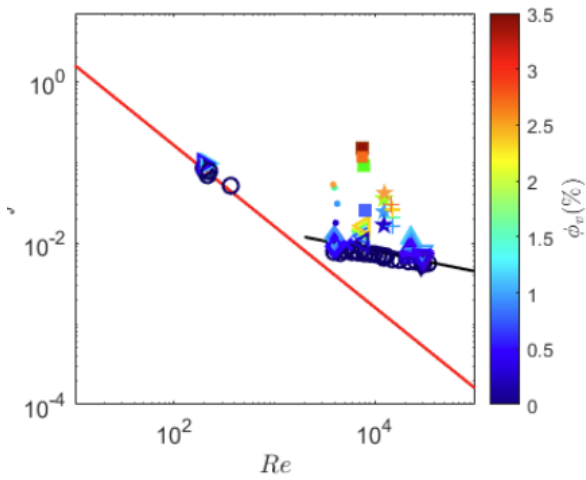


Figure 1: variation of the coefficient of skin friction with volume fraction (ϕ_v) of particles. Symbols represent different Froude numbers, while red and black lines are the correlations for laminar and turbulent single-phase flows.

This was true for all Stokes and Froude numbers considered ($St = 3$ to 120 , $Fr = 0.1$ to 4). The growth rate, β , of the friction factor ($\beta = df/d\phi_v$) was however observed to be only a function of the Froude number (see figure 2). A power-law fit to the data indicates that β scales as Fr^{-1} indicating that for Fr less than 1 , the influence of gravity cannot be neglected.

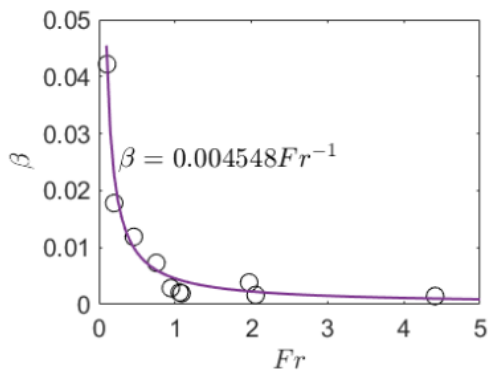


Figure 2: Growth rate (β) of the coefficient of skin friction as a function of the Froude number

By analysing the dispersed phase using Voronoi tessellation (see figure 3 for an example), we obtain a state map in the Stokes number – Froude number parameter space for the onset of turbophoresis. (see figure 4).

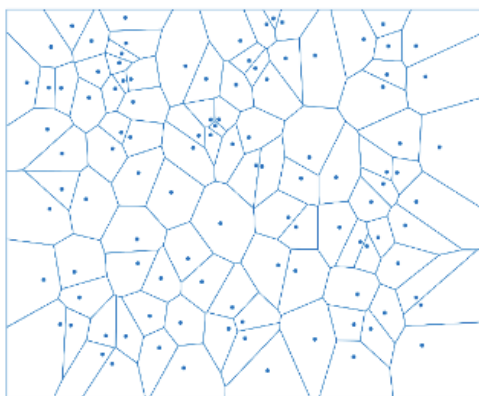


Figure 3: Sample Voronoi diagram at $St=10$ and $Fr=0.1$. Pipe wall is located at the left and right edges

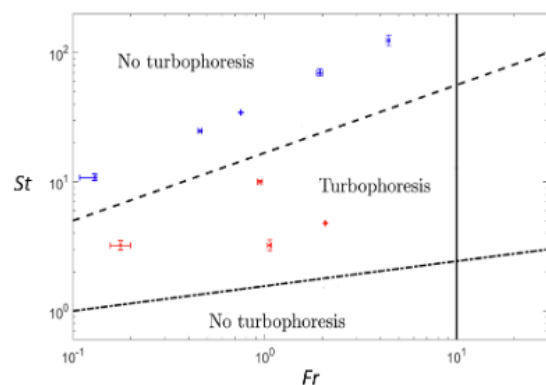


Figure 4: State map in the $St - Fr$ parameter space for the occurrence of turbophoresis

CONCLUSION

The dynamics of inertial particles in a vertical turbulent pipe flow have been investigated. An increase in skin friction drag with volume fraction was observed and a power-law growth rate dependent solely on the Froude number was established. The onset of turbophoresis was found to be influenced by the interplay between particle inertia and gravity, and the region in the Stokes number-Froude number parameter space where the phenomenon can be observed has been mapped out.

REFERENCES

Balachandar, S. & Eaton, J.K. Turbulent dispersed multiphase flow. *Annu. Rev. Fluid Mech.*, Vol. 42, pp. 111-133 (2010).

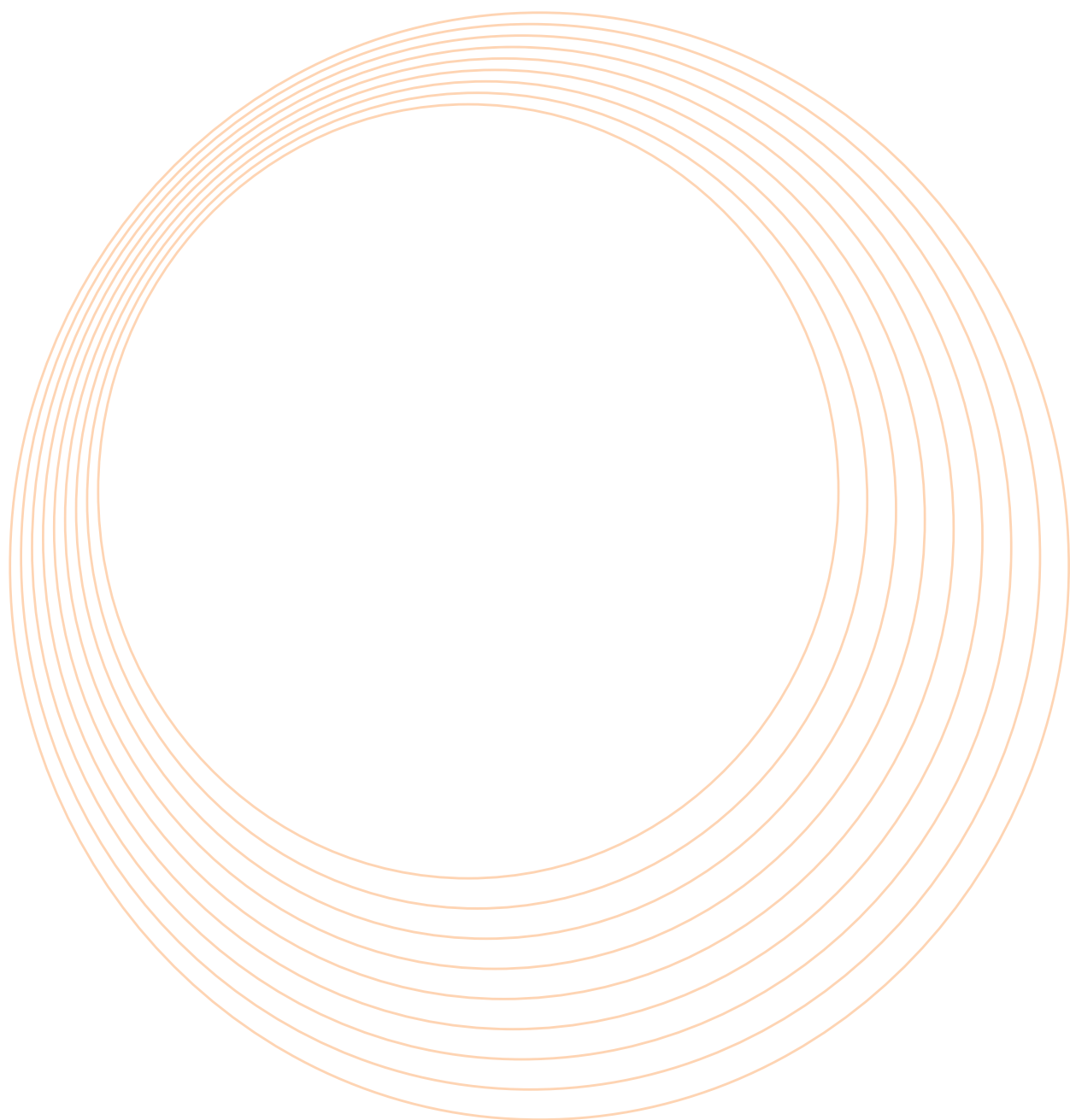
Brandt, L. & Coletti, F. Particle-laden turbulence: progress and perspectives. *Annu. Rev. Fluid Mech.*, Vol. 54, pp. 159-189 (2022).

Edition and Design:

Lívia Yohana

Marcia Ehmann

Núcleo Interdisciplinar de Dinâmica dos Fluidos (NIDF), Universidade Federal do Rio de Janeiro(UFRJ)





Tecnology Centre 2
Federal University of Rio de Janeiro (UFRJ)

Rua Moniz Aragão, 360 – Bl.01
Ilha do Fundão – Rio de Janeiro – Brazil